JOURNAL OF APPLIED PHYSICS

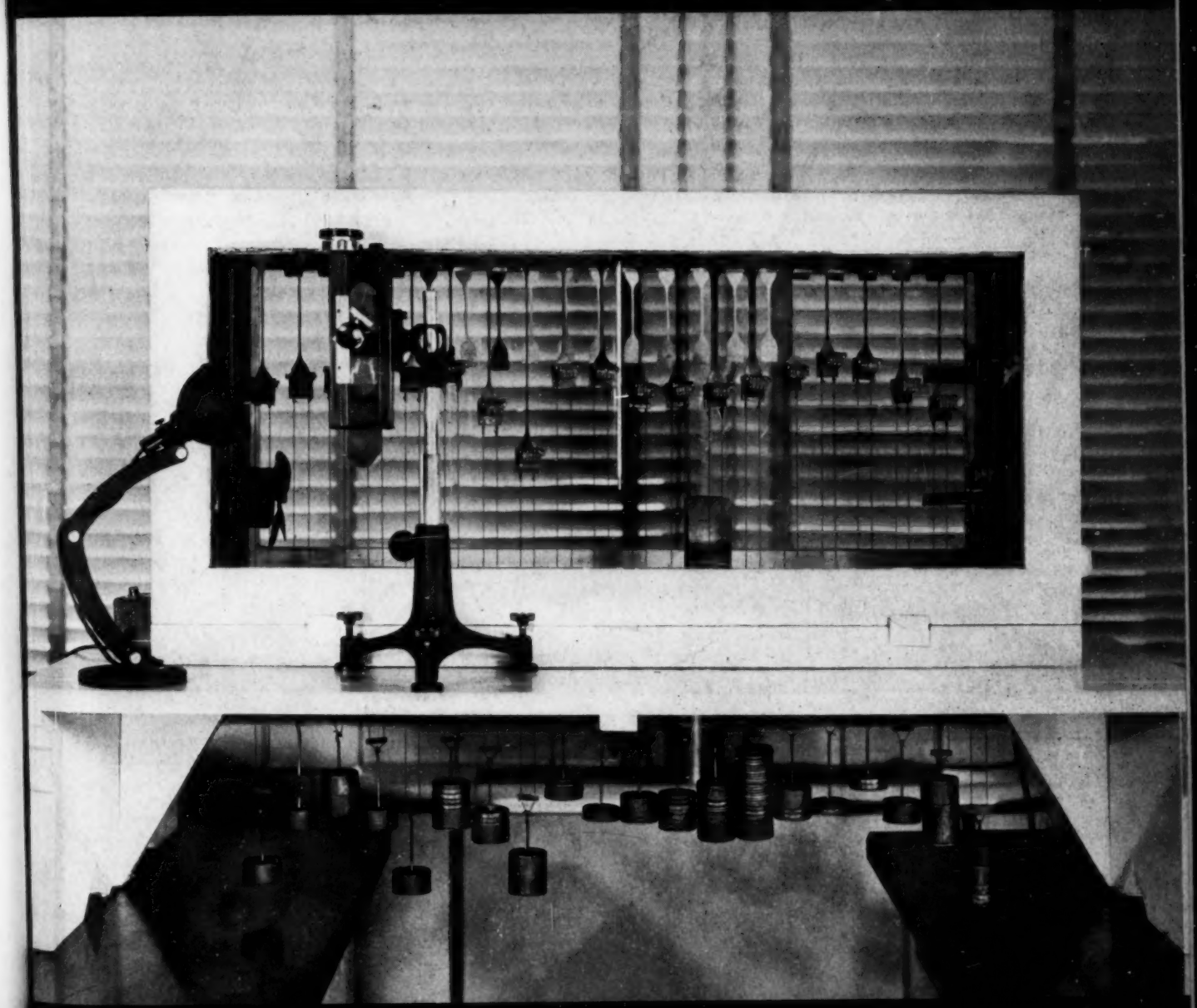

JOURNAL
OF
APPLIED PHYSICS

Vol. 19, No. 5 MAY, 1948

In This Issue

Special Issue on High Polymers

Page

Effects of Pile Bombardment on Uncured Elastomers
W. L. Davidson and I. G. Geib 427

Thermodynamics of a Strained Elastomer. I. General Analysis
M. Mooney 434

Thermodynamics of a Strained Elastomer. II. Compressibility
L. E. Copeland 445

Thermodynamics of a Strained Elastomer. III. The Thermal Coefficient of Modulus and the Statistical Theory of Elasticity
L. E. Copeland and M. Mooney 450

Creep, Recovery, and Permanent Set for GR-S and Hevea S. D. Gehman 456

Theory of Commercial Yarn Testing
Charles J. Geyer, Jr., C. H. Reichardt, and George Halsey 464

Errata: Infra-Red Spectra of Hydrocarbons. II. Analysis of Octane Mixtures by the Use of Infra-Red Spectra Obtained at Low Temperatures
W. H. Avery and J. R. Morrison 472

Method for the Absolute Measurement of Dynamic Properties of Linear Structures at Sonic Frequencies
W. James Lyons and Irven B. Prettyman 473

Regular Contributed Original Research

Electric Field Intensity Inside of Natural Clouds Ross Gunn 481

Apparatus for Weighing in Vacuum G. W. Monk 485

Ionosphere Reflections Recorded Mechanically by Means of a Repetition Frequency Converter W. Stoffregen 487

Quantitative X-Ray Investigations on the Crystallinity of Cellulose Fibers. A Background Analysis P. H. Hermans and A. Weidinger 491

Letters to the Editor:

Convenient Methods for Obtaining d/n Values from X-Ray Diffraction Patterns
C. B. Stewart and E. S. Lutton 507

Effect of Recrystallized Grain Size on Grain Growth Paul A. Beck 507

In Every Issue

Calendar of Meetings 449

New Booklets 509

Here and There 510

Index to Advertisers xxxvi

BOARD OF EDITORS

Elmer Hutchisson,
Editor

Associate Editors

R. Bowling Barnes
Otto Beeck
W. F. Busse
W. James Lyons
Philip Morrison
Paul E. Sabine
Frederick Seitz
J. R. Townsend
John Von Neumann

Publication of the
American Institute of Physics

ADMINISTRATIVE STAFF

Henry A. Barton,
Director

Cleveland Norcross,
Assistant Director

Ruth F. Bryans,
Publication Manager

Theodore Vorburger,
Business Manager

John T. Tate,
Adviser on Publications

GOVERNING BOARD

George R. Harrison,
Chairman

Wallace Waterfall,
Secretary

George B. Pegram,
Treasurer

Luis W. Alvarez
Robert B. Brode
E. U. Condon
A. J. Dempster
W. F. Fair, Jr.
Harvey Fletcher
R. C. Gibbs
W. V. Houston
Paul E. Klopsteg
F. W. Loomis
Philip M. Morse
A. H. Pfund
John T. Tate
M. W. White
A. G. Worthing

The Journal of Applied Physics, published monthly at Prince and Lemon Sts., Lancaster, Pa., is devoted to physics in its role as the science basic to other natural sciences and to the arts and industries. Previous to 1937 this publication was known as Physics. The Journal of Applied Physics publishes editorials, news of physicists, and reviews, as well as technical papers of applied physics.

Manuscripts should be submitted to Elmer Hutchisson, Editor, Case Institute of Technology, Cleveland 6, Ohio.

Subscriptions and orders for back numbers should be addressed to Prince and Lemon Streets, Lancaster, Pa. or to the American Institute of Physics, 57 East 55 Street, New York 22, N. Y.

Subscription Price

	U.S. and Canada	Elsewhere
To members and associate members of the American Institute of Physics	$6.00	$7.00
To all others	8.00	9.00

Back Number Prices

Complete set: Vol. 1, July, 1931–Vol. 18, 1947—$132.00
Yearly back number rate: $10.00
Single copies: $1.00 each.

Changes of address should be sent to the Business Manager, American Institute of Physics; corrected proofs should be sent to the Publication Manager, American Institute of Physics.

Advertising rates supplied on request. Orders, advertising copy, and cuts should be sent to the American Institute of Physics.

Entered as second class matter January 22, 1937, at the Post Office at Lancaster, Pennsylvania, under the Act of March 3, 1879.
Accepted for mailing at the special rate of postage provided for in the Act of February 28, 1925, authorized May 2, 1932.

Copyright 1948, by the American Institute of Physics.

Journal
of
Applied Physics

Volume 19, Number 5 May, 1948

Special Issue on High Polymer Physics

The Effects of Pile Bombardment on Uncured Elastomers*

W. L. Davidson

Clinton National Laboratory, Oak Ridge, Tennessee and The B. F. Goodrich Company, Akron, Ohio

AND

I. G. Geib

The B. F. Goodrich Company, Akron, Ohio

(Received January 28, 1948)

Previous work on the effects of ionizing radiations on hydrocarbons has established that four competitive processes are usually operative: (1) dehydrogenation, (2) condensation or polymerization, (3) hydrogenation (action of nascent hydrogen on any unsaturated matter present), (4) decomposition (C-C cleavage). The chain reacting nuclear pile offers an ideal means for subjecting relatively thick samples of matter (such as rubber) to uniformly high concentrations of radiation. Such studies on natural rubber, butyl rubber, and polyisobutylene allow one to draw the following conclusions. 1. Uncured natural rubber undergoes a slight curing action when exposed to pile radiations. 2. Polyisobutylene samples are appreciably degraded by pile radiations. 3. The same effects as noted in (1) and (2) are greatly enhanced by secondary alpha-particles, produced by an (n,α) reaction on boron^{10} (milled into the elastomer). However, even a 2-hour bombardment of natural rubber yields a product greatly inferior to sulfur vulcanizates. 4. Pile bombardment does not introduce measurable unsaturation in polyisobutylene and decreases the unsaturation in natural rubber but slightly. 5. A typical butyl rubber stock is permanently degraded by pile irradiation showing upon cure reduced tensile strength compared to that of a control sample. 6. Natural rubber shows a weak but measurable radioactivity days after bombardment, probably because of its mineral content. Polyisobutylene is not appreciably active.

INTRODUCTION

In the past numerous workers[1–6] have studied the behavior of simple hydrocarbons exposed to various kinds of ionizing radiations. Although a wide variety of experimental arrangements and techniques is described, remarkably similar effects were obtained by these workers. In fact, the results are so much alike that one is forced to conclude that for the same energy expendi-

* Part of the experimental work for this report was performed under Contract No. W-35-058, Eng. 71, for the Atomic Energy Commission while Dr. W. L. Davidson was a member of the Clinton Laboratories Training School on leave from The B. F. Goodrich Company. Presented at the Fifth Meeting of the Division of High-Polymer Physics, American Physical Society, Chicago, Illinois, December 29–30, 1947.

[1] S. C. Lind, D. C. Bardwell, and J. H. Perry, J. Am. Chem. Soc. **48**, 1556 (1926).

[2] S. C. Lind and D. C. Bardwell, J. Am. Chem. Soc. **48**, 2335 (1926).

[3] J. C. McLennan and W. L. Patrick, Can. J. Research **5**, 470 (1931).

[4] C. S. Schoepfle and C. H. Fellows, Ind. Eng. Chem. **23**, 1396 (1931).

[5] R. E. Honig and C. W. Sheppard, J. Phys. Chem. **50**, 119 (1946).

[6] M. Burton, (Manhattan Dist.), MDDC 17 (1947).

tures, electrons, deuterons, and alpha-particles are roughly equivalent as regards chemical changes induced in gaseous hydrocarbons.

The essential facts are these:

(1) Gases always constitute one type of reaction product. These gases consist of H_2 and various saturated hydrocarbons. Practically no unsaturated products are found in the gas phase, even though the target material may be unsaturated. This is in sharp contrast to the results obtained from thermal and photo-chemical decompositions or when hydrocarbons are passed through an electric discharge. For example, Yeddanapalli[7] finds that acetylene and ethylene are prominent products when CH_4 is passed through a glow discharge tube.

(2) A certain amount of high boiling liquid (polymer), or in some cases a solid residue, is also formed in the presence of ionizing radiations. These products do show unsaturation and normally yield a structure close to (C_nH_{2n}). Upon extended irradiation the gaseous phase becomes predominantly H_2, the remainder of the sample being converted to the liquid state. In fact, this behavior has led Lind to propose a radiation theory for the genesis of petroleum.

(3) The M/N yield (number of target molecules converted per ion pair) is approximately 2 for all saturated hydrocarbons which have been investigated. Unsaturated materials show an erratic behavior; C_2H_4 gives $M/N=5$, for C_2H_2 the figure is 20, while for benzene vapor $M/N=1$.

(4) In spite of the previous statement, the gaseous yield is much higher for saturated feed materials. As an example, Schoepfle and Fellows[4] obtained the following yields of gaseous products when the liquids listed were subjected to equal bombardments with 170-kev electrons:

Irradiated compound	Gas evolved (STP)
N-octane	48.3 cc
Diisobutylene	20.8
Benzene	2.2

(5) A corollary to (3) and (4) states that normally much more polymer product will be produced when the bombarded material is unsaturated. This can be confirmed by reviewing the following data taken from Burton's report MDDC 17. Here G denotes the number of molecules of target material converted to (a) gas or (b) polymer, per 100 electron volts absorbed. When liquids are under investigation, as was the case here, it is considered more proper to report results in terms of G rather than M/N, since the ionizing potential of a liquid is not easily determined. Interestingly enough the total conversion per 100 ev is the same for both materials. However, in one case the major product is gaseous, whereas for cyclohexene, polymerization is the predominant reaction.

Target material	G gas	G polymer
Cyclohexane	4.0	1.2
Cyclohexene	1.0	4.2

No one has yet succeeded in explaining satisfactorily all the previous facts. Early in the game Lind introduced his famous cluster theory. In this theory the first step consists of ionization. For ethane bombarded with α's he suggests:

$$C_2H_6 \xrightarrow{\alpha} C_2H_6^+ + e^-.$$

The positive ion then attracts a neutral ethane molecule to itself. This constitutes the cluster. (For acetylene the $C_2H_2^+$ ion is assumed to attract $19C_2H_2$ molecules in order to justify $M/N=20$.) The second step can be written

$$C_2H_6^+ + C_2H_6 \rightarrow (C_2H_6)_2^+.$$

The third step comprises neutralization of the cluster by a negative ion or electron. In the ethane case Lind found H_2, CH_4, C_2H_6, C_3H_8, and C_4H_{10} in the gas phase after bombardment. To explain these findings he assumes that on neutralization the cluster can break up in at least three ways:

1. $(C_2H_6)_2^+ + e^- \rightarrow C_4H_{10} + H_2$.
2. $(C_2H_6)_2^+ + e^- \rightarrow C_4H_8^* + 2H_2$
   $xC_4H_8^* \rightarrow (C_4H_8)_x$ polymer.

The butene is said to be formed in a nascent state, and immediately x molecules of butene react to form a molecule of liquid. This explains why no unsaturates appear in the gas phase.

3. $(C_2H_6)_2^+ + e^- \rightarrow CH_4 + C_3H_8$.

Reactions (1) and (2) correspond to condensation

[7] L. M. Yeddanapalli, J. Chem. Phys. 10, 249 (1941).

and dehydrogenation plus polymerization, whereas (3) represents a cleavage. Had we considered ethylene instead of ethane the cluster would have consisted of 5 molecules. On neutralization of this cluster a majority of the products would be unsaturated, which on Lind's picture requires that they immediately polymerize. This then explains why unsaturated materials yield more polymer and less gas.

The cluster theory has proved too naïve for many people; including Eyring, Hirschfelder, and Taylor.[8] They prefer to speak of chain reactions initiated by atoms and free radicals. In fact they partially discount the effects of ionization in radiation chemistry, saying that at least half of the initiating free radicals or atoms are formed by molecular dissociation from excited (not ionized) states. The other half are thought to be formed when the ions are neutralized. Even Lind admits that the cluster theory has to be abandoned for the case of radiochemical synthesis of HCl from H_2 and Cl_2 where $M/N > 1000$. The free radical-atom theory has been applied to only a few relatively simple radiochemical reactions, such as the conversion of *ortho*-H_2 to *para*-H_2 by α-particle bombardment and the synthesis or decomposition of HBr. Apparently too little is known about the excitation, ionization, and general ionic behavior of hydrocarbon fragments to attempt a detailed analysis of such experiments.

In the literature one finds few articles reporting the effects of radiations on unvulcanized elastomers. There are two German papers relating to the effect of the silent discharge on rubber solutions. However, these are not particularly helpful because they relate quite opposite results. Fromandi[9] finds a sharp decrease in solution viscosity, iodine number, molecular weight, and softening point of both natural rubber and polyisoprene.**

Hock and Leber[10] working at a later date in the same laboratory found equally large increases in these same properties. The latter workers explain Fromandi's results as due to small traces of oxygen present in the reactor system. The oxygen would be converted to ozone in the discharge and then degrade the rubber chains.

E. B. Newton[11] claims vulcanization of thin rubber films by subjecting them to short (20–25 sec.) bombardments with 250 kv cathode rays. He reported that the samples showed good tensile strength, were swelled but not dissolved by benzene and exhibited excellent resistance to accelerated aging tests. No tensile figures are included, however, so it is rather difficult to assess these results quantitatively.

With this meager background to build on, we will now describe the experiments performed in the nuclear pile at Oak Ridge on natural rubber, butyl rubber, and PIB.

TABLE I. Compounds studied.

	1	2	3	4	5
Smoked sheet	100	100		100	
Polyisobutylene			100		100
EPC black		30	30	30	30
Ammonium borate				26.4	26.4

	6	7
Butyl rubber	100	
Polyisobutylene		100
Carbon black	50	50
Zinc oxide	5	5
Stearic acid	1	1
Sulfur	2	2
Captax	0.5	0.5
Methyl Tuads	1	1
Ammonium borate	26.4	26.4

COMPOUNDS USED

The compounds used are given in Table I. Natural rubber was used in 1, 2, and 4. Stock 1 is smoked sheet as received at the factory. All other compounds were mixed on a laboratory mill and sheeted out to a thickness of 0.1". 30 parts of a typical reinforcing black were added to 100 parts of smoked sheet in 2, and 26.4 parts of ammonium borate equivalent to 5 parts boron were added to the compound in 4.

Compounds 3 and 5 are polyisobutylene compounds to be compared with the corresponding natural rubber compounds 2 and 4.

Compounds 6 and 7 were mixed to determine if a polyisobutylene stock can be cured like a

[8] H. Eyring, J. O. Hirschfelder, and H. S. Taylor, J. Chem. Phys. **4**, 479 (1936).

[9] G. Fromandi, Rubber Chem. Tech. **2**, 161 (1929).

** However, polyisoprene showed a small initial rise in all these properties.

[10] L. Hock and H. Leber, Rubber Chem. Tech. **13**, 831 (1940).

[11] U. S. patent 1,906,402.

TABLE II. Goodrich plasticity (70°C) for various exposures in Clinton pile.

Exposure→ stock ↓	0	1′	4′	16′	32′	60′	120′
1	3				4		
2	36				27		
3	5				13		
4	21	18	15	6	4	4	3
5	14	19	33	62	70		
7 (Uncured)	15						
7 (Cured)	16				80	89	

TABLE III. Unsaturation in stocks after various exposures in Clinton pile. Smoked sheet is 100 percent.

Exposure→ stock ↓	0	4′	32′	120′
1	89		82	
2	95		97	
3	1		0.5	
4	98	96	98	95
5	8	8	5	

butyl stock after irradiation. Compound 6 is a typical butyl rubber stock except for the addition of ammonium borate. Curing ingredients—zinc oxide, stearic acid, sulfur, Captax, and methyl Tuads—are added to the butyl rubber, carbon black, and ammonium borate. Compound 7 is to be compared with 6, polyisobutylene in 7 replacing butyl rubber in 6.

EXPERIMENTAL PROCEDURE

Small pieces of stock, about 2″×2″, were cut out and inserted in a "rabbit." The rabbit is a small cylindrical box which fits snugly inside a pneumatic tube and is driven through the tube by tank CO_2. The pneumatic tube extends to the center of the pile. Cooling air is drawn past the tube, so the temperature of the rabbit seldom exceeds 30°C, which eliminates the possibility of thermal effects on the samples. The time required by the rabbit to reach the center of the pile from outside is only 2 seconds, so the exposure can be precisely controlled. After exposure, Goodrich plasticity[12] and iodine number[13] were determined for representative samples. These data are summarized in Tables II and III.

The unsaturation data are not very illuminating. In general, pile bombardment of natural rubber seems to decrease the unsaturation present, although this trend is reversed in compound 2. It is somewhat disturbing that samples 3 and 5 should show such different iodine numbers when they are identical except for the ammonium borate content of 5. About all that can be said with regard to these latter samples is that they show no increase in unsaturation as a result of bombardment.

[12] E. Karrer, J. M. Davies and E. O. Dietrich, Ind. Eng. Chem. Anal. Ed. 2, 96 (1930).
[13] A. R. Kemp and H. Peters, Ind. Eng. Chem. Anal. Ed. 15, 453 (1943).

EXPERIMENTAL RESULTS

I. Neutron Intensities

In samples 1, 2, 3 any effects noted, either physical or chemical, can be assigned to:

(a) Ionization produced by fast electrons resulting from γ-radiation.
(b) Secondary ionization by fast neutrons.
(c) C−C and C−H cleavage by fast neutrons.
(d) C−H cleavage by H capture of slow neutrons due to recoil from γ-ray emitted.

Calculations indicate that processes (a) and (b) will be about equally effective in breaking chemical bonds, while (c) and (d) will be negligible by comparison.

From the dearth of previous work in this field it is impossible to predict which of the four processes listed in the Introduction will predominate here. However, it is interesting to speculate briefly concerning the relative bombardment times required to bring about certain changes in the elastomer, making in turn the hypothetical assumption that *every* broken bond acts to produce the particular change desired. The changes to be effected are:

1. Sufficient C−C cleavage to halve the molecular weight (decomposition). (45×10^{18} C−C bonds must broken per g rubber if mole. weight 140,000.)
2. Sufficient cross links to equal a sulfur cure (condensation or polymerization). (9×10^{19} cross links needed per g to assure 1 cross link per 100 C_5H_8 units.)
3. Creation of sufficient double bonds in PIB to equal the unsaturation present in butyl rubber (dehydrogenation) (1.8×10^{20} double

bonds needed to give 2 percent unsaturation; where natural rubber has 100 percent unsaturation).

Of course if the three processes are *equally* probable, degradation of the elastomer will predominate in every instance.

Even if processes (2) and (3) are highly favored, calculations imply that the bombardment times to achieve the desired end effects will be too long to arouse much technical interest. To accelerate the ionization effects we prepared stocks 4, 5, 6, and 7 containing 5 parts boron per 100 of elastomer (added as ammonium borate).

The slow neutron reaction $B^{10}+n^1 \rightarrow Li^7+He^4$ is a very prolific one. Total K.E. of the Li^7 and He^4 averages 2.4 Mev per event, and essentially all this will appear as excitation and ionization. If we can believe previous radiation studies, the effects produced will be identical with those for the non-boron stocks except in magnitude.

For equal bombardments we may anticipate an effect here some 80 times that deduced for the non-boron samples. Conversely, with boron present we might hope to achieve marked changes in times well within the range of technical interest.

II. Relation between Plasticity and Molecular Weight

In order to evaluate the increased effects of the added boron, we need to know what the plastometer readings correspond to in terms of molecular weight. Apparently no such relation has been established for this instrument. Karrer, Davies, and Dietrich[12] plot Goodrich plasticity as a function of milling time for a batch of crepe rubber. In addition, Wildschut[14] has published a curve showing molecular weight *vs.* milling time for a crepe sample. If we make the rough assumption that these two samples underwent equal mastication, it is possible to obtain a curve relating Goodrich plasticity and molecular weight for crepe rubber. This curve is depicted as the inset portion of Fig. 1. It would appear that the interpretation in terms of molecular weight should be limited to plasticity readings between 5 and 40. Although the curve is strictly applicable to crepe rubber only, we shall use it for our samples here in the absence of better information. Table IV records the molecular weights obtained in this manner.

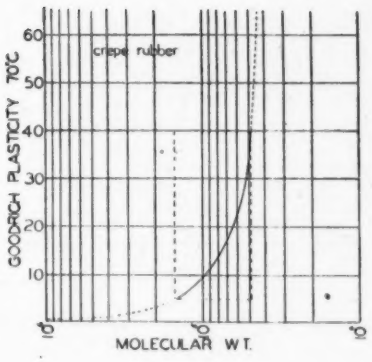

FIG. 1.

Compound 2 reveals an increase in molecular weight from 52,000 to 56,000 after 32 minutes bombardment, or a rate of $\frac{1}{4}$ percent per minute. Compound 4 shows a 100 percent increase in 16 minutes, which figures 6 percent per minute. Thus the boron accelerates matters here by only 25-fold instead of the calculated 80 times.

Comparing the degradation induced in PIB, a 32-minute irradiation of 3 goes 75 percent of the way toward halving the molecular weight. Roughly the same result is produced in 5 after 4

TABLE IV. Molecular weights ($X10^{-3}$) of stocks after various exposures in Clinton pile. Values obtained from plastometer-viscosity curve.

Exposure → stock ↓	0	1′	4′	16′	32′
1	—	—	—	—	—
2	52	—	—	—	56
3	140	—	—	—	88
4	62	69	80	125	—
5	82	67	53		

TABLE V. Radioactivity induced in stocks during pile bombardment.

Irradiation time (min.)	Net activity counts/min. No. 4	No. 5
1	19	13
2	13	13
4	38	6
8	64	6
16	77	19
32	218	6
60	460	—
120	730	—

[14] A. J. Wildschut, Rubber Chem. Tech. **7**, 34 (1934).

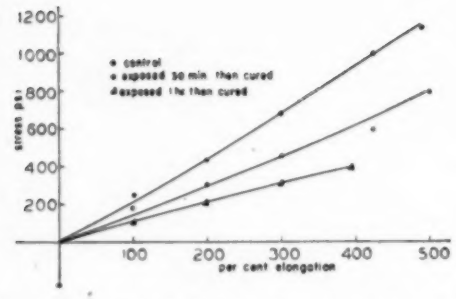

FIG. 2. Effect of pile bombardment on butyl rubber stock. Cure 80 min., 307°F.

minutes in the pile. This implies a mere 8-fold enhancement due to boron, although on the basis of chains broken we should raise this to 14-fold since 5 starts at a molecular weight of 82,000 compared to 140,000 for 3. In any event it seems clear that in neither instance does boron fully live up to expectations. It may be that the heavier ionization left in the wake of an alpha-particle (compared to that from a proton or electron) leads to considerable recombination within the ionization column, though this does not appear to be the case with gaseous targets.

III. Explanation of Experimental Findings

How does one explain the fact that natural rubber increases in molecular weight under pile bombardment while PIB is degraded? The explanation must lie with the unsaturation in natural rubber. The authors suggest that the first two steps, ionization and neutralization, are similar for both materials. If the ionization occurs at the expense of a valence electron belonging to a chain carbon, cleavage of the chain probably takes place. Upon neutralization free radicals are generated. In natural rubber these radicals are able to initiate chain reactions involving double bonds. Apparently the cross linking established in this way more than compensates for the broken chains. With PIB no chain reaction can be effected and so the end result has to be degradation.

In view of the large amount of H_2 found in previous radiation experiments involving hydrocarbons, it seems inevitable that some unsaturation would be induced in both types of elastomer. The apparent decrease in iodine number for natural rubber with radiation time is not unexpected in view of the chain reaction feature suggested above. The absence of an increase in iodine number for PIB, however, is somewhat disturbing. It is true that the unsaturation introduced in PIB would be only a few percent at most and the iodine method does not seem entirely satisfactory. Because of this uncertainty we formulated compound 7 and tried to cure same after extended irradiation in the pile. As is evident from Table II, this effort did not succeed. If any unsaturation had been created it was certainly overshadowed by the cleavage. This is further borne out by tests on 6, a butyl rubber compound. Figure 2 depicts the effect of pile bombardments on the stress-elongation curve of the cured material. It is evident that the degradation effects persist even after cure.

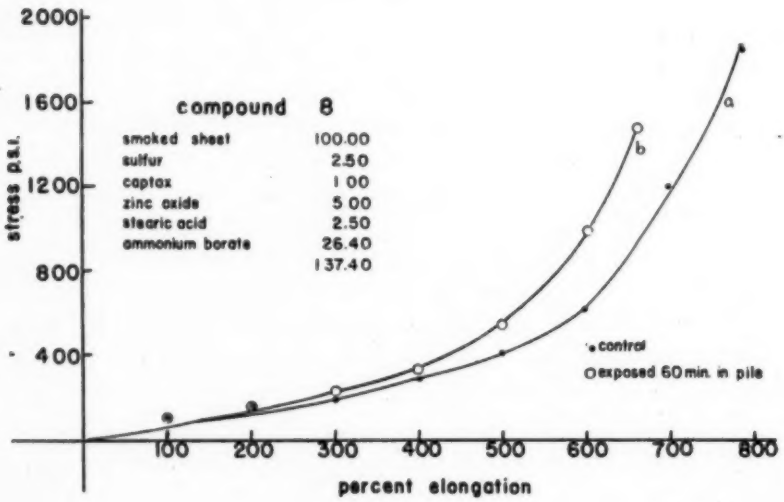

FIG. 3. Effect of pile bombardment on cured natural rubber stock. Cure 80 min., 280°F.

IV. Studies with Vulcanized Elastomers

(*a*) *Butyl Rubber*

It was deemed of interest to determine if pile bombardment would degrade a specimen of vulcanized butyl rubber as much as it did the uncured stock. Therefore a cured sample (80′ ×307°F) of compound No. 6 was exposed to the pile as before, for a period of 1 hour. A subsequent tensile test repeated within experimental error the curve of Fig. 2 for the sample which had been bombarded for an hour prior to cure. Apparently the degradation induced is essentially independent of the state of vulcanization. Fragments from this sample were subjected to three passes through a laboratory mill. This treatment resulted in a well knit material which might be classified as butyl rubber reclaim. This could be taken as superficial evidence that the pile has possibilities as a reclaiming agent for butyl rubber.

(*b*) *Natural Rubber*

It was also decided to ascertain the effect of pile radiations on cured natural rubber. Compound No. 8 was chosen for this test and given a cure of 80′×280°F. The resulting stress-elongation curve is presented in Fig. 3a. The low tensile strength is accounted for by the poor dispersion of the borate in the compound. A sample of this cured compound was likewise subjected to 1 hour in the pile. The curve of Fig. 3b, illustrates the stress-elongation characteristics after bombardment. It is clear that the modulus has increased appreciably while a corresponding decrease has occurred in the tensile strength. This is typical of accelerated rubber stocks that have been subjected to a long overcure. From the weak vulcanizing effect of a 1-hour pile exposure on uncured rubber it seems impossible to account for the present change as a conventional over-cure phenomenon. It may be true that the sulfur linkages that are already present here in some way suppress the degrading effects of pile bombardment, thus allowing the vulcanizing tendencies to be more pronounced. At the moment there is insufficient evidence to permit speculation as to the mechanism for this suppression.

ACTIVITY OF IRRADIATED SPECIMENS

Specimens of 1, 2, 3, 4, and 5 were tested for radioactivity several days after irradiation. $\frac{1}{2}''\times\frac{1}{2}''$ specimens from each irradiated piece were placed in a standard position below the 10 mg/cm² mica window of the Geiger tube. The natural rubber compounds 1, 2, and 4 had a small but measurable activity. The PIB compounds showed practically no activity. Activities are given in Table V. The background for the counting tube used was 60 counts/minute. The activity in natural rubber is doubtlessly accounted for by its mineral content.

We wish to thank the Monsanto Chemical Company and the personnel of Clinton National Laboratory for the privilege of utilizing the pile facilities in carrying out these studies while one of us (W. L. Davidson) was a member of the Training School at Clinton Laboratories.

The Thermodynamics of a Strained Elastomer. I. General Analysis*

M. Mooney
General Laboratories, United States Rubber Company, Passaic, New Jersey
(Received February 18, 1948)

The thermodynamic functions of principal interest in a strained elastomer are the entropy and energy of deformation. The volume is of secondary importance, and it can be assumed, with sufficient accuracy for most purposes, that the volume is linear in the temperature and the mean pressure. The basic partial differential equations of thermodynamics can then be integrated, yielding expressions for the energy and entropy of deformation in terms of observable quantities.

In the present analysis the volume effects caused by changes in mean pressure and crystallinity are taken into account, and the effects associated with change in shape are sharply separated from those associated with change in volume. It is shown that the superelastic functions of deformation previously published (M. Mooney, J. App. Phys. **11**, 582–92 (1940)) have a very general validity.

INDEX OF NOTATION

Subscripts; usual significance.

i, j, k—directions of principal strain and stress axes.
0—initial state of sample.
1, 2, 3—directions of principal strain and stress axes.
1—amorphous phase.
2—crystalline phase.

Variable	Eq. No.	Variable	Eq. No.	Variable	Eq. No.
f	9	A	4	α	20
h	58	C	36, 57, 58	β	15, 18–22
m	1	D	26	γ	60
r	5, 67	F	10, 79	δ	13
s	69	G	59	θ	33, 36, 58, 76
u	79	H	59	κ	15, 18–22
v	67, 71, 79	L	1	λ	6
w	79	P	9	μ	66
x	18, 30	Q	12	σ	9
		R	59	ϕ	35, 74
		S	28	ψ	33, 68
		T	15	ω	16, 19–22
		U	28	Φ	78
		V	1, 15, 17, 18	Ψ	78
		W	24, 52		
		X	44		
		Z	10		

INTRODUCTION

THIS article is the first of a series, written by the present author and associates, devoted to the thermodynamics of strained elastomers. The first article is entirely theoretical and will present theory and equations to be applied in the analysis of experimental data.

There have been published a number of treatments of the thermodynamics of stretched rubber. In most cases, the treatment presented was limited to that required for the analysis of a particular type of experimental data. The present treatment is intended to be quite general in scope and serve as the basis for analyzing any conceivable type of data having to do with the thermodynamic properties of a strained sample of a cured gum elastomer. It is assumed that the elastomeer is isotropic, in a sense later to be precisely defined, and that all deformations and changes of state are reversible.

Several points of view in the present analysis may be mentioned as being new. In the first place, recognizing that effects which occur with change in shape of an elastomer sample are usually of primary concern while those occurring with change in volume are of secondary concern, we begin the analysis by assuming a volume equation of state which will be sufficiently exact for our purpose. We assume that, at any deformation, the volume is a linear function of temperature and pressure. This neglect of second-order temperature and pressure effects seems to be entirely justified for the limited ranges of temperature and pressure involved in most experimental investigations. With this assumption regarding the volume, it then becomes possible to integrate the basic differential equations of thermodynamics and obtain explicit

* Presented at the Fifth Meeting of the Division of High-Polymer Physics, American Physical Society, Chicago, Illinois, December 29–30, 1947.

relationships between entropy, energy, and observed stresses or temperature changes in a deformed sample. If, at any time, experimental data become available which require inclusion of the second or higher terms of temperature and pressure, such terms can readily be included in a more exact analysis following the same procedure.

Another respect in which the present differs from previous treatments lies in the choice of the deformation variables. Following classical methods, the total strain is resolved into its two components, dilatation and pure shear, or change in volume and change in shape. Then, instead of length or dimension variables, we use deformation variables which refer exclusively to changes in shape and are independent of changes in volume.

Some elastomers crystallize when stretched. Certain limited thermodynamic analyses are valid in spite of any such change in phase composition which may occur. In cases where this is not true, the analyses in the literature have been limited to low elongations or to types of elastomers which do not crystallize at any elongation. In the present analysis we take account of crystallization, subject to the assumption that percent crystallinity, like the volume of the sample, is a linear function of pressure and temperature, and that the volume change resulting from crystallization is small.

The first of these assumptions would not be valid for raw Hevea and certain other elastomers which have, in the raw state, a fairly sharp melting point. Cured elastomers, on the other hand, have never been found to have a melting "point." Here again, the method of analysis can be carried through with higher powers of pressure and temperature retained if this is later found desirable. If a second-order transition occurs within the temperature range covered in a particular experiment, the slight changes in specific heat and coefficient of expansion would have, in many cases, only negligible effects. When, however, exact analysis is required, two solutions could be fitted to the experimental data, one on each side of the transition temperature.

Finally, as a further step beyond previous work, we incorporate in the present thermodynamic analysis the results obtained by the writer in a previous general treatment of the strain-work function for a large elastic deformation.[1] (This paper will hereafter be designated as reference 1.) It will be shown that this analysis of the work function can be applied generally to any thermodynamic function of a deformed elastomer, subject only to certain very mild conditions which will be satisfied by nearly all cured elastomers.

Particular mention may be made at this point of the work of Elliott and Lippmann.[2] These authors were the first to recognize the theoretical importance of distinguishing between deformation at constant pressure and at constant volume. However, their treatment is limited to small deformations and is made somewhat awkward mathematically by the fact that they followed custom and used lengths to measure the deformation instead of the more suitable λ-variables employed in the present theory.

ANALYSIS OF STRAIN

We consider an unstrained rectangular sample of a cured elastomer of mass m and dimensions L_{10}, L_{20}, L_{30}. If we represent by the V_0 the specific volume in the undeformed state at initial temperature and pressure, we may write

$$mV_0 = L_{10}L_{20}L_{30}. \tag{1}$$

In the deformed state at any temperature and pressure, we have

$$mV = L_1L_2L_3. \tag{2}$$

We postulate, without loss in generality, that the three dimensions of the sample lie parallel to the principal strain axes. The principal strains are therefore $(L_i/L_{i0}) - 1$.

Obviously,

$$m\,dV = \sum_1^3 A_i\,dL_i$$

where

$$A_i = L_jL_k. \tag{4}$$

We now define r, the mean relative length, by the equation

$$r = (V/V_0)^{\frac{1}{3}}, \tag{5}$$

[1] M. Mooney, J. App. Phys. **11**, 582 (1940).
[2] D. R. Elliott and S. A. Lippman, Rubber Chem. and Tech. **18**, 579 (1945); *ibid.*, J. App. Phys. **16**, 50 (1945).

and then introduce the deformation variables λ_i by the definition

$$\lambda_i = (L_i/rL_{i0}). \tag{6}$$

It follows directly from these defining equations that

$$\lambda_1\lambda_2\lambda_3 = 1, \tag{7}$$

$$\sum_1^3 (d\lambda_i/\lambda_i) = 0. \tag{8}$$

The deformation variables λ_i, which we shall call the principal deformations, measure exclusively the change in shape of the sample, independent of changes in volume. Thus, Eq. (6) states that λ_i is the ratio of the length in direction i to the length which the sample would have in the same direction if reduced to its original shape while retaining the same volume it has in the deformed state, at whatever temperature and pressure.

ANALYSIS OF STRESS

For later convenience, we shall employ separate notation for the atmospheric or hydrostatic pressure and the mechanical stresses used to deform the sample. In an isotropic material the stress axes will coincide with the strain axes. We denote the principal mechanical stresses by f_i, the hydrostatic pressure by P, and the total stress by σ_i. Then

$$\sigma_i = f_i - P. \tag{9}$$

In terms of F_i, the mechanical force, the mechanical stress, f_i, is

$$f_i = F_i/A_i = \lambda_i Z_i/r^2, \tag{10}$$

where Z_i is the conventional "stress" based on the original section, A_{i0}, or

$$Z_i = F_i/A_{i0}. \tag{11}$$

The mean stress is

$$Q = \tfrac{1}{3}\sum_1^3 \sigma_i = \tfrac{1}{3}\sum_1^3 f_i - P, \tag{12}$$

and the effective deforming stresses are the stress deviations,

$$\delta_i = \sigma_i - Q. \tag{13}$$

From these definitions it follows that

$$\sum_1^3 \delta_i = 0. \tag{14}$$

In the equations to be developed below, we shall use as our independent variables the deformation variables, λ_i, the mean stress, Q, and the absolute temperature, T. The stress deviations, δ_i, are to be thought of as dependent variables, their values being determined by the mechanical reactions of the sample while in the state of deformation λ_i at mean stress Q and temperature T. There is a degree of indeterminacy in the f_i, since each of them can be increased by an arbitrary amount, ϵ, without changing either Q or the δ_i, if at the same time P is also increased by ϵ. This indeterminacy is generally resolved by some arbitrary condition in the experimental procedure, such as, for example, the use of a single deforming force applied in only one direction. With this procedure, P must then be considered as being adjusted in accordance with Eq. (12) so as to give the independent variable Q arbitrarily assigned values. Thus, if a deformation is to be carried out at constant Q, P must be varied so as to compensate continuously and exactly for variations in the mean mechanical stress, $\frac{1}{3}\sum f_i$. Although actual experiments have not been and perhaps need never be carried out in this manner, it is nevertheless necessary to treat such a hypothetical experiment in the mathematical analysis.

VOLUME EQUATION OF STATE

In setting up an equation for the volume of the sample in terms of the independent variables, we wish to allow for the possibility of partial crystallization. For each phase, amorphous and crystalline, we assume a volume equation which is linear in T and Q. Thus, if we indicate the amorphous and crystalline phases by subscripts 1 and 2, respectively,

$$\left.\begin{aligned} V_1 &= V_{10}(1+\beta_1\Delta T+\kappa_1\Delta Q),\\ V_2 &= V_{20}(1+\beta_2\Delta T+\kappa_2\Delta Q),\end{aligned}\right\} \tag{15}$$

where V_{10} and V_{20} are the specific volumes at the reference temperature and mean stress, and β_1, β_2 and κ_1, κ_2 are, respectively, the thermal coefficients of expansion and the moduli of com-

pressibility. The constancy of β_1 and κ_1 at high deformations may be open to question. We shall assume in the present analysis that any effects, so far unobserved, caused by variability of β_1 and κ_1, are negligible in comparison with the effects included in the analysis, all of which have been observed.

If we now represent by m_2 the mass in the crystalline state, the fractional mass is

$$\omega = m_2/m. \tag{16}$$

In accordance with assumptions previously stated, we write

$$\omega = \omega_0 + \Delta\omega + (\partial\omega/\partial T)_{\lambda_i,Q}\Delta T + (\partial\omega/\partial Q)_{\lambda_i,T}\Delta Q, \tag{17}$$

where

$$\left.\begin{aligned} \Delta\omega &= \omega_{\lambda_i 0} - \omega_0, \\ \Delta T &= T - T_0, \\ \Delta Q &= Q - Q_0. \end{aligned}\right\} \tag{18}$$

Here the subscript 0 in ω_0 denotes the reference state, $\lambda_i = 1$, $T = T_0$, $Q = Q_0$; subscript $\lambda_i 0$ denotes a deformation λ_i at $T = T_0$, $Q = Q_0$. We note that the assumption of linearity in T and Q implies that the partial derivatives in Eq. (7) must be constant within the experimental range involved.

The mean specific volume of the sample is

$$V = V_1 + \omega(V_2 - V_1). \tag{19}$$

From Eqs. (15) to (19), it follows that, to the first approximation in the various volume increments,

$$V = V_0(1 + \alpha\Delta\omega + \beta\Delta T + \kappa\Delta Q), \tag{20}$$

in which

$$V_0 = V_{10} + \omega_0(V_{20} - V_{10}), \tag{21}$$

$$\left.\begin{aligned} \alpha V_0 &= V_{20} - V_{10}, \\ \beta V_0 &= \beta_1 V_{10} + \omega_{x0}(\beta_2 V_{20} - \beta_1 V_{10}) + (V_{20} - V_{10})(\partial\omega/\partial T)_{\lambda_i,Q}, \\ \kappa V_0 &= \kappa_1 V_{10} + \omega_{x0}(\kappa_2 V_{20} - \kappa_1 V_{10}) + (V_{20} - V_{10})(\partial\omega/\partial Q)_{\lambda_i,T}. \end{aligned}\right\} \tag{22}$$

It is to be noted that $\Delta\omega$, β, and κ are all functions of the deformation. $\Delta\omega$ is a function also of T and Q. Corresponding to Eq. (20) we have, to the first approximation

$$r = 1 + (\alpha\Delta\omega/3) + (\beta/3)\Delta T + (\kappa/3)\Delta Q. \tag{23}$$

THE DIFFERENTIAL OF WORK

If we denote by dW the work done on unit mass in an infinitesimal change in strain, then

$$m dW = \sum_1^3 (f_i - P) A_i dL_i. \tag{24}$$

Now by applications of Eqs. (3) to (14), this expression for dW can be put into the forms

$$dW = (1/m)\sum_1^3 (\delta_i + Q) A_i dL_i = Q dV + V \sum_1^3 \delta_i (d\lambda_i/\lambda_i). \tag{25}$$

If we now let dD represent the increment in work associated with the stress deviations, we have

$$dD = V \sum_1^3 \delta_i (d\lambda_i/\lambda_i) = V \sum_1^3 f_i (d\lambda_i/\lambda_i) = V_0 \sum_1^3 r Z_i d\lambda_i, \tag{26}$$

the latter forms of this equation being derived again by the application of Eqs. (8) to (14).

The expression for the total work increment now takes the form

$$dW = Q dV + dD. \tag{27}$$

THE THERMODYNAMIC DIFFERENTIAL EQUATIONS

The first and second laws of thermodynamics are expressed by the equation

$$T dS = dU - dW = dU - Q dV - dD, \tag{28}$$

where S and U are, respectively, the entropy and energy per unit mass. We wish to include in our treatment all possible types of deformation. In order to do this conveniently, we let x be a parameter which varies with extent of the deformation; and we suppose that each of the λ's is expressed as a function of x, the three functions being subject to the condition (7). Any possible path of deformation can thus be represented, while we have only a single deformation variable, x, to deal with directly in the following differential equations.

If we divide Eq. (28) successively by the

differentials ∂T, ∂Q, and ∂x, we obtain

$$\left.\begin{aligned}(\partial S/\partial T)&=(1/T)[(\partial U/\partial T)-Q(\partial V/\partial T)],\\(\partial S/\partial Q)&=(1/T)[(\partial U/\partial Q)-Q(\partial V/\partial Q)],\\(\partial S/\partial x)&=(1/T)[(\partial U/\partial x)-Q(\partial V/\partial x)\\&\qquad-(\partial D/\partial x)].\end{aligned}\right\}\quad(29)$$

In these and all subsequent equations it is to be understood, unless otherwise indicated, that a partial differentiation with respect to any of the variables T, Q, or x implies that the other two independent variables are constant in that differentiation. The derivatives $\partial D/\partial T$ and $\partial D/\partial Q$ are omitted in Eqs. (29) because, by Eq. (26), the increment dD has no component in dT or dQ. It is obvious that

$$\partial D/\partial x=\sum_1^3(\partial D/\partial\lambda_i)(d\lambda_i/dx)$$

$$=V_0\sum_1^3 rZ_i(d\lambda_i/dx).\quad(30)$$

Now, by equating $\partial^2S/\partial Q\partial T$ and $\partial^2S/\partial T\partial Q$ derived from Eqs. (29.1) and (29.2), we obtain the equation

$$(\partial U/\partial Q)=Q(\partial V/\partial Q)+T(\partial V/\partial T).\quad(31)$$

INTEGRATION OF THE EQUATIONS

The only dependent variable found in the right member of Eq. (31) is V, for which we have assumed an equation of state. Hence, we substitute Eq. (18) into (31) and obtain

$$\partial U/\partial Q=V_0(\kappa Q+\beta T),\quad(32)$$

which can be integrated to yield

$$U=V_0(\kappa/2)(Q^2-Q_0^2)+V_0\beta T(Q-Q_0)+\theta(T-T_0)+\psi.\quad(33)$$

θ and ψ are arbitrary functions of x. Since we are limiting ourselves to linear functions of T and Q, the arbitrary function of T takes the simple form indicated. Constants and arbitrary functions are chosen so that $U=0$ in the reference state, $Q=Q_0$, $T=T_0$, $x=0$. Obviously, ψ is the energy of deformation at Q_0, T_0.

Now substituting Eqs. (20) and (33) into Eqs. (29.1) and (29.2), we obtain a pair of partial differential equations

$$\partial S/\partial T=(1/T)(\theta-\beta V_0Q_0),\quad\partial S/\partial Q=\beta V_0.\quad(34)$$

Integration leads to

$$S=(\theta-\beta V_0Q_0)\ln(T/T_0)+\beta V_0(Q-Q_0)+\phi,\quad(35)$$

in which ϕ is an arbitrary function of x. Again, the choice of arbitrary constants and the function ϕ is such that $S=0$, in the reference state. Obviously, ϕ is the entropy of deformation at T_0, Q_0. Also, $\theta-\beta V_0Q_0$ is the specific heat at constant x, and $Q=Q_0$, while θ is the specific heat at constant x and $Q=Q_0=0$. In later equations we shall set

$$Q_{\lambda Q}=\theta-\beta V_0Q_0.\quad(36)$$

In order now to obtain D, we can first write (29.3) in the form,

$$\frac{\partial D}{\partial x}=\frac{\partial}{\partial x}(U-TS-QV).\quad(37)$$

We thus see that D is closely related to the Gibbs free energy, $U-TS+PV$; and in fact D is the free energy at constant mean stress, Q, in contrast to the free energy at constant atmospheric pressure, which is the Gibbs free energy.

If we were content to use D only in differential expressions such as Eq. (37), it would be sufficient to set D equal to the parenthesis in this equation. However, following the logic of our method, we can make use of the arbitrary functions of integration to make D vanish at $x=0$. Thus, we set

$$\begin{aligned}D&=U(x,T,Q)-TS(x,T,Q)-QV(x,T,Q)\\&\quad-U(0,T,Q)+TS(0,T,Q)\\&\quad+QV(0,T,Q),\quad(38)\\&=\psi-T\phi-QV_0\alpha\Delta\omega-V_0(\beta-\beta_0)\Delta T\Delta Q\\&\quad-\tfrac{1}{2}V_0(\kappa-\kappa_0)(\Delta Q)^2,\end{aligned}$$

where β_0 and κ_0 are the respective values in the undeformed state $x=0$. Obviously, D is a linear function of T.

It is readily understood that D as defined by this equation is still the free energy at constant T and Q, except for an additive function of T and Q, which yields zero under the operation $(\partial/\partial x)_{T,Q}$. At the same time, D as defined here is the total work done by the deviatory stresses, δ_i, in producing deformation x at constant T and Q.

The last two terms of Eq. (38) vanish if Q is Q_0, the reference mean stress. The term $QV_0\alpha\Delta\omega$

represents the interchange of work between the deviatory stresses and the mean stress as a result of the change in volume $\alpha\Delta\omega$. This term vanishes at $Q=Q_0=0$, and in this case D reduces to $\psi-T\phi$.

The two functions ψ and ϕ are the functions of primary theoretical interest. We have seen here that they are directly related to the temperature-dependent and temperature-independent components of D, except for some small correction terms associated with certain changes in volume.

STRESS EQUATIONS

For the analysis of experimental data on deforming force as a function of temperature, stress equations are required which are derivable from the preceding equations. In reference 1 it was shown that, in our present notation,

$$\sigma_i-\sigma_j=(1/V)[\lambda_i(\partial D/\partial\lambda_i)-\lambda_j(\lambda D/\partial\lambda_j)]. \quad (39)$$

This equation was derived on the assumption of constant volume, but it is still valid in the present application with variable volume, since we have changed the definition of the λ_i so that Eqs. (7) and (8) still hold. To express the stresses in terms more commonly used for elastomer systems, Eq. (39) can be readily transformed into

$$V_0r(\lambda_iZ_i-\lambda_jZ_j)=\lambda_i(\partial D/\partial\lambda_i)-\lambda_j(\partial D/\partial\lambda_j). \quad (40)$$

This is a general equation, applicable to the deformation produced by any combination of stresses. Let us consider the special case most commonly involved in experimental work, that in which the sample is stretched by a tensional force applied in only one direction, i. Then $Z_j=Z_k=0$, and

$$\sigma_j=\sigma_k=-P, \quad \lambda_j=\lambda_k=1/(\lambda_i)^{\frac{1}{2}}. \quad (41)$$

By means of Eq. (41.2), D can be transformed into a function of λ_i only. Then, Eq. (39) becomes

$$\sigma+P=(\lambda/V)(\partial D/\partial\lambda), \quad (42)$$

the subscript i being omitted as being no longer necessary. Likewise, Eq. (40) becomes

$$V_0rZ=\partial D/\partial\lambda. \quad (43)$$

If we now compare Eqs. (37) and (43), we see that rZ must be a linear function of T. On the other hand, experimentalists report that Z is a linear function of T. However, if rZ is strictly linear, the curvature in Z within the temperature range of reported experiments would not be detectable. Hence, the reported linearity of Z is no evidence against our deduction that rZ should be linear; and if we set

$$X=rZ, \quad (44)$$

we can expect experimental data to agree within experimental error with an equation of the form,

$$X=X_0(\lambda)+TX_1(\lambda). \quad (45)$$

From Eq. (38) and later equations it follows that

$$\left.\begin{aligned} -(d\phi/d\lambda)&=V_0(\partial X/\partial T),\\ d\psi/d\lambda&=V_0[X-T(\partial X/\partial T)\\ &\quad+V_0Q\alpha(\partial\omega/\partial\lambda),\end{aligned}\right\} \quad (46)$$

and also

$$V_0X=(d\psi/d\lambda)-T(d\phi/d\lambda)-V_0Q\alpha(\partial\omega/\partial\lambda).^{**} \quad (47)$$

Equation (46) expresses the entropy and energy functions of primary interest in terms of the measurable quantities. However, in applying these equations to stress measurements as usually made, certain corrections are required. Evaluation of the derivative $\partial X/\partial T$ requires the temperature variation of X at constant λ and Q; whereas measurements are actually made with unidirectional stretching force at constant P instead of constant Q; and usually at constant L instead of constant λ.

We seek a correction formula for converting a measurement at $T=T_0+\Delta T$, $\lambda=\lambda_a+\Delta\lambda$, $Q=Q_a+\Delta Q$ to the measurement which would be obtained at $T=T_0+\Delta T$, $\lambda=\lambda_a$, $Q=Q_a$. The subscript a signifies a reference state other than $Q=Q_0$, $\lambda=0$. $\Delta\lambda$ and ΔQ are here the increments caused by the imposed change ΔT under the customary experimental conditions of constant P and L. We begin with the general equation

$$X(\lambda, T, Q)=X(\lambda_a, T, Q_a)+(\partial X/\partial\lambda)_{T,Q}\Delta\lambda+(\partial X/\partial Q)_{\lambda,T}\Delta Q. \quad (48)$$

We have, making use of Eqs. (80.4) and (81.2)

** The constant α and the function ω cannot be independently determined with precision by any method yet developed, but the product $\alpha(\partial\omega/\partial\lambda)$ can be determined in a stretch dilatometer. See, for example, reference (4). Data obtained by this procedure require correction for the volume change due to the increase in mean stress when the sample is stretched.

in Appendix II,

$$\begin{cases} \Delta\lambda = \dfrac{L_a}{L_0}\dfrac{\partial}{\partial T}\left(\dfrac{1}{r}\right)_{L,P}\Delta T \\ \qquad\qquad \doteq -\lambda_a\left[\dfrac{\beta}{3}+\dfrac{\kappa\lambda}{9}\left(\dfrac{\partial X}{\partial T}\right)_{\lambda,P}\right]\Delta T, \quad (49) \\ \Delta Q = \left(\dfrac{\partial Q}{\partial T}\right)_{L,P}\Delta T \doteq \dfrac{\lambda_a}{3}\left(\dfrac{\partial X}{\partial T}\right)_{\lambda,P}\Delta T. \end{cases}$$

To a sufficient approximation in the correction terms,

$$\begin{aligned} (\partial X/\partial\lambda)_{T,Q} &\doteq (\partial X/\partial\lambda)_{T,P}, \\ (\partial X/\partial Q)_{\lambda,T} &\doteq -\alpha(\partial\omega/\partial\lambda). \end{aligned} \quad (50)$$

From (48), (49), and (50),

$$\begin{aligned} X(\lambda_a, T, Q_a) &= X(\lambda, T, Q) \\ &+\Delta T\left\{\left(\frac{\partial X}{\partial\lambda}\right)_{T,P}\left[\frac{\beta\lambda_a}{3}+\frac{\kappa\lambda_a^2}{9}\left(\frac{\partial X}{\partial T}\right)_{\lambda,P}\right]\right. \\ &\left.+\frac{\alpha\lambda_a}{3}\frac{\partial\omega}{\partial\lambda}\left(\frac{\partial X}{\partial T}\right)_{\lambda,P}\right\}. \quad (51) \end{aligned}$$

In experiments of the kind under discussion, the correction terms in α and κ will be small compared to the term in β. As an adequate correction formula we therefore have

$$\begin{aligned} X_a = X(\lambda_a, T, Q_a) &= X(\lambda, T, Q) \\ &+(\beta\lambda_a/3)(\partial X/\partial\lambda)_{T,P}\Delta T. \quad (52) \end{aligned}$$

X_a, substituted for rZ in Eq. (46), now gives correct expressions for $d\phi/d\lambda$ and $d\psi/d\lambda$ in terms of observables. But a word of caution is necessary regarding the derivative $(\partial X/\partial\lambda)_{T,P}$. The $\Delta\lambda$ involved in this case is always quite small, and Wiegand and Snyder[3] have shown that the slope in a small stress-strain cycle is appreciably greater than the local slope of the total stress-strain curve. The same statement would apply to X or rZ, which signifies that $\partial X/\partial\lambda$ for the correction formula (51) should be determined by measurements in a short cycle of deformation.

TEMPERATURE EQUATION

The equation for the Joule heat effect, or temperature change in adiabatic reversible strain, involves a number of small correction terms. The type of strain normally employed in such experiments is that produced by a unidirectional tension imposed in an atmosphere of constant pressure. We limit the following analysis to this case, and we write, for an adiabatic deformation,

$$\begin{aligned} (\partial S/\partial\lambda)_P &\equiv (\partial S/\partial\lambda)_{T,Q}+(\partial S/\partial Q)_{\lambda,T}(\partial Q/\partial\lambda)_{S,P} \\ &+(\partial S/\partial T)_{\lambda,Q}(\partial T/\partial\lambda)_{S,P}=0. \quad (53) \end{aligned}$$

In this equation $(\partial T/\partial\lambda)_{S,P}$ is the measured effect. Approximate expressions for the other partial derivatives are given in Appendix II. Substituted into Eq. (53) they lead to the result

$$\begin{aligned} -\frac{d\phi}{d\lambda} &= V_0\left(\frac{\partial X}{\partial T}\right)_{\lambda,Q} \\ &=\left(\frac{\partial T}{\partial\lambda}\right)_{S,P}\left[\frac{C_{\lambda Q}}{T}+\frac{\beta\lambda V_0}{3}\left(\frac{\partial Z}{\partial T}\right)_{\lambda,P}\right] \\ &\quad+\frac{\beta V_0}{3}\left[Z+\lambda\left(\frac{\partial Z}{\partial\lambda}\right)_{T,P}\right] \\ &=\left(\frac{\partial T}{\partial\lambda}\right)_{S,P}\left[\frac{C_{LP}}{T}-\frac{\beta\lambda V_0}{3}\left(\frac{\partial Z}{\partial T}\right)_{\lambda,P}\right. \\ &\quad\left.-\frac{\kappa\lambda^2 V_0}{9}\left(\frac{\partial Z}{\partial T}\right)^2_{\lambda,P}\right] \\ &\quad+\frac{\beta V_0}{3}\left[Z+\lambda\left(\frac{\partial Z}{\partial\lambda}\right)_{T,P}\right]. \quad (54) \end{aligned}$$

$$\begin{aligned} C_{LP} &= C_{\lambda Q}+T[(2\beta V_0\lambda/3)(\partial Z/\partial T) \\ &+(\kappa\lambda^2 V_0/9)(\partial Z/\partial T)^2]. \quad (55) \end{aligned}$$

The specific heat at constant $Q=Q_0$, represented by θ, arose as an arbitrary function of x in Eq. (37). It is obvious, however, that θ can be expressed in terms of the specific heats of the amorphous and crystalline phases, C_{10} and C_{20}, the latent heat of crystallization, h, the phase composition, ω, and rate of change of ω with T. Thus

$$\theta = C_{10}+\omega(C_{20}-C_{10})-h(\partial\omega/\partial T)_{\lambda,Q}. \quad (56)$$

It is not necessary to assume here that h is independent of λ and Q.

[3] W. B. Wiegand and J. W. Snyder, Trans. Inst. Rubber Ind. 10, 234 (1934).

THE GENERAL FORM OF DEFORMATION FUNCTIONS

The general form of the strain-work function was derived in reference 1 on the assumption of constant volume. The same derivation applies also to the case of variable volume if we let the λ_i be the principal deformations, instead of the principal strains, with the result that Eq. (7) still holds. Consequently, we conclude that ϕ and ψ, which express the variation of D with the deformations λ_i, must each have the general form given by Eq. (47) of reference 1. This form is

$$R(\lambda_i)=\sum_{n=1}^{\infty}\left[\frac{G_{2n}}{4n}\sum_{i=1}^{3}(\lambda_1^{2n}+1/\lambda_i^{2n}-2)+\frac{H_{2n}}{4n}\sum_{i=1}^{3}(\lambda_i^{2n}-1/\lambda_i^{2n})\right], \quad (57)$$

in which G_{2n} and H_{2n} are constants. G_2 will be the temperature dependent or the temperature independent component of the modulus of rigidity for moderate deformations, depending on whether R represents ψ or ϕ. In general, R will contain, in addition to the terms in Eq. (57), a constant term $R_0 \neq 0$. Also, in general, the parameters G_{2n} and H_{2n} will be functions of T and Q.

If the deformation is a simple shear of magnitude, γ, R can be expressed in the form, Eq. (49) of reference 1,

$$R(\gamma)=\sum_{q=1}^{\infty}\frac{\gamma^{2q}}{(2q)!}\sum_{n=q}^{\infty}\frac{G_{2n}}{n}n^2[n^2-1^2]\cdots\times[n^2-(q-1)^2]. \quad (58)$$

The proof that ϕ and ψ, the entropy and energy of deformation, must have the form of (57), is indirect; for the initial assumptions in the proof were related to stress-strain relationships, the connection with entropy and energy being established through necessary relationships between stresses, work of deformation, and entropy and energy of deformation. This question naturally arises: What assumptions or postulates must be made regarding ϕ, ψ, themselves, or any other function of deformation, in order to arrive at the functional forms (57) and (58)?

It is sufficient to make the following postulates concerning the elastomer material and the deformation function considered. Such an elastomer and such a deformation function may, for convenience, be referred to as "normal."

1. The elastomer is isotropic in the unstrained state, and in any state of strain having axial symmetry, remains isotropic in the plane normal to the symmetry axis.
2. In any strain the deformation function considered is an analytic function of the deformation variables, λ_i, over the range of physically attainable λ_i. In any simple shear in an isotropic plane, this function is expressible as an even power series in the shear, γ.
3. The specific volume of the material conforms to postulates 1 and 2.

The proof that these three postulates lead to the deformation functions (57) and (58) is given in Appendix I.

The symmetry required by the postulate 1 means that the power series in γ referred to in postulate 2 must be either even or odd and cannot be mixed. Since for every even function, $R(\gamma)$, there is also an odd function, $dR/d\gamma$, and vice versa, our choice of an even power series in postulate 2 does not reduce the number of functions of deformation covered by our analysis. This choice of an even function corresponds, for example, to a choice of the work, instead of the deforming stress, as the deformation function to which the postulates apply. The analysis in any case applies directly to an even function of γ.

If a deformation is produced by a unidirectional tension or pressure, so that the deformation is characterized by Eq. (41), then Eq. (57) reduces to

$$R(\lambda)=\sum_{n=1}^{\infty}\frac{G_{2n}}{4n}\left[\lambda^{2n}+\frac{1}{\lambda^{2n}}+2\left(\lambda^n+\frac{1}{\lambda^n}\right)-6\right]+\sum_{n=1}^{\infty}\frac{H_{2n}}{4n}\left[\lambda^{2n}-\frac{1}{\lambda^{2n}}-2\left(\lambda^n-\frac{1}{\lambda^n}\right)\right]. \quad (59)$$

If the deformation function is adequately represented, within a limited range of deformation, by the first terms only; i.e., for $n=1$,

Eqs. (57) to (59) then reduce to

$$R(\lambda_i)=\frac{G}{4}\sum_{i=1}^{3}\left(\lambda_i^2+\frac{1}{\lambda_i^2}-2\right)+\frac{H}{4}\sum_{i=1}^{3}\left(\lambda_i^2-\frac{1}{\lambda_i^2}\right), \quad (60)$$

$$R(\gamma)=(G/2)\gamma^2, \quad (61)$$

$$R(\lambda)=\frac{G}{4}\left[\lambda^2+\frac{1}{\lambda^2}+2\left(\lambda+\frac{1}{\lambda}\right)-6\right]+\frac{H}{4}\left[\lambda^2-\frac{1}{\lambda^2}-2\left(\lambda-\frac{1}{\lambda}\right)\right]. \quad (62)$$

It seems appropriate at this point to state, without proof, certain facts concerning the applicability of the operator Eq. (39) or (40), and (42) or (43). It is obvious that the inherent symmetry of Eq. (59) in the λ_i will be formally destroyed if any one of the three λ_i's is eliminated by a substitution $\lambda_i=1/\lambda_j\lambda_k$. It is interesting to find that if now the operations indicated in Eqs. (39) or (40) are applied to the transformed deformation function, the result is still correct. This means, for example, that $\sigma_i-\sigma_j$ as expressed by Eq. (39) is invariant under any transformation of D permitted by Eq. (7).

With regard to the operator Eq. (42) and (43), the situation is somewhat different. If the deformation considered is subject to any condition, $F(\lambda_1, \lambda_2, \lambda_3)=0$, in addition to Eq. (7), then the deformation function can be reduced to a function of only one of the λ_i, such as Eq. (59) or (62). However, the only case in which the single-term operator of Eq. (42) is valid is the particular case represented by condition (41).

Here the condition $\sigma_j=\sigma_k$ is necessary, but not $\sigma_j=0$. If $\sigma_j=\sigma_k\neq 0$, Eq. (42) has the slightly more general form

$$\sigma_i-\sigma_j=(\lambda_i/V)[dD(\lambda_i)/d\lambda_i]. \quad (63)$$

DISCUSSION

Previous thermodynamic analyses of strained elastomers have been developed in terms of the strain variables, L_i/L_{i0} (principal strain $+1$). Our choice of the deformation variables L_i/rL_{i0}, has led naturally and easily to two important consequences; first, that the entropy and energy of strain are separated, respectively, into entropy and energy of deformation, and other terms representing effects of pressure, temperature and dilatation; second, that the entropy and energy of deformation must each have the form of a particular multiparameter function of the principal deformations provided only that the undeformed elastomer is isotropic and normal as defined in this paper.

These consequences, aside from their scientific interest, have a certain practical value in the analysis of data. With foreknowledge of the necessary form of the entropy and energy functions of deformation, the task of fitting curves to experimental data is reduced to the determination of certain parameters to give the best fit.

The conclusion that such a variable as ω, the fractional crystallinity, can be represented by the general deformation function does not imply that the curve of ω *versus* deformation should resemble the curve for the work of deformation. The form of a particular deformation function will vary greatly with the values assigned to the parameters in the function. Also, the form may vary with temperature and mean stress, since the parameters may be functions of T and Q.

The properties of an elastomer which have been defined as normal are to be expected unless there is some peculiarity in the curing procedure which causes anisotropy in the cured material. On the other hand, reversibility in stress-strain cycles, assumed in the analysis, does not exist in reality. The experimentalist must use special techniques in order to attain even approximate reversibility; and it is still an open question whether the techniques employed have been as adequate as they seemed. This point will be discussed further in later communications.

A number of synthetic elastomers are known which, when stretched, give x-ray diffraction patterns indicating ordered states of incomplete regularity, as compared with the crystalline state, having 3-dimensional periodicity. In order to apply the present analysis to such elastomers, it is only necessary to assume a density change and latent heat in the transition from the amorphous to the semi-ordered state.

Equations (46) show that the entropy and energy of deformation are more directly related to X, or rZ, than to Z itself. This is under-

standable if we recognize that, in order to produce a given change in deformation, a given force, A_0Z, must act through a distance which is proportional to r, $r-1$ being the mean linear expansion of the sample.

In articles which are to follow the present theoretical analysis, the equations developed will be applied to experimental data and conclusions will be drawn regarding the thermodynamic properties of various cured elastomers.

APPENDIX I

Proof of General Validity of the Deformation Function

We assume the validity of the preceding postulates 1–3. The principal stretch variables, μ_i, are defined by

$$\mu_i = L_i/L_0 = r\lambda_i. \tag{64}$$

We shall consider a general state of strain as being produced in two steps, a and b. In the first step the strain is such as is produced by a unidirectional stesss in direction 1. Then we have the relations

$$\mu_1\mu_n{}^2 = v_a = r_a{}^3, \quad \mu_1 = r_a\lambda_a, \tag{65}$$

where μ_n is the stretch in the 2–3 plane, and v_a is the relative volume in state a.

By postulate 2, any deformation function, R, will vary continuously with the strain, and for the step a we may write

$$\Delta R_a = \psi(\lambda_a), \tag{66}$$

ψ being an unknown analytic function of λ_a.

Now to complete the general deformation, we impose a shear, γ, in the 2, 3 plane while holding L_1 constant. The shear is related to s_2 and s_3, the principal deformations in the 2–3 plane referred to state a, by the equation

$$\gamma = s_2 - s_3. \tag{67}$$

By definition of a principal deformation, we must have

$$s_2 s_3 = 1. \tag{68}$$

If we denote by μ_2, μ_3 the final 2, 3 stretches, and by v_b the volume expansion in step a to b, we must have

$$\mu_2 = s_2 v_b{}^{\frac{1}{3}}\mu_n, \quad \mu_3 = s_3 v_b{}^{\frac{1}{3}}\mu_n. \tag{69}$$

Hence

$$\begin{aligned} \mu_2\mu_3 &= v_b\mu_n{}^2 = v_a v_b/\mu_1, \\ \mu_1\mu_2\mu_3 &= v_a v_b = r_a{}^3 r_b{}^3 = r^3, \\ \mu_i &= r\lambda_i, \end{aligned} \tag{70}$$

r being the mean linear expansion in state b compared with the undeformed state.

Now by appropriate substitution in Eq. (69), we find

$$\gamma^2 = \lambda_1(\lambda_2 - \lambda_3)^2. \tag{71}$$

The change produced in R by the change in strain from state a to state b is, by postulate 2, expressible as a power series in γ^2. The coefficients in this series will depend upon the extent of the deformation in state a. The total change in R will therefore be of the form

$$\Delta R = \psi(\lambda_a) + \sum_1^\infty \phi_n(\lambda_a)\lambda_1{}^n(\lambda_2 - \lambda_3)^{2n}. \tag{72}$$

We must now eliminate λ_a from this equation. From preceding equations,

$$\lambda_1 = \frac{\mu_1}{r} = \frac{r_a\lambda_b}{r_a r_b} = \frac{\lambda_a}{r_b}. \tag{73}$$

By postulate 3,

$$r_b = 1 + \sum_1^\infty \theta_n(\lambda_a)\gamma^{2n}, \tag{74}$$

where the coefficients θ_n are such that this series is convergent and analytic. We can now express λ_a in the form

$$\lambda_a = \lambda_1\left[1 + \sum_1^\infty \theta_n\gamma^{2n}\right]. \tag{75}$$

Substitution into (72) gives an expression for ΔR which can be written in the form

$$\Delta R = \Psi(\lambda_1) + \sum_1^\infty \Phi(\lambda_1)(\lambda_2 - \lambda_3)^{2n}. \tag{76}$$

We have thus reduced ΔR to the same form as Eq. (34) of reference 1. This condition, together with equation $\lambda_1\lambda_2\lambda_3 = 1$ is all that is mathematically required in the derivation of the general deformation function $R(\lambda_i)$.

APPENDIX II

Approximate Equations for Partial Derivatives

The following expressions for certain selected partial derivatives apply to the strains produced

by a unidirectional stretching force. They are obtained in most cases by means of general formulas of the type

$$(\partial F/\partial u)_c=(\partial F/\partial u)_{v,w}+(\partial F/\partial v)_{w,u}(dv/du)_c+(\partial F/\partial w)_{u,v}(dw/du)_c, \quad (77)$$

where u, v, w represent T, Q, and X or λ_f and the subscript c signifies any experimental condition which fixes the variation of v and w with u. The approximations are carried, as a rule, to the first degree in α, β, and κ and the partial derivatives $(\partial\omega/\partial T)_{\lambda,Q}$ and $(\partial\omega/\partial Q)_{\lambda,T}$. Even the first-degree terms are omitted in the expressions for the derivatives of Q, Eqs. (79), since these expressions, in application, are combined with κ. It is frequently helpful to remember that, to the first approximation, it makes no difference in the following derivatives whether c signifies constant L or constant λ. Also, since approximately $X\cong Z$, X and Z may be interchanged at will in any term having α, β, or k as a factor.

$$r=1+\tfrac{1}{3}(\alpha\Delta\omega+\beta\Delta T+\kappa\Delta Q), \quad (23)$$

$$=1+\tfrac{1}{3}[\alpha\Delta\omega+\beta\Delta T+(k\lambda Z/3)]. \quad (53)$$

$$\left.\begin{aligned}&(\partial r/\partial\lambda)_{T,Q}=(\alpha/3)(\partial\omega/\partial\lambda)_{T,Q},\\&(\partial r/\partial\lambda)_{T,P}=(\alpha/3)(\partial\omega/\partial\lambda)_{T,Q}+(\kappa/9)[Z+\lambda(\partial Z/\partial\lambda)_{T,P}],\\&(\partial r/\partial T)_{\lambda,Q}=\beta/3,\\&(\partial r/\partial T)_{\lambda,P}=(\beta/3)+(\kappa\lambda/9)(\partial Z/\partial T)_{\lambda,P},\\&(\partial r/\partial Q)_{\lambda,T}=\kappa/3.\end{aligned}\right\} \quad (78)$$

$$Q=(\lambda Z/3r^2)-P. \quad (12)$$

$$\left.\begin{aligned}&(\partial Q/\partial\lambda)_{T,P}=\tfrac{1}{3}[Z+\lambda(\partial Z/\partial\lambda)_{T,P}]+\cdots\\&(\partial Q/\partial T)_{L,P}=(\lambda/3)(\partial Z/\partial T)_{\lambda,P}+\cdots,\\&(\partial Q/\partial\lambda)_{S,P}=\tfrac{1}{3}[Z+\lambda(\partial Z/\partial\lambda)_{T,P}]+(\lambda/3)(\partial Z/\partial T)_{\lambda,P}(\partial T/\partial\lambda)_{S,P}+\cdots.\end{aligned}\right\} \quad (79)$$

$$\lambda=L/rL_0=(L/L_0)[1-\tfrac{1}{3}(\alpha\Delta\omega+\beta\Delta T+\kappa\Delta Q)]$$

$$=L/L_0[1-\tfrac{1}{3}(\alpha\Delta\omega+\beta\Delta T+(\kappa\lambda Z/3))], \quad (6)$$

(for $\Delta P=0$).

$$\left.\begin{aligned}&(\partial\lambda/\partial T)_{L,Q}=-\beta\lambda/3,\\&(\partial\lambda/\partial T)_{L,P}=-(\beta\lambda/3)-(\kappa\lambda^2/9)(\partial Z/\partial T)_{\lambda,P}.\end{aligned}\right\} \quad (80)$$

$$X=rZ, \quad (44)$$

$$\left.\begin{aligned}&(\partial X/\partial Q)_{\lambda,T}=-\alpha(\partial\omega/\partial\lambda)_{T,Q},\ \text{(by Eq. (47)).}\\&(\partial X/\partial\lambda)_{T,Q}=r(\partial Z/\partial\lambda)_{T,Q}+(\alpha Z/3)(\partial\omega/\partial\lambda)_{T,Q},\\&(\partial X/\partial\lambda)_{T,P}=r(\partial Z/\partial\lambda)_{T,P}+(\kappa/9)[Z^2+\lambda Z(\partial Z/\partial\lambda)_{T,P}]+(\alpha Z/3)(\partial\omega/\partial\lambda)_{T,P},\\&\quad=r(\partial Z/\partial\lambda)_{T,Q}-(\alpha\lambda/3)\times(\partial\omega/\partial\lambda)_{T,Q}(\partial Z/\partial\lambda)_{T,P},\\&\qquad\text{(by Eq. (81.1))}\\&(\partial X/\partial T)_{\lambda,Q}=r(\partial Z/\partial T)_{\lambda,Q}+\beta Z/3,\\&(\partial X/\partial T)_{\lambda,P}=r(\partial Z/\partial T)_{\lambda,P}+(\beta Z/3)+(\kappa\lambda Z/9)(\partial Z/\partial T)_{\lambda,P},\\&\quad=r(\partial Z/\partial T)_{\lambda,Q}+\beta Z/3-(\alpha\lambda/3)(\partial\omega/\partial\lambda)_{T,Q}(\partial Z/\partial T)_{\lambda,P}.\end{aligned}\right\} \quad (81)$$

$$\left.\begin{aligned}&(\partial Z/\partial Q)_{\lambda,T}=-\kappa Z/3-\alpha(\partial\omega/\partial\lambda)_{T,Q},^*\\&(\partial Z/\partial\lambda)_{T,P}=(\partial Z/\partial\lambda)_{T,Q}-[(\kappa Z/3)-\alpha(\partial\omega/\partial\lambda)_{T,Q}][Z+\lambda(\partial Z/\partial\lambda)_{T,Q}]\\&(\partial Z/\partial T)_{L,P}=(\partial Z/\partial T)_{\lambda,Q}[1-(\kappa\lambda Z/9)-(\alpha\lambda/3)(\partial\omega/\partial\lambda)_{T,Q}]-(\partial Z/\partial\lambda)_{T,P}[(\beta\lambda/3)+(\kappa\lambda^2/9)(\partial Z/\partial T)_{\lambda,P}],\\&(\partial Z/\partial T)_{\lambda,P}=(\partial Z/\partial T)_{\lambda,Q}[1-(\kappa\lambda Z/9)-(\alpha\lambda/3)(\partial\omega/\partial\lambda)_{T,Q}].\end{aligned}\right\} \quad (82)$$

$$S=C_{\lambda Q}\ln(T/T_0)+\beta V_0(Q-Q_0)-\phi, \quad (35)$$

$$C_{\lambda Q}=\theta-\beta V_0Q_0, \quad (36)$$

$$\left.\begin{aligned}&(\partial S/\partial\lambda)_{T,Q}=d\phi/\partial\lambda=-V_0(\partial X/\partial T)_{\lambda,Q},\\&(\partial S/\partial Q)_{T,\lambda}=\beta V_0,\\&(\partial S/\partial T)_{\lambda,Q}=\theta-\beta V_0Q_0/T=C_{\lambda Q}/T.\end{aligned}\right\} \quad (83)$$

* Obtained by substituting $X=rZ$ in (83.1).

The Thermodynamics of a Strained Elastomer. II. Compressibility

L. E. COPELAND*
General Laboratories, United States Rubber Company, Passaic, New Jersey
(Received February 18, 1948)

Adiabatic compressibility coefficients were measured on a series of cured polymers of commercial types under pressures up to 5000 lb./in.^{2}. In most cases, the second order as well as the first order coefficient could be determined from the data. The linear isothermal compressibility also was calculated from the measured linear adiabatic coefficient.

Preliminary measurements of the thermal expansion of a stretched Hevea gum stock show that there is a slight decrease in expansion at the 200 percent elongation, presumably due to partial crystallization.

INTRODUCTION

IN the first paper of this series,[1] a number of equations were developed which included the coefficients of compressibility and thermal expansion as parameters. In order to apply such equations in the analysis of experimental data on thermoelasticity, it is obviously necessary to know the values of these parameters for the different polymers and for different states of deformation. The present paper deals primarily with the compressibilities of a group of polymers at zero deformation. Certain incidental associated data also are presented, including the effect of elongation up to 200 percent on the thermal expansion of a Hevea gum stock.

APPARATUS AND METHOD

The apparatus for measuring the compressibility consists of a water-jacketed chamber, A, $\frac{9}{16}''$ inside diameter, 15 inches in length, and made of Shelby steel tubing. The bottom of the chamber is connected through a valve, B, to a high pressure oil pump, C, while the top of the chamber is connected through a second valve, D, to a burette, E. A pressure gauge, F, is placed in the line connecting the chamber to the pump (Fig. 1).

The elastomer sample, S, used for the determination of compressibility was cured in the form of a round rod $\frac{1}{2}''$ in diameter and about 14" long. It was placed in the chamber and oil pumped through the chamber and overflow pipe, G, until the air was swept out of the system so far as possible. The oil was a standard hydraulic fluid which had no measurable effect on the rubber during the time of the experiment. Removal of air was facilitated by wetting the sample with oil before placing it in the apparatus. It was also found that closing the upper valve, D, pumping oil into the system until the pressure was between 5000 and 10,000 lb./in.^{2}, and then suddenly releasing the pressure by opening the upper valve, aided in removing the air. When it was evident that no more air could be removed, the oil level was adjusted to the zero mark on the burette with the upper valves, D and G, closed. The pressure was then raised to a predetermined value, the lower valve closed and the upper valve, D, opened. In this manner pressure was applied to the sample and released in a comparatively short time, less than 20 seconds. The increase in volume of the oil and rubber in returning to atmospheric pressure was read in the burette after closing the valve, D. The measurement was repeated three times at each pressure. The pressure was increased in steps of 500 lb./in.^{2} up to 5000 lb./in.^{2}

A thermometer, H, was kept in the water jacket, but no change in temperature was observed during the course of any experiment. Since the change in pressure from atmospheric to P and back to atmospheric was so rapid, the compressibility observed was the adiabatic compressibility.

It is obvious that the observed increase in volume will be due in part to the compressibility of (1) the oil, (2) any air bubbles present in the system, and (3) the rubber. Consecutive tests on

* Present address: Portland Cement Association, Chicago, Illinois.

[1] M. Mooney, "The thermodynamics of a strained elastomer I. General Analysis," J. App. Phys. 19, 434 (1948).

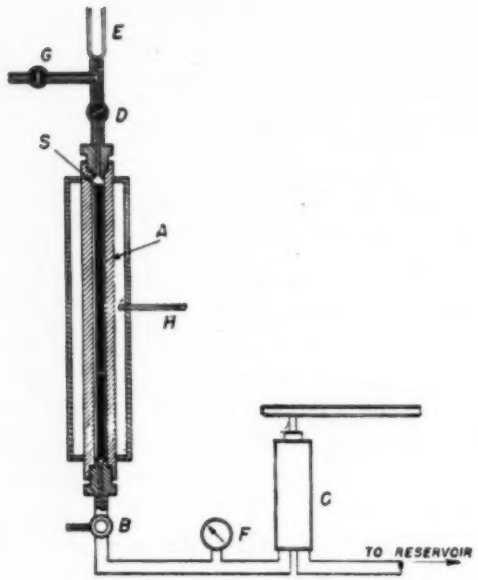

FIG. 1.

the same sample showed that the swelling by the oil was too small to influence the results. The compressibility of the oil may be obtained by comparing the volume changes obtained with oil alone in the chamber to those obtained with a steel rod as the sample. The compressibility of the steel is so small it may be considered zero.

METHOD OF ANALYSIS

The apparatus was not designed to obtain a high degree of accuracy, but when the data for rubber were plotted, the curvature appeared to be significant. Consequently, a method of analysis of the data was used which would take advantage of the unexpected precision.

Assume a volume of residual air in the system equal to A_0 in the case of oil, A_s when the steel rod is in the system, and A_r with the rubber sample. We assume that the air behaves as a perfect gas compressed isothermally; and we express the pressure in lb./in.^{2} Then, with oil in the chamber at pressure P

$$A_0\frac{14.7}{P+14.7}+\left(V_c-A_0\frac{14.7}{P+14.7}\right)=V_c. \quad (1)$$

After releasing the pressure

$$A_0+\left(V_c-A_0\frac{14.7}{P+14.7}\right)(1+A_0P+b_0P^2) = V_c+M_0, \quad (2)$$

where c' = volume of chamber (cc), P = pressure, lb./in.^{2} above atmospheric, M_0 = observed increase in volume of oil in the burette, and a_0 and b_0 = compressibility coefficients of the oil defined by

$$V=V_0[(1-a_0P-b_0P^2)]. \quad (3)$$

These two equations give

$$A_0\frac{P}{14.7+P}+\left(V_c-A_0\frac{14.7}{P+14.7}\right) \times(a_0P+b_0P^2)=M_s. \quad (4)$$

Similarly, with the steel rod,

$$A_s\frac{P}{P+14.7}+\left(V_c-V_s-A_s\frac{14.7}{P+14.7}\right) \times(a_0P+b_0P^2)=M_s, \quad (5)$$

where V_s = volume of steel rod, and M_s = observed volume increase with steel rod in the chamber. Solution of these last two equations gives

$$(A_0-A_s)+[V_s(P+14.7)-(A_0-A_s)14.7] \times[a_0+b_0P]=(M_0-M_s)\left(\frac{P+14.7}{P}\right) \quad (6)$$

or

$$y=a+bP+cP^2, \quad (7)$$

where

$$\begin{aligned} y&=M_0-M_s[P+14.7/P],\\ a&=(A_0-A_s)(1-14.7a_0)+14.7V_sa_0,\\ b&=V_sa_0+14.7b_0[V_s-(A_0-A_s)],\\ c&=V_sb_0, \end{aligned} \quad (8)$$

from which

$$\begin{aligned} b_0&=c/V_s,\\ a_0&=b/V_s, \end{aligned} \quad (9)$$

since the second term in the equation for b may be neglected.

As P was varied in equal steps, the second-degree equation in P was easily fitted to the data by using orthogonal polynomials.[1a]

The same method of analysis for the system

[1a] R. L. Anderson and E. E. Houseman, "Tables of orthogonal polynomials extended to $N=104$," Research Bull. No. 297, April, 1942, Agr. Exp. Sta., Iowa State College of Agr. and Mechanical Arts.

TABLE I. Adiabatic compressibility coefficients. $V = V_0(1 - a_r P - b_r P^2)$, P = pressure in lb./in.^{2}.

Stock	$a_r \times 10^6$	$-b_r \times 10^{12}$
I Hevea 100, S-8	3.51	0.8
II Hevea gum	3.28	—
III Hevea carbon black	2.83	0.3
III Hevea in above*	3.38	0.4
IV GR-S gum	3.36	0.8
V GR-S carbon black	2.67	0.2
V GR-S in above*	3.52	0.2
VII GR-I carbon black	2.79	0.15
VII GR-I in above*	3.38	0.2
VIII Hycar OR 15 gum	2.44	—
IX Perbunan gum	2.51	—

* Calculated from data for carbon black stock by correcting for compressibility of carbon black, assuming that the compressibility of carbon black was equal to that of graphite (3×10^{-6} atm.$^{-1}$, I.C.T.).

containing rubber leads to

$$A_r \frac{P}{14.7+P} + \left(V_c - V_r[1 - a_r P - b_r P^2] - A_r \frac{14.7}{P+14.7} \right)(a_0 P + b_0 P^2) = M_r. \quad (10)$$

Solution of (6) and (10) gives an equation of the form

$$y = k + BP + CP^2 + DP^3 + EP^4, \quad (11)$$

where

$$\begin{aligned} y &= (M_r - M_s)[(P+14.7)/P], \\ k &= 14.7\,V_r a_r + (A_r - A_s)(1 - 14.7 a_0) \\ &\quad + 14.7 a_0 (V_s - V_r) \approx A_r - A_s, \\ B &= V_r a_r (1 + 14.7 a_0) + 14.7\,V_r b_r + a_0 (V_s - V_r) \\ &\quad + 14.7[V_s - V_r - (A_r - A_s)]b_0 \\ &\quad \approx V_r a_r + a_0 (V_s - V_r), \\ C &= V_r (b_r - b_0 + a_r a_0 + 14.7 a_r b_0 + 14.7 b_r a_0) \\ &\quad + V_s b_0 \approx V_r (b_r + a_r a_0) + b_0 (V_s - V_r), \\ D &= V_r (b_r a_0 + b_0 a_r + 14.7 b_r b_0) \approx V_r (b_r a_0 + b_0 a_r), \\ E &= V_r b_r b_0. \end{aligned} \quad (12)$$

From the experimental data on a GR-S stock the compressibility coefficients, a_r and b_r, were calculated by neglecting the third- and fourth-degree terms in Eq. (11). From these coefficients the values of D and E and the resulting error in a_r and b_r were estimated. The error was much too small to be significant; consequently no terms in Eq. (11) higher than the quadratic term need be considered.

We define the adiabatic compressibility coefficient by the equation

$$\beta_S = -(1/V)(\partial V/\partial P)_S.$$

TABLE II. Composition of compounds.

	I	II	III	IV	V	VI	VII	VIII	IX
Pale Crepe	100	100	100						
GR-S				102	102				
GR-I						101.5	101.5		
Hycar OR-15								100	
Perbunan									100
Channel Black			47		46		46		
Zinc Oxide		5	8	5	5	5	5	5	5
Stearic Acid		2	5	1.5	1.5	3	3	1	1.5
BLE		1	1						
AgeRite Powder								1	
Captax		1	1	1.5	1.5				
Altax								1	1
XKA						1	1		
Sulfur	8	2.5	2.5	1.5	1.5	0.5	1.5	1	1.2
Cure: Minutes	180	43	37	37	55	37	55	37	20
Temperature, °C	147	134	142	148	148	148	148	148	148

The adiabatic volume of rubber is adequately represented by an equation of the form

$$V = V_0[1 - a_r P - b_r P^2],$$

from which

$$\beta_S = a_r + 2 b_r P.$$

EXPERIMENTAL RESULTS

Values of a_r and b_r for all the stocks investigated are given in Table I. Composition of these stocks is given in Table II. The error in a_r is about 3 percent, based upon the standard deviation of the regression coefficient. However, since according to this estimate of error the compressibility of the rubber in a carbon black compound is not significantly different from the compressibility of the gum compound (Table I), this should be a valid estimate. The error in b_r ranges from about 3 percent up, depending upon the material. It was impossible to obtain some of the stocks in the form of rods free from air bubbles; e.g., gum stocks of Neoprene, Thiokol, and GR-I. The values of a_r for GR-I were calculated from the value obtained on a carbon black stock, after correcting for the amount of carbon black present.

Isothermal compressibilities were calculated from the adiabatic compressibilities by the equation[2]

$$\beta_T = \beta_S + (T\alpha^2/C_p d),$$

where β_T = isothermal compressibility, β_S = adiabatic compressibility, T = temperature, α = volume coefficient of thermal expansion, C_p = heat

[2] G. N. Lewis and M. Randall, *Thermodynamics* (McGraw-Hill Book Company, Inc., New York, 1923), p. 164.

TABLE III. Some thermodynamic properties of elastomers. C_p = heat capacity, international joules per gram. α = volume thermal expansion (degree^{-1}) from measurements made in this laboratory by Dr. C. F. Eckert, Mr. W. R. Carlson, and Dr. E. M. Grabbe. β_S = adiabatic compressibility, dynes^{-1} cm.^{2} β_T = isothermal compressibility, dynes^{-1} cm^2.

Compounds[a]	C_p	$\alpha\times10^3$	$\beta_S\times10^{12}$	$\beta_T\times10^{12}$	Density
I Hevea, 8 S			51	59	0.997
II Hevea gum	1.890[a]	68	48	55	0.98
IV GR-S gum	1.905[b]	64	49	55	1.00
VII GR-I	1.962[c]	51	49	53	1.00
VIII Hycar OR 15 gum	1.970[d]	59	35	39	1.04
IX Perbunan	1.97[e]	59[e]	36	40	1.02

[a] N. Bekkedahl and H. Matheson, J. Research Nat. Bur. of Stand. **15** 503 (1935).
[b] R. D. Rands, Jr., W. J. Ferguson, and J. L. Prather, J. Research Nat. Bur. of Stand. **33**, 63 (1944).
[c] Value for polyisobutylene. See J. D. Ferry and G. S. Parks, J. Chem. Phys. **4**, 70 (1936).
[d] N. Bekkedahl and R. B. Scott, J. Research Nat. Bur. of Stand. **29**, 87 (1942).
[e] Assumed value.

TABLE IV. Internal pressure of elastomers. (Cal. cm^{-3}) at 298°K. Column 1 lists values calculated from compressibilities, determined in this work, and coefficients of expansion. Column 2 is calculated from published values of compressibility and coefficient of thermal expansion. 3 contains Scott, Burns, and Magat's values obtained from swelling (private communication). 4 lists Gee's values obtained from swelling.[a]

Compound	P_i 1	2	3	4
Hevea, 8 S	83			
Hevea gum	88	85	70.0	63.7
GR-S gum	83		73.1	65.5[b]
GR-I	68			
Hycar OR 15 gum	108			
Perbunan	105			
Neoprene GN			84.6	67.0
Buna N			88.4	88.0
Polybutadiene			70.6	

[a] G. Gee, I.R.I. Trans. **18**, 266 (1943).
[b] Value given for Buna S.

capacity, and d = density. The values of the compressibilities and other properties necessary for the calculations are given in Table III.

The internal pressure of the elastomer may be calculated from the compressibility and coefficient of expansion, by the equation[3]

$$P_i = T(\alpha/\beta_T).$$

Values of P_i for these stocks as well as values obtained for similar stocks by other workers are given in Table IV. P_i calculated from the thermodynamic properties is higher than P_i estimated from swelling experiments, although the comparative values between different polymers are roughly the same. The error in the isothermal compressibility and thermal expansion measurements is about 5 percent, making the error in P_i approximately 7 percent. The calculation of the numerical value of P_i from the coefficients of compressibility and thermal expansion requires the assumption that the change of internal energy of a system resulting from a change in volume at constant temperature is equal to the work done in overcoming the internal pressure. This assumption would appear to be valid for cases in which no transition between thermodynamic states of the system is involved. The assumptions underlying calculation of P_i from swelling data are more complex. It is assumed that maximum swelling is obtained in solvents with the same cohesive energy density (the cohesive energy density is equal to P_i). The cohesive energy densities of the solvents are obtained from their heats of vaporization. The assumptions involved here are such as to make P_i low.[4] For this reason, it would be expected that the values of P_i calculated from thermal expansion and compressibility measurements would be more reliable.

The internal pressures of rubber and GR-S are the same. GR-I has an internal pressure below that of rubber, while the internal pressures of Hycar OR and Perbunan are higher than that of rubber.

Effect of Elongation on Thermal Expansion

In precise analysis of thermoelastic data of stretched elastomers, it is necessary to know how the thermal expansion and volume compressibility vary with elongation. A preliminary experiment was performed to determine the coefficient of thermal expansion of moderately stretched rubber. Samples of Hevea gum (II) were stretched to 100 percent and 200 percent elongation and tightly wrapped with Cellophane which was cemented in place. A turn of wire at each end of the wrapping kept it from splitting when the tension on the rubber was released.

The coefficient of thermal expansion, α, on these samples was determined in a dilatometer employing mercury or alcohol as the immersion

[3] S. Glasstone, *Textbook of Physical Chemistry* (D. Van Nostrand Company, Inc., 1940), p. 472.

[4] J. H. Hildebrand, *Solubility of Non-Electrolytes* (Reinhold Publishing Corporation, New York, 1936), p. 73.

TABLE V. Thermal expansion of elongated rubber.

Percent Elongation	α
0	68×10^{-5}/°C
100	67.5×10^{-5}
200	62.6×10^{-5}

liquid (Table V). The temperature range was −80 to 12°C.

At 100 percent elongation α is the same within experimental error as it is at 0 percent. At 200 percent elongation there appears to be a significant decrease in α. This may be explained as due to partial crystallization of the sample. The appearance of a crystalline phase will have two effects upon the coefficient of expansion of rubber. The first effect will be to decrease the coefficient of thermal expansion, since α for the crystalline phase is less than a third that of the liquid phase. The second effect is to raise the coefficient of expansion, since in raising the temperature part of the crystals will melt and there will be an increase in volume due to the change in volume of rubber upon melting. At room temperature and those elongations where only a small amount of crystallization is produced, it may be that the first effect will predominate.

These preliminary results suggest that at elongations not greater than 200 percent, thermal expansion of elastomers is not much affected by elongation, but that larger effects may be expected at higher elongations if the polymer crystallizes. It seems reasonable to assume that similar remarks would apply to the compressibility.

ACKNOWLEDGMENTS

The author wishes to express his thanks to Dr. M. Mooney for many helpful discussions during this work and to Mr. W. R. Carlson for technical assistance in measuring the coefficients of thermal expansion.

Calendar of Meetings

May

27–29 Canadian Association of Physicists (Third Annual Council), Ottawa, Canada

May 30–June 2 American Society of Refrigerating Engineers, Swampscott, Massachusetts

May 30–June 4 American Society of Mechanical Engineers (Semi-Annual Meeting), Milwaukee, Wisconsin

June

6–11 Society of Automotive Engineers (Summer Meeting), French Lick, Indiana

14–18 American Association of Physics Teachers and American Society for Engineering Education, Austin, Texas

14–19 Symposium on Molecular Structure and Spectroscopy, Columbus, Ohio

17 American Mathematical Society, University of British Columbia, Vancouver, British Columbia

21–23 American Physical Society, Madison, Wisconsin

21–25 American Institute of Electrical Engineers (Summer General Meeting), Mexico City, Mexico

21–25 American Society for Testing Materials (Annual Meeting), Detroit, Michigan

21–September 3 Gordon Research Conferences (formerly Gibson Island Research Conferences), American Association for the Advancement of Science, New London, New Hampshire

23–25 National Colloid Symposium, Cambridge, Massachusetts

24–26 American Physical Society, Pasadena, California

28–July 1 American Astronomical Society, Pasadena, California

28–July 16 Northwest Conference on Nuclear Science, Reed College, Portland, Oregon

July

8–11 General Assembly, International Union of Pure and Applied Physics, Amsterdam, Holland

12–18 Conference on the Physics of Metals, under auspices of Netherlands Physical Society and Netherlands Committee of the International Union of Pure and Applied Physics, Amsterdam, Holland

12–18 International Commission of Optics, Schveningen (The Hague), Netherlands

21–23 American Society of Civil Engineers, Seattle, Washington

29–31 Second Symposium on Applied Mathematics, American Mathematical Society with the cosponsorship of the American Institute of Physics, Cambridge, Massachusetts

28–August 3 International Union of Crystallography, Cambridge, Massachusetts

29–31 Second Symposium on Applied Mathematics, American Mathematical Society with the cosponsorship of the American Institute of Physics, Cambridge, Massachusetts

August

2– 6 Instrumentation Conferences (Gordon Research Conferences) New London, New Hampshire

10 International Astronomical Union, Zurich, Switzerland

18–20 Society of Automotive Engineers (West Coast Meeting), San Francisco, California

19–28 International Union of Geophysics, Oslo, Norway

24–27 American Institute of Electrical Engineers (Pacific General Meeting), Spokane, Washington

24–September 1 18th International Geological Congress, London, England

30–September 4 American Chemical Society (Eastern Session), Washington, D. C.

The Thermodynamics of a Strained Elastomer. III. The Thermal Coefficient of Modulus and the Statistical Theory of Elasticity*

L. E. COPELAND** AND M. MOONEY
General Laboratories, United States Rubber Company, Passaic, New Jersey
(Received February 18, 1948)

Published thermoelasticity data are critically analyzed by means of thermodynamic equations developed in the first paper of this series. Equations known to be of the proper form are fitted by least squares to the experimental data, which were first corrected to allow for the changes in shape when tested under variable temperature and constant length. If the measurements are accepted as truly reversible, the data show that several different elastomers depart considerably in some respects from the predictions of the statistical theory of elasticity.

Some thermoelasticity measurements in torsion are reported which seem to give the most reliable evidence that stress is proportional to absolute temperature.

INTRODUCTION

IN the derivation of the equation of state of an elastomer by statistical mechanical methods, the assumption is made that the only effect of stretching a sample is to alter the possible number of configurations of the cross-linked network of flexible chain molecules. Then it follows that the resulting decrease in entropy is the only source of the observed retractive force and the force is proportional to absolute temperature. To a first approximation the theoretical equations obtained agree with experimental data, both as to form of the stress-strain curve and as to the dependence of modulus on temperature.

However, significant departures from the theory occur. In the present paper the available thermoelastic data[1] have been analyzed statistically in an attempt to determine, as precisely as the data permit, what are the relative contributions of the two factors, entropy and energy, in developing the retractive force. Also, the variation of the entropy component of force with elongation is critically examined.

In carrying out this analysis use is made of a stress-strain equation previously published by one of us.[2]

THE STRESS-STRAIN EQUATION

The equation referred to has the form

$$F=\frac{G}{2}(\lambda+1)\left(1-\frac{1}{\lambda^3}\right)+\frac{H}{2}(\lambda-1)\left(1-\frac{1}{\lambda^3}\right), \quad (1)$$

where F is the retractive force per unit initial area of a stretched elastomer, λ is the stretch, or $1+e$ (e being the elongation), and G and H are the two moduli of superelasticity. This equation was derived from phenomenological considerations, on the assumptions:

(a) the rubber is isotropic and remains so in a plane normal to the stretch,
(b) the deformation occurs at constant volume, and
(c) the traction in simple shear in any isotropic plane is proportional to the shear.

It has been found that this equation fits experimental elongation stress-strain data fairly well up to the point of inflection.[2,3]

Since all thermo-stress experiments have shown that the stress is a linear function of the temperature, it follows that the moduli G and H must be linear functions of temperature. Equation (1) can therefore be expressed in the more complete form

$$F=a+bT=\tfrac{1}{2}G_0P(\lambda)+\tfrac{1}{2}H_0Q(\lambda)+\tfrac{1}{2}G_1TP(\lambda)+\tfrac{1}{2}H_1TQ(\lambda), \quad (2)$$

where

$$P=(\lambda+1)(1-1/\lambda^3) \quad \text{and} \quad Q=(\lambda-1)(1-1/\lambda^3).$$

* Presented at the Fifth Meeting of the Division of High-Polymer Physics, American Physical Society, Chicago, Illinois, December 29–30, 1947.

** Present Address: Portland Cement Association, Chicago, Illinois.

[1] While this work was in progress some additional thermoelasticity results were published by G. Gee, Trans. Faraday Soc. **42**, 585 (1946), but the data are not given in sufficient detail for critical analysis by the method employed in the present paper.

[2] M. Mooney, J. App. Phys. **11**, 582 (1940).

[3] L. R. G. Treloar, Nature **159**, 231 (1947).

Obviously, the stress intercept, a, and the slope, b, of a stress temperature curve can be expressed by the equations

$$\begin{cases} a=(G_0/2)P(\lambda)+(H_0/2)Q(\lambda), \\ b=(G_1/2)P(\lambda)+(H_1/2)Q(\lambda). \end{cases} \quad (3)$$

Calculations involved in fitting experimental data to the equation can be further simplified by rewriting Eqs. (3) in the form

$$\begin{cases} a\lambda^3/(\lambda^3-1)=(G_0/2)(\lambda+1) \\ \qquad\qquad +(H_0/2)(\lambda-1)=A+B\lambda, \\ b\lambda^3/(\lambda^3-1)=(G_1/2)(\lambda+1) \\ \qquad\qquad +(H_1/2)(\lambda-1)=C+D\lambda. \end{cases} \quad (4)$$

A large part of the published data was obtained by observing the stress as a function of the temperature while holding the sample at a constant length. An experiment conducted in this manner does not give directly or exactly the stress at constant deformation. If λ is to measure pure deformation; i.e., change in shape, it must be defined as $\lambda=L/L_u$, where L is length and L_u is undeformed length at the same volume. Since L_u increases with temperature, L must also be increased with temperature if λ is to be kept constant.

This matter has been analyzed in the first paper[4] of the present series, where it is shown that general superelastic functions, of which Eq. (1) is an example, are still valid when assumption (b) above is only approximately valid. As part of this analysis, an equation was derived for calculating stress at constant λ from observed stress at constant L. In our present notation and with sufficient approximation, this equation is

$$F(\lambda,T)=F(L,T)-(\beta/3)(T-T_0)L(\partial F/\partial L). \quad (5)$$

We have ignored here the volume changes resulting from changes in mean pressure acting on the bulk compressibility, but calculations show that in the experiments to be analyzed such volume changes are quite negligible.

A check on the equivalence of the two experimental procedures (i.e., observing the stress as a function of the temperature at constant elongation or, in the second method, at constant length) is provided by the data on GR-S obtained by Roth and Wood.[5]

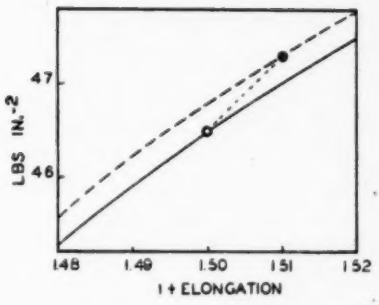

FIG. 1. The solid curve is a portion of the stress-strain curve obtained from data observed at constant elongations; the dashed curve was obtained from observations at constant length by correcting for the temperature change.

The results obtained by the two methods are illustrated in Fig. 1, where a portion of the stress-strain curves at 0° is plotted in the neighborhood of $\lambda=1.5$. The solid curve is a stress-strain curve obtained by plotting the stress temperature data at a constant elongation. The dashed curve is the stress-strain curve obtained from the data observed at constant length, after correcting, by Eq. (5), for the effect of the change in temperature upon the elongation. It is seen that the stress corrected to constant elongation lies above the stress observed at constant elongation.

One explanation for the discrepancy described here may be that the temperature cycle involved in the experiment where the length of the sample

TABLE I. Values of coefficients in Eq. (2). Units of values in parenthesis are lbs./in.² for G_0 and H_0, lbs./in². degree^{-1} for G_1 and H_1. All other values are in g/cm^{-2} and g/cm^{-2} degree^{-1}.

Compound	$\frac{1}{4}G_0$	$\frac{1}{4}G_1$	$\frac{1}{4}H_0$	$\frac{1}{4}H_1$
1. Hevea-commercial gum[a]	1030	4.5	−1860	6.2
2. Hevea 100-S8[b]	900	5.0	−2640	6.6
3. Hevea gum[c]	385	7.4	−1180	5.2
	(5.5)	(0.10)	(−16.8)	(0.074)
4. GR-S gum[d]	−343	8.0	−245	1.9
	(−4.9)	(0.11)	(−3.5)	(0.027)
5. Hycar[e]	150	4.8	−9510	24.
6. Neoprene[f]	2390	0.7	−8470	39.

[a] See reference 12.
[b] Unpublished data from Professor Guth.
[c] Anthony, Gaston, and Guth, J. Phys. Chem. **46**, 826 (1942).
[d] L. A. Wood and F. L. Roth, J. App. Phys. **15**, 781 (1944).
[e] L. E. Peterson, R. L. Anthony, and E. Guth, Ind. Eng. Chem. **34**, 1349 (1942).
[f] L. R. G. Treloar, Trans. Faraday Soc. **36**, 538 (1940).

[4] M. Mooney, J. App. Phys. **19**, 434 (1948).

[5] F. L. Roth and L. A. Wood, J. App. Phys. **15**, 749 (1944).

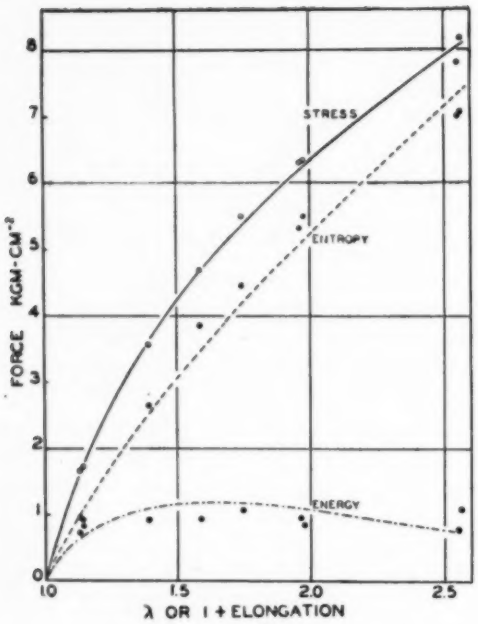

FIG. 2. Hevea, compound 1, commercial stock dur. 40.

is held constant produces a small elongation cycle, and that the slope of the line joining the corrected stress and the observed stress corresponds to the dynamic modulus of the stock in such small cycle rather than to the local slope of the over-all stress-strain curve. The latter slope was the only one derivable from published

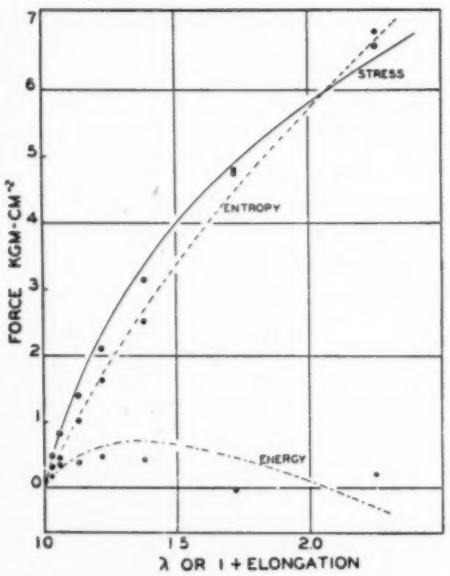

FIG. 3. Hevea, compound 2, 100 rubber—8 sulfur.

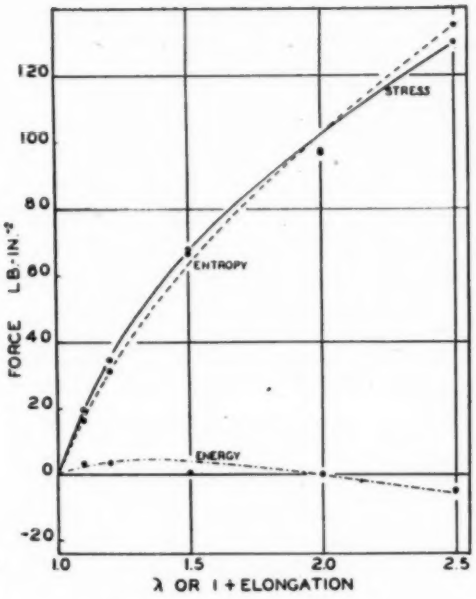

FIG. 4. Hevea, compound 3.

thermoelasticity data; but Wiegand and Snyder[6] have shown that the modulus of elasticity in a short cycle of elongation about a mean value different from zero is much larger than the modulus obtained from the "equilibrium" stress-strain curve. In view of this work, it is felt that, if it is possible to apply thermodynamic methods to this system at all, the correct modulus for use in Eq. (5) is the one obtained by executing an elongation cycle comparable in amplitude to the cycle produced by the temperature changes. The discrepancy shown in Fig. 1 is in the direction to be expected on the basis of this discussion.

ANALYSIS OF THERMOELASTICITY DATA

Since the discrepancy between the observed and calculated curve is small, it was ignored and the value of the coefficients in Eq. (2) were calculated from the experimental data after being corrected by Eq. (5) for the effect of temperature upon the elongation. The coefficients are given in Table I.

The entropy contribution to the stress is

$$T(\partial F/\partial T)=\tfrac{1}{2}G_1TP(\lambda)+\tfrac{1}{2}H_1TQ(\lambda). \quad (6)$$

The energy contribution to the stress is

$$F-T(\partial F/\partial T)=\tfrac{1}{2}G_0P(\lambda)+\tfrac{1}{2}H_0Q(\lambda). \quad (7)$$

[6] W. B. Wiegand and J. W. Snyder, Trans. Inst. Rub. Ind. 10, 324 (1934).

The curves obtained at a single temperature with these coefficients are plotted in Figs. 2–7. The three points at a given elongation show the total (observed) stress, the slope multiplied by the absolute temperature or the entropy part of the stress, and the intercept on the stress axis or the energy part of the stress. The constants of A, B, C, and D in Eq. (4) were fitted to the data by the method of least squares. The agreement between the calculated curves and the observed data is fairly good.

TESTS OF STATISTICAL MECHANICAL THEORY OF ELASTICITY

The coefficients of Eq. (2) provide two tests for the statistical theory of elasticity. The fundamental assumption of the statistical theory is that the entropy change is responsible for the stress. If this is true, then

$$-\lim_{\lambda\to 1}[(\partial S/\partial\lambda)_{T,P}/F] \equiv [G_1T/(G_0+G_1T)]=1. \quad (8)$$

Wall[7] observed that the statistical theory predicted that H would be equal to G in Mooney's equation. Since the statistical method considers only the entropy of deformation, we take the prediction to mean

$$H_1/G_1=1. \quad (9)$$

These two predictions can be tested with the values of the moduli listed in Table I. Results are shown in Table II.

Variance analyses have been made to determine if the deviations from unity of the two ratios of Eqs. (8) and (9) are significant. This was done by computing the variances for the independent coefficients A, B, C, and D in Eq. (4). From these variances, the variance of each ratio was calculated by the theory of propagation of errors. Values of the ratios, their standard deviations, and an estimate of their significance is given in Table II. Columns 2 and 4 in Table II give the probability, obtained by applying Student's t test, that the departure of the observed ratio from unity is due to chance errors. A probability of 0.05 indicates that the difference between the observed ratio and unity is significant. A probability less than 0.01 is an indication that the difference is highly significant. It is to be remembered that variance analysis deals only with chance errors; systematic errors are beyond its power.

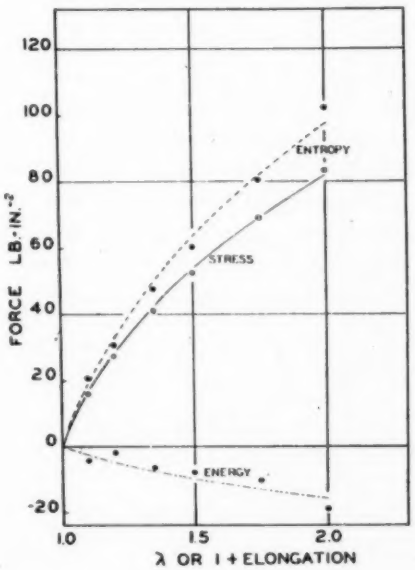

FIG. 5. GR-S, compound 4.

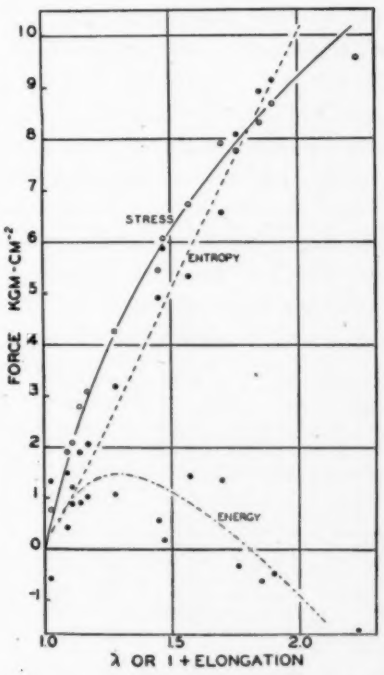

FIG. 6. Hycar, compound 5.

[7] F. T. Wall, J. Chem. Phys. 10, 485 (1942).

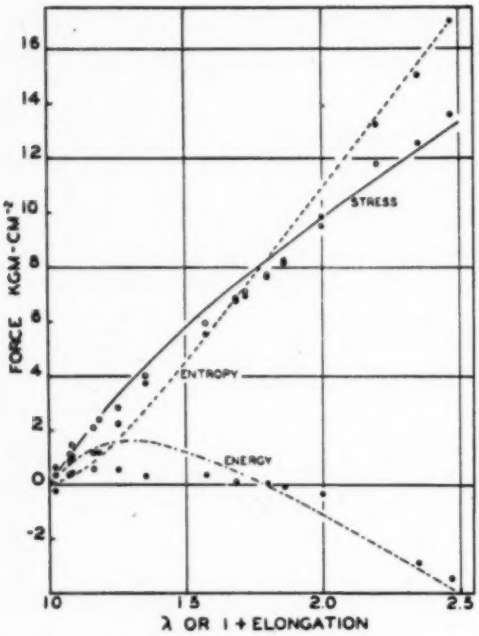

FIG. 7. Neoprene, compound 6.

CONCLUSIONS DERIVED FROM THE STATISTICAL ANALYSIS

A. Hevea Gum Compounds

For all the Hevea compounds, Figs. 2–4,*** the ratio H_1/G_1 is not significantly different from unity. Hence the equation of state derived from the statistical theory adequately represents the entropy contribution to the stress. The ratio $G_1T/(G_0+G_1T)$ is significantly different from unity. Hence the energy change makes a significant contribution to the stress at low elongations. The fact that the internal energy first increases, then decreases rapidly, suggests that there may be two mechanisms by which the energy changes with elongation. The decrease in energy can be attributed to crystallization induced by high stretch, but the cause of the initial rise in energy is not obvious.

TABLE II. Ratios and their significance. By the statistical theory, $H_1/G_1=G_1T/(G_0+G_1T)=1$. P is the probability that the observed value in the preceding column differs from 1 because of chance errors.

Compound	H_1/G_1, or α		P	$G_1T/(G_0+G_1T)$		P
1. Hevea-commercial gum[a]	1.37	±0.58	>0.5	0.57	±0.05	<0.001
2. Hevea 100-88[b]	1.32	±0.38	>0.5	0.63	±0.04	<0.001
3. Hevea gum[c]	0.71	±0.18	0.22	0.85	±0.03	0.018
4. GR-S gum[d]	0.24	±0.13	0.005	1.18	±0.09	0.10
5. Hycar[e]	5.26	±2.8	0.14	0.28	±0.10	<0.001
6. Neoprene[e]	60	±265	>0.5	0.77	±0.33	<0.05

*** The authors are indebted to Professor Guth for the data shown in Fig. 2.

B. GR-S

For the one GR-S compound reported, Fig. 5, the ratio $G_1T/(G_0+G_1T)$ is not significantly different from one, showing that the entropy contribution is practically the whole stress. On the other hand, H_1/G_1 is significantly and considerably different from one; hence in this case the statistical equation of state does not represent even approximately the form of the entropy-elongation curve. Since, by x-ray analysis, GR-S does not crystallize appreciably, the negative energy component of stress is unexpected and, so far, unexplained.

C. Hycar and Neoprene

The scattering of the data, Figs. 6 and 7, for these two stocks at low elongations is large, and the precision of the ratio H_1/G_1 is very low. However, the statistical equation will fit the data within their experimental error. The ratio $G_1T/(G_0+G_1T)$ is significantly different from one in both cases, showing that the energy contributions are significant.

THERMOELASTIC EFFECTS FROM TWISTING COUPLE MEASUREMENTS

Recently in this laboratory a series of experiments were performed to determine with high precision the thermoelasticity effects at very small deformations. The need for such measurements arises from two facts: (1) the statistical theory of elasticity ignores crystallization effects and hence is vaid only for low elongations before crystallization or any other phase change is induced by the elongation, and (2) current methods

TABLE III. Relative coefficient of thermoelasticity.

Compound	$J=(\Delta C/C)(T/\Delta T)$
Hevea gum (6 compounds)	0.96–1.00
GR-S (2 compounds)	1.18*
Hycar OR-15	1.16*
Neoprene GN	1.01
Polymethylpentadiene	1.15*
Polyisoprene	1.21*
Perbunan	1.16*
Butyl	1.04
Thiokol FA	1.04

* Significantly different from 1 at the 5 percent level.

of measuring thermoelasticity in elongation are relatively inaccurate at low elongations.

The specimen, a cured gum stock, was in the form of a rectangular rod, approximately $\frac{1}{10} \times \frac{1}{10} \times 3$ in. It was first held twisted 1 revolution for 15 minutes in a Dewar flask of water at 70°C to permit relaxation to an approximately steady value of the twisting couple. The temperature was then changed repeatedly from 2°C to 50°C and back, while the twisting couple of the sample was measured by means of an opposing steel suspension ribbon. The sample is permitted to expand freely in the longitudinal as well as lateral direction, and consequently the extent of the shearing deformation in any element of the sample is unaltered by thermal expansion.

The relative coefficient of thermoelasticity calculated from the measurements is

$$J = (\Delta C/C)(T/\Delta T),$$

where C is the twisting couple and T is absolute temperature. If the stress results entirely from entropy, $J=1$; and if it is found experimentally that $J=1+j$, then $-j$ is the fractional contribution to the total stress arising from internal energy change. The value of J has been determined for nine different polymers. The data are presented in Table III. J is approximately 1 in all cases; the small departures from 1.0 are significant in five cases. In all cases where there is a significant departure from 1, $j>0$, and the internal energy decreases with deformation.

The agreement between the two methods of determining the entropy contribution to the stress is not good. However, the experimental evidence indicates that the torsional test is the more reliable of the two and the results obtained with it give stronger support to the statistical theory of elasticity than can be found in measurements with the elongation method.

While these data thus conform approximately to the prediction that the stress is proportional to the absolute temperature, we can infer nothing from these results regarding the predicted relationship between the factor of proportionality and the molecular structure of the material.

It is to be observed that in this analysis we have accepted the usual assumption that the experimental technique in this field is adequate to yield essentially true equilibrium stress-strain curves. This assumption may be questionable.

Gee[4] shows that if a loaded sample is swelled with a volatile liquid and then deswelled, the stable length is increased. With the swelling technique, Gee finds that force at a given λ is proportional to absolute temperature within experimental error; but the stress-strain curves do not follow the kinetic theoretical relationship, $f=G(\lambda-1/\lambda^3)$. It is possible to calculate α from the form of Gee's curves (for the dry stocks), and it is found that $\alpha \lessapprox .1$ for Hevea, Buna-N, Thiokol, Neoprene-GN, and GR-S. These results are definitely in disagreement with the statistically significant values of α in Table II of the present paper. It is possible, that these differences in α are due to differences in compounding and curing; but it seems much more probable that they are due to differences in experimental procedures.

The outstanding conclusion from this critical work is that experimental techniques in this field need improvement. Even the extremely laborious swelling and deswelling technique may not give true equilibrium curves, as Gee himself rightly points out.

In spite of imperfections of method, it now seems definitely established that force at a given deformation is closely, but probably not exactly, proportional to absolute temperature. But there is still considerable doubt concerning α and the precise form of the stress-strain curve; and whether the statistical theory of elasticity is correct in this respect remains an open question. In deciding this question, stress-strain curves in both elongation and compression of the same samples would probably be helpful.

Creep, Recovery, and Permanent Set for GR-S and Hevea*

S. D. GEHMAN
*Research Laboratories, The Goodyear Tire and Rubber Company, Akron, Ohio***
(Received January 23, 1948)

A study was made of creep, recovery, and permanent set for Hevea and GR-S over a 1000-hr. period and a range of elongations at 35° C. Creep for GR-S is greater than for Hevea. The stress for GR-S is considered to be supported to a greater extent by a relatively unstable secondary bond structure. This is consistent with the large creep values for GR-S at low elongations and the large ratio of primary or recoverable creep to permanent set. Hevea, in contrast, shows low creep at both high and low elongations and maximum creep at intermediate elongations for which the structure is heterogeneous, consisting of amorphous and crystalline phases.

A procedure was worked out for determining the contribution of permanent set to the observed creep. The creep curves were concave to the strain axis when plotted against logarithmic time. After correction was made for permanent set, they were found to be approximately linear, thus extending the range of application of the Tobolsky-Eyring theory of creep.

At the start of the creep test the flow appears to be due largely to the reversible yielding of relatively weak bonds which can reform under the action of the elastic network when the stress is removed. For longer periods of time, or for higher elongations, the flow involves more deep seated changes in structure. Larger units of structure are displaced or stronger bonds broken with resultant permanent molecular displacements upon removal of the stress. For Hevea at high elongations all of the flow was accounted for by permanent set.

CREEP, the slow progressive deformation or flow which occurs under stress for a great many materials, is especially prominent for elastomers. But creep also presents technical problems in the use of metals at high temperatures and has been observed in nature on a grand scale for ice and rocks and in the laboratory for glass and all sorts of high polymers, including natural and synthetic textiles, rubbers, and plastics. Against this background of information, the fact emerges that many aspects of creep phenomena are very much the same wherever they are observed. Since the time of Maxwell, creep has been thought of and described in terms of ideal molecular mechanical models consisting of springs and dashpots.[1–3] These models have sufficed to explain the general character of the results, but calculations become unwieldy and of limited significance for systems with unspecified molecular units of flow and distributions of relaxation times. Because of the variety of types of molecular structures for which creep occurs, it is apparent that any molecular theory must be on a very broad basis. Since creep phenomena for diversified materials are so similar, it is to be expected that definite and convincing deductions from experimental curves in regard to the molecular structure and flow units and mechanisms of flow will be difficult. The reaction rate concepts of molecular flow developed by Eyring are sufficiently general to be used for molecular theories of creep.[4–7] In applying the theory to a network molecular structure,[4] Tobolsky and Eyring assumed that the primary network units did not break and that segment motion could be neglected. The flow under constant stress because of breaking or slipping of secondary bonds was deduced to obey an equation of the form

$$S=a+b\log t, \tag{1}$$

where S is the strain and a and b are parameters, the values of which depend upon the temperature and the molecular magnitudes used in the theory. The theory does not apply directly for creep recovery, which is activated by internal molecular forces.

* Presented at the Fifth Meeting of the Division of High-Polymer Physics, American Physical Society, Chicago, Illinois, December 29–30, 1947.

** Contribution No. 151 from Goodyear Tire and Rubber Company Research Laboratory.

[1] J. M. Burgers, "First report on viscosity and plasticity," Acad. Sci. Amsterdam (1935).

[2] H. Leaderman, "Elastic and creep properties of filamentous materials and other high polymers," Textile Foundation, Washington, 1943.

[3] C. Mack, J. App. Phys. **17**, 1086 (1946).

[4] A. Tobolsky and H. Eyring, J. Chem. Phys. **11**, 125 (1943).

[5] P. J. Blatz and A. V. Tobolsky, J. Chem. Phys. **14**, 113 (1946).

[6] W. Kauzmann, Metals Tech. **8**, 57 (1941).

[7] Dushman, Dunbar, and Huthsteiner, J. App. Phys. **15**, 108 (1944).

Although the deductions from this molecular theory of creep conform in a general way to the observations, there is much to be desired in regard to specificity as to the types of bonds, bond strengths, or activation energies and units of flow involved. It is doubtful if the molecular constants, which must be deduced from experimental creep results, are really constant for a very wide range of experimental conditions. These difficulties may be inherent in the character of molecular network structures, since it is reasonable to suppose that a distribution of secondary bond strengths exists so that confusion may arise in trying to distinguish between effects from strong secondary bonds and primary bonds. Likewise, there may be an indefiniteness in the size of the units of flow.

Andrews, Tobolsky, and Hanson[8] have proposed a molecular theory of permanent set for rubber during relaxation at elevated temperatures which assumes that new network chains are formed during relaxation. These new chains are at equilibrium in the stretched condition. They are considered, therefore, to resist retraction when the load is removed. The general ideas would be applicable for permanent set occurring during a creep test, but it is doubtful if many new primary bonds of the type contemplated are formed at more moderate temperatures. Hence it is desirable to explain the permanent set observed after creep tests such as will be described on the basis of some irreversible flow mechanism without using the idea of new primary bond formation.

The experiments here reported were undertaken with the idea that additional information on creep and flow processes, and hence molecular structure for GR-S and other rubbers, might be obtained by measuring creep for a range of elongations and cures and correlating the results with the corresponding observations of creep recovery and permanent set. In the case of Hevea, creep phenomena at higher elongations are complicated by the occurrence of progressive crystallization during the tests,[9,10] Comparison with GR-S should be instructive for studying this effect.

The occurrence of creep is one of the fundamental limitations of elastomers in many applications, so that a better understanding of how it comes about may have technical importance as well as significance for the general knowledge and theory of the molecular structure of elastomers. Creep is a manifestation of imperfect elasticity which, under other circumstances, may become apparent as stress relaxation and hysteresis. A review of creep studies, from the engineering standpoint, has been given in a recent British publication.[11] The general mathematical relationships between creep and relaxation based on the superposition principle and linear mechanical models have been recently presented by Gross.[12]

METHODS OF DESIGNATING CREEP

In engineering usage, creep for rubber is usually defined as the percent change in elongation, compression, or shear in any specified time. Figure 1 represents a plot of the gauged length of a test piece against the time. The initial elongation is $100(l_s-l_0)/l_0$. The elongation at time t is $100(l_t-l_0)/l_0$. The increase in elongation is $100(l_t-l_s)/l_0$. The percent increase in elongation is $100(l_t-l_s)/(l_s-l_0)$. This is usually used as a measure of the creep. One of the ideas behind this definition is to secure a result which is relatively independent of the magnitude of the initial deformation. It will be seen from the

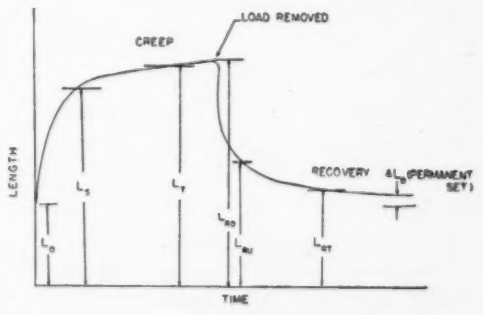

FIG. 1. Diagram of deformations in creep and recovery processes.

[8] Andrews, Tobolsky, and Hanson, J. App. Phys. **17**, 352 (1946).
[9] J. E. Field, J. App. Phys. **12**, 23 (1941).
[10] A. J. Wildschut, Rubber Chem. and Tech. **17**, 854 (1944); Physica **10**, 571 (1943).
[11] "Creep phenomena, natural and synthetic rubbers," Users' Memo. No. U 12, The Services Rubber Investigations, London.
[12] B. Gross, J. App. Phys. **18**, 212 (1947).

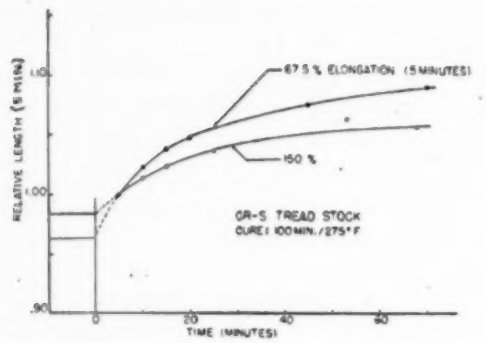

FIG. 2. Curves illustrating extrapolation to zero time.

data presented later that the definition does not accomplish this purpose very well.

A complication arises in the use of the definition in that it is necessary to select some arbitrary time interval as marking the end of the initial elongation and at which to measure l_s. To avoid uncertainty in determining this initial elongation, the ratio l_t/l_0 has been used by Wildschut[10] to designate creep. This has the disadvantage of not furnishing any basis for distinguishing between the ordinary elastic deformation and the subsequent slow deformation usually thought of as creep.

In this work it will be assumed that creep processes of flow start simultaneously with the ordinary elastic deformation, so that the ordinary elastic deformation is to be deduced by extrapolation of a suitable long term creep curve to zero time. In the experiments to be described, this procedure applies a correction but does not change the results materially from those secured by using the period of extrapolation as the arbitrary start of the creep process.

The same notation as that shown in Fig. 1 may be used, but l_s is now thought of as being the stretched length resulting from the ordinary elastic deformation alone, a correction having been made for any contribution caused by creep. l_0 is the initial unstretched length, and l_t the stretched length at any time t. The relative length, $R.L.$, is here defined as the ratio l_t/l_s.

The ordinary elastic elongation, E_0, is given by

$$E_0=\frac{100(l_s-l_0)}{l_0}. \tag{1}$$

It follows that

$$\frac{l_t}{l_0}=R.L.\left(\frac{E_0}{100}+1\right). \tag{2}$$

The elongation, E_t, at any time, t, is given by

$$E_t=R.L.(E_0+100)-100. \tag{3}$$

The percent creep, as previously defined, can now be expressed as

$$\text{percent creep}=100\frac{E_t-E_0}{E_0}$$

$$=100(R.L.-1)\left(\frac{E_0+100}{E_0}\right). \tag{4}$$

During a creep test the rubber usually acquires a permanent set which becomes apparent when the test is discontinued at time t. Let Δl_0 be the increment to l_0 due to permanent set. The contribution which Δl_0 made to the length, l_t, is, to a first approximation

$$\Delta l_0\left(\frac{E_0+100}{100}\right).$$

To secure the value of the primary, i.e., reversible or recoverable, creep, the observed value should be corrected for the permanent set. This can be done by subtracting the above quantity from l_t in the definition of creep as given by Eq. (4). When this is done, it follows that

$$\text{primary creep}=\text{observed creep}$$

$$-\left(\frac{E_0+100}{E_0}\right)\cdot\text{permanent set}. \tag{5}$$

The values are in percents.

An advantage of expressing the creep as percent change in elongation is that it permits this simple subtractive correction for the permanent set.

A method which appears to permit the determination of the ordinary elastic elongation with an accuracy which is satisfactory for these experiments will now be described. With the relative length is plotted against the time, curves are secured such as those of Fig. 2. These can be extrapolated from the five minute point to zero time with reasonable precision, so that the length

measured at five minutes after load application can be corrected to give the length corresponding to the ordinary elastic deformation. Usually the correction is not very large. For the curves shown in Fig. 2, it is 1.5 percent and 3.5 percent, respectively, for the high and low elongation.

When the load is removed after the creep test, there is an initial rapid retraction followed by a slow retraction which is called "recovery." Recovery, like creep, is a flow process. Analogously to creep, it may be defined as the percent change in the initial deformation, the initial deformation being the rapid retraction when the load is removed. Or, to avoid the ambiguity involved in determining the initial deformation, the ordinary elastic deformation for recovery can be determined in the same manner as previously described for creep, i.e., by extrapolating the curve of relative length *vs.* time to zero time. According to these ideas,

$$\text{percent recovery} = 100\frac{l_{ru}-l_{rt}}{l_{r0}-l_{ru}}, \tag{6}$$

where

l_{r0} is the stretched length before the load is removed,
l_{rt} is the length at time t,
l_{ru} is the length corresponding to the ordinary elastic retraction.

For recovery, let the relative length be defined as

$$R.L.=\frac{l_{rt}}{l_{ru}}. \tag{7}$$

Then,

$$\text{percent recovery} = 100\frac{(1-R.L.)l_{ru}}{l_{r0}-1}. \tag{8}$$

This definition may be readily understood when it is realized that it has the same form as for the case of the creep of a test piece under compressive stress. The sequence of length changes which ensue upon removal of the load are analogous to those which occur for a test piece loaded in compression.

EQUATIONS FOR CREEP CURVES

The empirical description of creep curves for many different types of materials favors an equation in which the strain is essentially a linear function of the logarithm of the time in the earlier stages of the creep process. This has been suggested by both Braun[13] and Wildschut[10] for rubber.

Lyons[14] has advocated, as the most generally acceptable empirical law of creep, an equation of the form

$$\epsilon=\epsilon_1+at+b\log t. \tag{9}$$

ϵ is the strain at time t. ϵ_1, a, and b are parameters, the values of which depend upon the material and experimental conditions.

At the start of the creep process the logarithmic term predominates. For longer times, the linear term becomes more important. The result of this is that when the strain is plotted against logarithmic time, the straight line obtained at the start tends to bend toward the strain axis as time goes on.

EXPERIMENTAL METHOD

The procedure for making the creep measurements consisted of hanging weights on $\frac{1}{8}$-in. wide, 2-mm gauge, dumbbell test pieces in a constant temperature cabinet with glass sides through which the samples could be observed with a measuring microscope. The arrangements are apparent in Fig. 3. The temperature was 35°C. It has been found advantageous to determine the gauged length as the distance between the ends of two lines ruled parallel to the length of

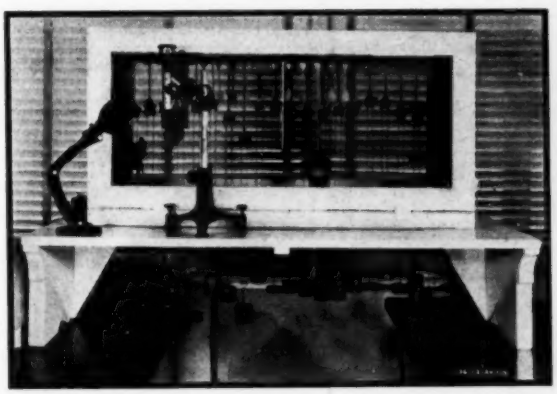

FIG. 3. Photograph of creep test apparatus.

[13] M. L. Braun, Physics **7**, 421 (1936).
[14] W. J. Lyons, J. App. Phys. **17**, 472 (1946).

the test piece with a ruling pen and white, pigmented rubber cement. If the lines are ruled across the test piece, they are broadened upon stretching. When ruled parallel to the length of the test piece, the ends are sharpened upon stretching and furnish very satisfactory points upon which to set the cross hair of the measuring microscope.

The creep tests were made under constant load conditions, the stress increasing during the test because of reduction of cross section as creep progressed. An experimental procedure has been used by Speakman[15] to avoid this effect. It would also be possible to make corrections for the change in area from a family of curves at different elongations, as suggested by Wildschut.[10] Since this involves the assumption that the structure is independent of the time-load relationship, it did not seem advisable to do this.

Constant stress conditions would permit more exact comparison with present theories, but the results would have less practical significance.

Permanent set was determined 1000 hrs. after the load was removed, the test pieces remaining in the thermostat at 35°C. To determine the permanent set resulting from various durations of the creep test, it was, of course, necessary to use a different test piece for each point of the curve.

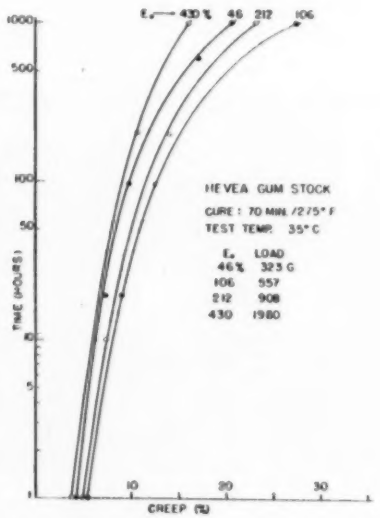

FIG. 4. Effect of elongation on creep.

[15] J. B. Speakman, J. Textile Inst. **17**, T472 (1926).

COMPOUNDS

The formulas for the compounds used are given below:

GR-S	100		
Hevea		100	100
Sulfur	2.0	2.75	3.0
Zinc oxide	5.0	5.0	3.0
Captax	1.5	1.35	1.0
Stearic acid	2.0	3.0	4.0
Softener	3.0	3.0	3.75
Phenyl-β-naphthylamine	1.0	2.0	1.0
E.P.C. black	50.0	50.0	

RESULTS

Figures 4 and 5 show plots of percent creep *vs.* logarithmic time for a series of elongations for Hevea gum stock and Hevea and GR-S tread stocks. The structural changes which occur because of crystallization make the creep phenomena for Hevea complicated and difficult to interpret. It is noteworthy that the Hevea stocks show the greatest creep rates for intermediate elongations where the structure is partly amorphous and partly crystalline, a fact which has

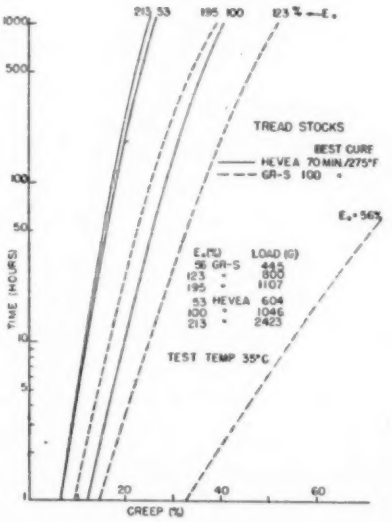

FIG. 5. Effect of elongation on creep.

already been recorded in the literature.[9] For GR-S, on the other hand, creep diminishes monotonously for higher elongations. This contrast in the effect of elongation on the creep for the two types of rubber correlates to some extent with hysteresis and relaxation observations which show GR-S to improve relative to Hevea

in respect to both relaxation and hysteresis at higher elongations.[16] The mechanical instability of the molecular structure of GR-S at low elongations appears to be a fundamental weakness in comparison with Hevea.

All of the creep curves shown exhibit a characteristic concavity toward the strain axis when the ordinate is logarithmic time. Figures 6, 7, and 8 illustrate creep curves before and after correcting for permanent set. The correction improves the linearity of the creep curves. Frequently, it results in a slight curvature in the opposite direction. Considering the approximate

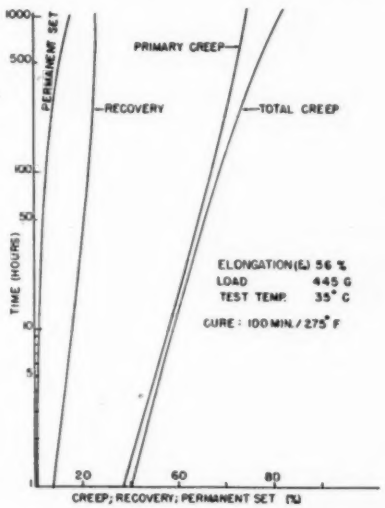

FIG. 6. Creep, recovery, and permanent set for GR-S tread stock.

nature of the correction, the assumption that the true primary creep curve would be essentially linear in this type of plot seems to be well justified.

The general empirical equation for creep curves, Eq. (9), accounts for the curvature on the semilog plot by means of a linear term representing a viscous type, constant-rate flow. Permanent set is not linear with time, as shown by the curves of Fig. 9, although it becomes linear after a relatively short time. Hence the contribution of permanent set to creep does not correspond exactly to this linear term, although correction for permanent set has the effect of making the creep very closely a logarithmic function of the time for the cases studied.

[16] H. A. Braendle and W. B. Wiegand, J. App. Phys. **15**, 304 (1944).

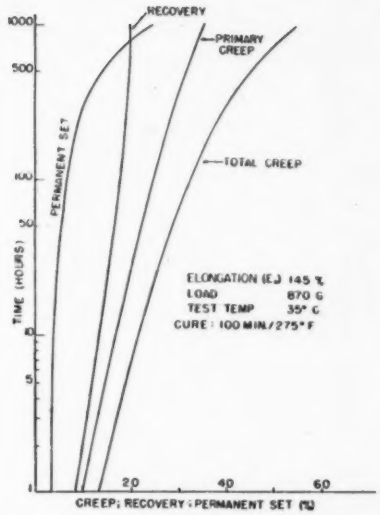

FIG. 7. Creep, recovery, and permanent set for GR-S tread stock.

Figures 6, 7, and 8 also show recovery curves. The rate of recovery is considerably less than the creep rate. The recovery curves show some curvature in the opposite direction from that of the creep curves since a constant length must be approached asymptotically as time goes on, whereas in a creep test the length may increase indefinitely until rupture. Recovery is activated by the residual retractive tendencies of the network structure, a return to a condition of higher entropy. Theories of creep which require an external force to supply the activating stress do not apply directly.

Although, from Figs. 6 and 7, the recovery curves for GR-S are rather insensitive to the elongation for the creep test, they show a systematic dependence on the duration of the creep test, as illustrated in Fig. 10. As might be expected, the residual elastic forces in the network structure depend upon the deformation which remains because of primary creep when the load is removed after the creep test. The

TABLE I. Creep and permanent set for GR-S tread stock; $E_0 = 83\%$.

Cure	A Permanent set (%)	B Creep (%) (1000 hrs.)	C Primary creep (%)	$\frac{C}{A}$ Primary creep permanent set
50/275	34	138	63	1.9
70/275	23	89	38	1.7
140/275	11	44	20	1.8

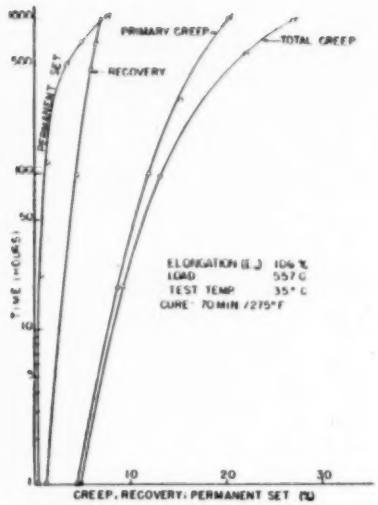

FIG. 8. Creep, recovery, and permanent set for Hevea gum stock.

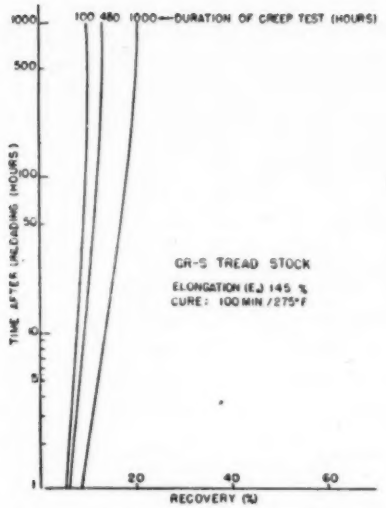
100 480 1000—DURATION OF CREEP TEST (HOURS)
GR-S TREAD STOCK
ELONGATION (E_o) 145 %
CURE: 100 MIN /275°F
TIME AFTER UNLOADING (HOURS)
RECOVERY (%)

FIG. 10. Recovery after creep test.

magnitude of this deformation depends, in turn, upon the duration of the creep test.

The effect of cure on creep and permanent set for GR-S is shown by the curves in Figs. 11 and 12. The 35- and 50-minute cures are decidedly under optimum cure and show large values for creep and permanent set.

Table I gives data on the relative proportion of permanent set and primary creep in dependence on cure.

The strengthening of the primary valence network structure by vulcanization could reduce flow by reducing the rate, the magnitude, or both the rate and magnitude of the molecular displacements. It is reasonable to suppose that only the larger unit molecular flow processes result in permanent set. Since the proportion of primary creep to permanent set was not affected appreciably by the extent of the vulcanization, it is most probable that vulcanization reduced the rate of the unit molecular flow processes rather than affecting their size distribution or general character. As vulcanization progresses, a larger part of the stress is carried by the relatively stable primary valence network, but the molecular units of flow which remain appear to function in essentially the same way. For short term creep tests, up to about 48 hours, it was found that vulcanization did tend to reduce primary creep relative to permanent set, but the

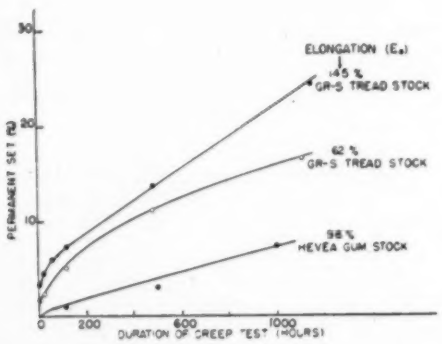

FIG. 9. Dependence of permanent set on duration of creep test.

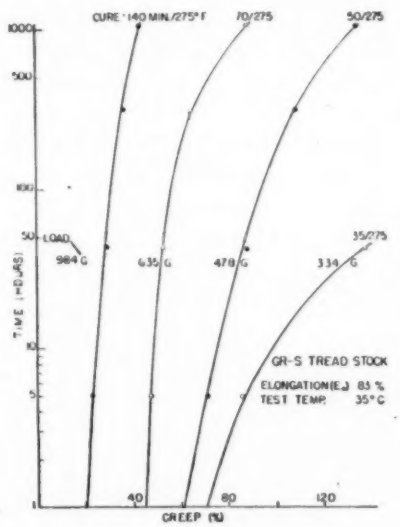

FIG. 11. Effect of cure on creep.

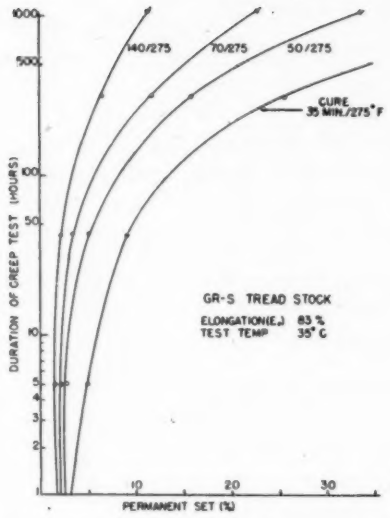

FIG. 12. Effect of cure on permanent set.

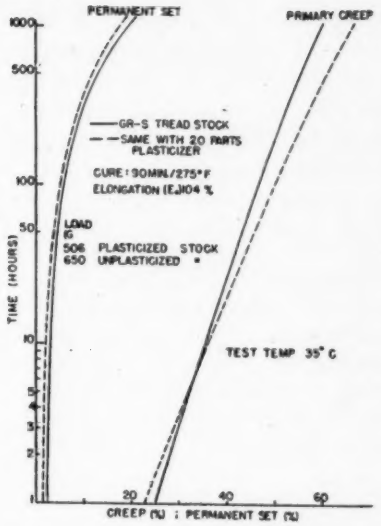

FIG. 13. Effect of plasticizer on creep.

long term tests here reported seem to be of more general significance.

Figure 13 presents data secured for the GR-S tread stock with 20 parts of plasticizer (Paraflux) added. The possible lubrication of secondary valence bonds by the plasticizer has a surprisingly small effect on both the permanent set and the primary creep, although some enhancement of primary creep is definitely indicated. Any instability introduced into the molecular structure by the plasticizer was very nearly compensated for, as far as flow was concerned, by the lower stress applied to the plasticized stock in this test. It would be very desirable to extend the experiments to other temperatures to determine activation constants for the flow resulting in permanent set as compared to primary creep. This would be a means of securing additional information as to the molecular flow mechanisms responsible for the two types of flow.

For Hevea tread stock at high elongations all of the creep was accounted for by permanent set. What is known of the structure of Hevea at high elongations leads to the suggestion that, in this case, flow occurs in the amorphous material between the crystallites, with whole crystallites being displaced with reference to each other. Under such circumstances, the original relative molecular configurations cannot be reassumed upon removal of the stress.

ACKNOWLEDGMENT

The author wishes to express his thanks to the Goodyear Tire and Rubber Company and Dr. L. B. Sebrell for permission to publish this work, and to P. J. Jones for securing some of the data.

This investigation was carried out under the sponsorship of the Office of Rubber Reserve, Reconstruction Finance Corporation, in connection with the Government's synthetic rubber program.

A Theory of Commercial Yarn Testing*

CHARLES J. GEYER, JR.,** C. H. REICHARDT,*** AND GEORGE HALSEY†

(Received January 30, 1948)

A method has been devised for the application of the theory of the three-element shear model of Eyring and co-workers to textiles which does not necessitate the location of the "basic spring line" and thus is readily applicable to both yarn and fiber tests and to the commercial inclined-plane and pendulum-type testers. It is also applicable as a first approximation to those textiles which do not possess a "basic spring line" as such. The method employs the conventional spring constants or elastic moduli, but determination of the viscous constant involves the magnitude of the relaxation in constant rate of elongation experiments (or the magnitude of the creep in constant rate of loading experiments) from the upper envelope per interval of time. The relationship has been employed to establish the correlation between the viscoelastic properties of "slashed" and "unslashed" viscose tire cord rayon yarns and also to show the identity of single filament stress-strain relationships with those of yarns of normal twist of the same textile. The simplicity of technique which enables this method to be used as a routine laboratory test for the determination of the viscoelastic properties of textiles affords it an advantage over previous methods, which were often unsatisfactory from both a theoretical and an experimental viewpoint.

A THEORY OF COMMERCIAL YARN TESTING

IT might be expected that tests which measure the stress-strain relationships of yarns and filaments should agree, when the yarn is manufactured of continuous filaments. With staple fibers such as cotton and wool, where the yarn is constructed of short lengths held together by friction, agreement would not be expected. One feature of a yarn which prevents it from being considered as a bundle of filaments is the twist. It has been shown, however, that the twist of a yarn up to normal degrees of twist, i.e., approximately five turns per inch, has no apparent effect on the stress-strain characteristics of a textile.

Proceeding further in the consideration of yarn and single filament testing, it is known that the majority of the yarn tests on commercial testing devices, because of the magnitudes of the forces involved, does not obtain the sensitivity with which practically all single filament tests are carried out. Therefore, many of the theories advanced to explain the stress-strain relationships of textiles, requiring complicated procedures performed on a sensitive apparatus, have been worked out for single filament experiments. These theories are not readily applied to or obtained from yarn tests because of their complexity.

The mechanical properties of a number of textile fibers and filaments have been treated successfully on the basis of the theory of the three-element shear model of Eyring and coworkers.[1] This model (Fig. 1) is made up of a spring, S_2, in parallel with a Maxwell unit consisting of a spring, S_1, in series with a non-Newtonian dashpot, the dashpot being defined by the hyperbolic sine law of Eyring's theory of viscosity. Application of the theory of this model involves the location of a "basic spring line." The spring line (cf. dotted line in Fig. 3) may be defined as the locus of points of no relaxation, i.e., points in a stress-strain plot at which there is no instantaneous relaxation in either direction. The distance between the spring line and the upper envelope of the stress-strain curve represents the force on the Maxwell unit, and therefore on the dashpot, at any given elongation. The elastic moduli are given by the two slopes. From the shape of the curve in the yield region, the shape of the relaxation curve, or the difference between the forces on the dashpot at differing rates of elongation, or loading, the viscous constants can be calculated. These four constants are then used to characterize a textile

* Contribution of The Textile Foundation, Frick Chemical Laboratory of Princeton University, and The American Viscose Corporation. Presented at the Fifth Meeting of the Division of High-Polymer Physics, American Physical Society, Chicago, Illinois, December 29–30, 1947.

** American Viscose Corporation, Front Royal, Virginia
*** Fellow of the Textile Research Institute.
† Fellow of the Textile Research Institute. Present address: Mallinckrodt Chemical Laboratories, Harvard College, Cambridge, Massachusetts.

[1] G. Halsey, "Non-linear viscous elasticity and the Eyring shear model," J. App. Phys. 18, 1072 (1947).

and knowledge of them allows the prediction of the stress-strain curve of a textile.

Applications of this theory had two major drawbacks: 1. the experimental technique was complicated and often required the use of several samples to obtain the viscous constants; 2. for the majority of fibers, the three-element model is applicable to the first approximation only.

To explain the limitations introduced by this latter point, it would be advantageous first to consider the properties of the three-element model. Cellulose acetate obeys the theory of the three-element model extremely well. For one, determination of the spring line is straightforward and, secondly, each loop of a recycling curve is superimposable on any other loop. On the other hand, in the case of viscose rayon or wool a single basic spring line is either nonexistent or cannot be determined experimentally. This does not exclude altogether the use of the three-element model theory for these textiles, since by assuming a spring line which by definition must pass through the origin and be parallel to the upper envelope, these textiles can be fairly well characterized. One might say then, that the three-element model theory applies in these cases to the first approximation. To illustrate the difficulties arising when the three-element model theory is applied in this manner to viscose rayon it is advantageous to examine a typical stress-strain curve of viscose rayon (Fig. 2). First, the return loops of a recycling curve are not superimposable, but the yield points broaden as the load and elongation increase. Secondly, instead of a simple basic spring line, viscose rayon shows an area below which a relaxation upward occurs and above which a relaxation downward occurs regardless of direction of approach. Furthermore, a point of no relaxation can be located anywhere within the area by the process of bracketing. It is easy to see that such conditions make it extremely difficult to employ the three-element model theory since the location of the spring line and the shape of the yield point are both used in calculating the constants. Thus a method of applying the theory of Eyring and co-workers to textiles, which does not necessitate the location of the spring line or the shape of the yield point, would make the theory more applicable to routine laboratory testing, as well as to research, on single filaments and yarns.

With respect to yarn testing, the present routine laboratory tests to determine the viscoelastic behavior of textile yarns are inadequate, and a reduction to basic parameters is necessary. For example, the stress-strain curves of slashed and unslashed yarns are very dissimilar, although both may have been manufactured from the same stock. Again, the elongation to break curves of two rayons may be superimposable, although they may have been manufactured from dissimilar stocks and have very dissimilar elastic or recovery properties.

The spring constants or elastic moduli are familiar constants, being merely the ratios of stress to strain and are obtained from the slopes of the stress-strain envelope. The first slope is equal to k_1 and k_2, that is, to the sum of the spring constants of the open spring, S_2, and of the closed spring, S_1. The value of k_2 is obtained directly from the second slope. Viscous constants, however, are less tangible terms and require definition. Considering a constant rate of elongation experiment, a viscous constant β may be defined by

$$\beta = \frac{\rho}{K},$$

where ρ is the experimental rate of elongation and K is the rate at which the fiber would lengthen at zero force, if every molecular jump

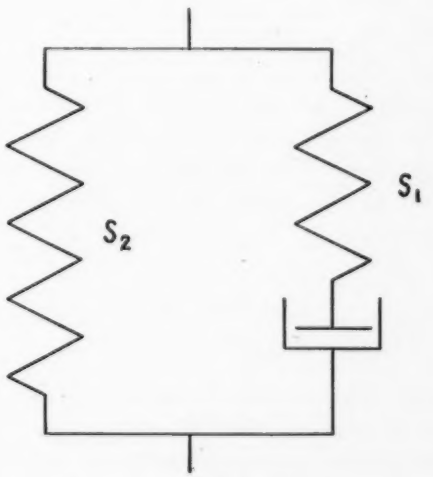

FIG. 1. Three-element model.

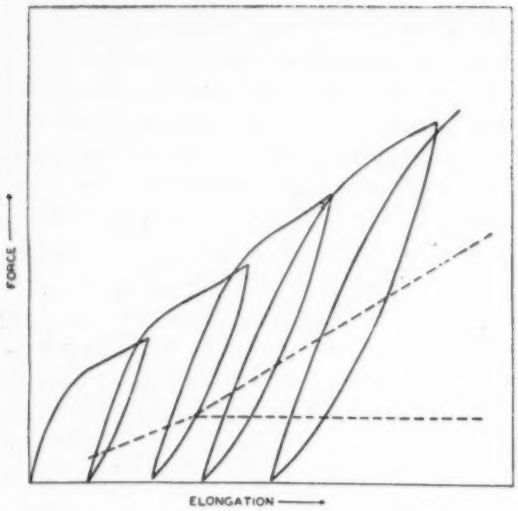

FIG. 2. Typical recycling stress-strain curve of viscose tire cord rayon.

which shortens fibers were suppressed and all jumps which lengthen fibers were allowed. For constant rate of loading experiments,

$$\beta = \frac{P}{Kk_2},$$

where P is the experimental rate of loading, K is as defined before, and k_2 is the spring constant of the open spring S_2. A related viscous constant, α, may be defined by the hyperbolic sine law governing the non-Newtonian dashpot. Thus assuming a symmetrical barrier opposing flow

$$\frac{dl_1}{dt} = K \sinh \alpha f,$$

where dl_1/dt is the rate of extension of the dashpot, f is the force acting on it, and K is as defined above. The constant α is very largely a function of the molecular structure. For large values of β,

$$\alpha \approx \frac{1}{f_\infty} \ln 2\beta.$$

The normal method of calculating the viscous constants requires the use of the basic spring line and the two envelopes obtained at two very different rates of loading or elongation. A logical first approach to the problem of determining the viscous constants without recourse to an experimentally determined spring line would be to attempt to calculate the viscous constant from a formula involving three rates of elongation or loading. However, the nature of the equation governing the viscous element is such that the ratio between the rates is independent of the viscous constants.[1]

The new method of applying the three-element model theory was suggested by the experimental work of another person.[2] Unfortunately, the original data of Meredith, which covered almost the entire range of textile types and which were more than adequate for his work, could not be analyzed by this new method of applying the three-element theory since, as was discovered by subsequent correspondence, they did not have need for or adhere to a rigid time cycle which is needed for the new method. By a slight modification of Meredith's original technique this difficulty was easily overcome.

II. THEORETICAL

Every previous method of determining the various constants involving change of rate required, naturally, a large change in rate of elongation or loading, which in general necessitated the use of two or more samples of the yarn or filament, and a knowledge of the location of the basic spring line. Determination of a viscous constant by the method set forth here involves the amount of relaxation in constant rate of elongation experiments or the amount of creep in constant rate of loading experiments per interval of time, requires no knowledge of the basic spring line, and can be carried out on one sample of a particular yarn or filament.

A. Constant Rate of Elongation Experiments

Consider the family of stress-strain curves (Fig. 3) obtained in a series of constant rate of elongation experiments from the fast rate 1 down to the fractional rate n, where curve AB represents the relaxation curve from the fast rate. From the theory of the three-element model the

[2] R. Meredith, "A comparison of the tensile elasticity of some textile fibers," J. Textile Inst. **36**, T147 (1945).

force†† on the viscous element is given by

$$f=k_1(l-l_1),$$

which on differentiation yields

$$\frac{df}{dt}=k_1\left(\frac{dl}{dt}-\frac{dl_1}{dt}\right)=k_1\left(\rho-\frac{dl_1}{dt}\right),$$

where $\rho=dl/dt$, the rate of elongation of the sample. In the steady state,

$$\frac{df}{dt}=k_1\rho.$$

Now

$$\left.\frac{df}{dt}\right|_0=\left.\frac{d\Delta f}{d\Delta t}\right|_0=k_1\rho,$$

where $\left.\frac{df}{dt}\right|_0$ denotes the initial rate of relaxation, because the instantaneous rate of relaxation is determined by the force, which in the steady state under a constant rate equals $k_1\rho$. Therefore, any

$$\frac{d\Delta f}{d\Delta t}=nk_1\rho_1, \tag{1}$$

where ρ_1 is the rate for the fast rate 1, and $n\rho_1$ gives the rate for the constant rate curve that has the instantaneous value f_n for f_∞.

Now, taking the dimensional datum $\Delta f=f_n-f_1$ as the measured quantity, we have from previous considerations[1]

$$f_n-f_1=\frac{1}{\alpha}(\text{arc sinh}n\beta-\text{arc sinh}\beta).$$

If the spring line is sufficiently distant from the upper envelope to make β large, then the approximation for arc sinh can be employed, and

$$f_n-f_1=\frac{1}{\alpha_\infty}\ln n$$

or

$$\alpha_\infty=\frac{\ln n}{f_n-f_1}=\frac{\ln n}{\Delta f}. \tag{2a}$$

†† It should be noted that "force" is used in this instance, although the term "stress" might be more precise. However, this practice appears to be justified in the light of the simplicity of using "force" in plotting the data. No confusion should result from this usage.

The symbol α_∞ denotes a limiting value of dimensional α as β becomes very large. Equation (2a) may be written

$$n=e^{\alpha_\infty\Delta f} \tag{2b}$$

and substitution in (1) gives

$$\frac{d\Delta f}{d\Delta t}=k_1\rho_1e^{\alpha_\infty\Delta f}. \tag{3}$$

Integration gives

$$e^{-\alpha_\infty\Delta f}=-\alpha_\infty k_1\rho_1\Delta t+\text{constant}.$$

When $\Delta f=0$, $\Delta t=0$, and the constant $=1$. Thus

$$e^{-\alpha_\infty\Delta f}-1=-\alpha_\infty k_1\rho_1\Delta t,$$

where Δf is measured in the negative sense. For positive Δf,

$$e^{\alpha_\infty\Delta f}-1=\alpha_\infty k_1\rho_1\Delta t. \tag{4}$$

The magnitude of relaxation, Δf, in time, Δt, is measured, $k_1\rho_1$ is known, and a plot of the solution of

$$e^x-1=ax, \tag{5}$$

where $x=\alpha_\infty\Delta f$ and $a=k_1\rho_1\Delta t/\Delta f$, can be used to determine α_∞. Values of x *vs.* a for the equation $e^x-1=a$ are given in Table III.

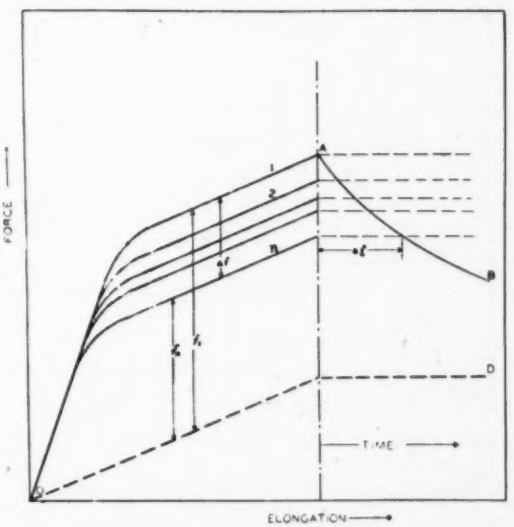

FIG. 3. Family of stress-strain curves for constant rate of elongation experiments.

B. Constant Rate of Loading Experiments

The family of stress-strain curves obtained in constant rate of loading experiments from a fast rate 1 down to the fractional rate n, is represented in Fig. 4. From the theory of the three-element model, the forces involved can be represented by

$$F-f=k_2 l.$$

Differentiating,

$$\frac{dF}{dt}-\frac{df}{dt}=P-\frac{df}{dt}=k_2\frac{dl}{dt},$$

where $P=dF/dt$, the rate of loading. In the steady state,

$$P=k_2\frac{dl}{dt}.$$

Therefore, any

$$\frac{d\Delta l}{d\Delta t}=\frac{nP_1}{k_2}, \tag{6}$$

where P_1 is the rate of loading at the fast rate 1, and nP_1 gives the rate for the constant rate of loading curve that has the instantaneous value f_n for f_∞. Since the instantaneous rate of creep is determined by the force, which is given by

$$\left.\frac{df}{dt}\right|_0=-k_2\frac{dl}{dt},$$

then

$$\Delta f=-k_2\Delta l. \tag{7}$$

As before,

$$n=e^{\alpha_\infty \Delta f}. \tag{8}$$

Substitution of (7) gives

$$n=e^{-\alpha_\infty k_2\Delta l}. \tag{9}$$

From (6) and (9)

$$\frac{d\Delta l}{d\Delta t}=\frac{P_1}{k_2}e^{-\alpha_\infty k_2\Delta l}.$$

Integration gives

$$e^{\alpha_\infty k_2\Delta l}=\alpha_\infty P_1\Delta t+\text{constant}.$$

Where $\Delta l=0$, $\Delta t=0$, and constant $=1$. Thus

$$e^{\alpha_\infty k_2\Delta l}-1=\alpha_\infty P_1\Delta t, \tag{10}$$

the extent of creep, Δl, in time, Δt, is measured, P_1 and k_2 are known, and a plot of the solution of

$$e^x-1=ax, \tag{5}$$

where $x=\alpha_\infty k_2\Delta l$ and $a=P_1\Delta t/k_2\Delta l$, can be used to determine α_∞.

III. EXPERIMENTAL

The experimental procedure to be used is easily perceived from the previous diagrams. The fiber is elongated or loaded at constant rate

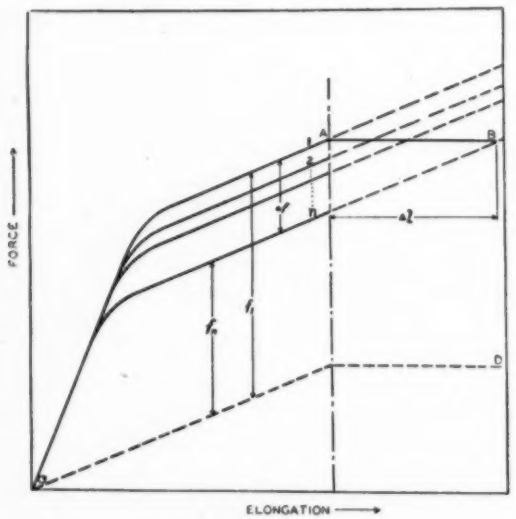

FIG. 4. Family of stress-strain curves for constant rate of loading experiments.

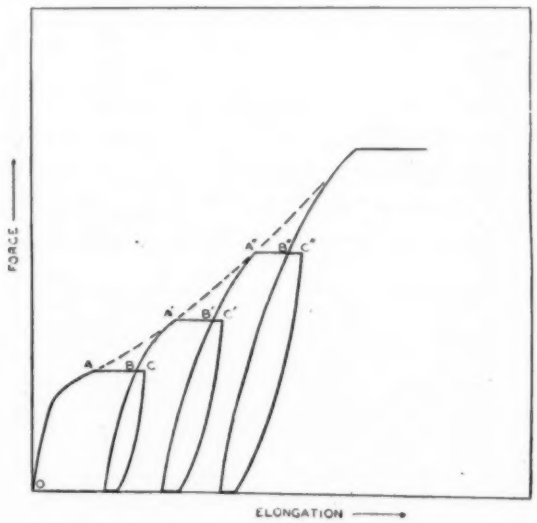

FIG. 5. Typical experimental curve for constant rate of loading experiments.

TABLE I. Unslashed yarn.

No.	Denier / filament	Sample length (cm)	Rate of loading ($\frac{\text{dynes}}{\text{cm}^2\ \text{sec.}}$)	Rate of elongation (sec.^{-1})	Breaking strength average ($\frac{\text{g}}{\text{denier}}$)	Breaking strength sample ($\frac{\text{g}}{\text{denier}}$)	k_1 ($\frac{\text{dynes}}{\text{cm}^2}$)	k_2 ($\frac{\text{dynes}}{\text{cm}^2}$)	Δt	Stress ($\frac{\text{g}}{\text{denier}}$)	α_∞ ($\frac{\text{cm}^2}{\text{dyne}}$)
1170/440 yarn											
12	1170/490	100	1.101×10^{8}	—	3.5	>2.7	1.77×10^{11}	2.15×10^{10}	60	1.07	0.670×10^{-8}
									60	1.50	0.703
19	1170/490	50	1.101	—	3.5	3.00	1.33	2.14	300	1.31	0.800
									300	2.01	0.787
21	1170/490	50	1.101	—	3.5	2.42	1.21	2.16	30	1.20	0.580
									30	1.67	0.625
22	1170/490	50	1.101	—	3.5	3.08	1.09	2.19	30	1.03	0.645
									30	1.65	0.605
									30	1.89	0.740
									30	2.38	0.612
Single filaments 1170/490 yarn											
3	2.386	6.1	—	5.19×10^{-5} 4.67×10^{-4}	3.5	2.86	1.16	2.24	290	1.88	0.880
									30	2.16	0.675
									40	2.16	0.690
									50	2.16	0.667
9	2.386	6.45	—	7.42×10^{-4}	3.5	>2.07	1.20	1.65	30	2.07	0.572
									60	2.07	0.678
1	2.386	6.45	—	4.42×10^{-4}	3.5	3.82	1.14	1.90	30	1.70	0.670
									60	1.70	0.624
									30	2.06	0.645
									60	2.06	0.685

to some force, allowed to relax or creep for a definite unit of time, contracted or unloaded at constant rate, allowed to recover for a definite time, again elongated or loaded at constant rate until the envelope is reached, and then allowed to relax or creep for a definite time; then the cycle is repeated until break. The theoretical calculations of the recovery at zero force in each cycle are easily made for a three-element model textile; however, these calculations cannot be applied to textiles such as viscose rayon where the theory of the three-element model appears to break down to a large degree in this region. The experimental measurements made, however, can be used to qualitatively describe the recovery properties of such a textile.

The temperature and humidity conditions used in all of the tests were the same, namely, 75°F and 60 percent relative humidity.

As the exact knowledge of the duration of creep or relaxation is important, it would be assumed that the longer the duration of creep or relaxation the more precise the experimental data would be. However, the rate of creep or relaxation is very high during only small intervals of time, and small errors in time of starting the unloading or loading cycle would result in large errors in the magnitude obtained. On the other hand, after a short time the rate of creep or relaxation becomes very slow—the rate varies exponentially with time—and the accuracy of the value obtained depends on the sensitivity and response of the apparatus employed. For this reason a period of creep or relaxation of one minute was employed throughout the work. A time of thirty seconds was observed to be too short, and a period of two or more minutes was thought to be too long for the latter reason, as well as too time consuming for commercial testing purposes.

In determining k_2, the second spring constant, the slope to be used is the straight upper portion of the stress-strain curve, the shorter, more horizontal portion, which occurs in the case of viscose, Nylon, wool, and other textiles, being neglected. This is discussed further in Section IV.

IV. DISCUSSION

This technique was carried out on samples of normal 1170/490 viscose rayon tirecord yarn at constant rate of loading and some single filaments of the same yarn at constant rate of elongation. The various constants were calculated and the results are shown in Table I. It can be seen that the data agree very well. It might be pointed out that the yarn has a twist of approximately

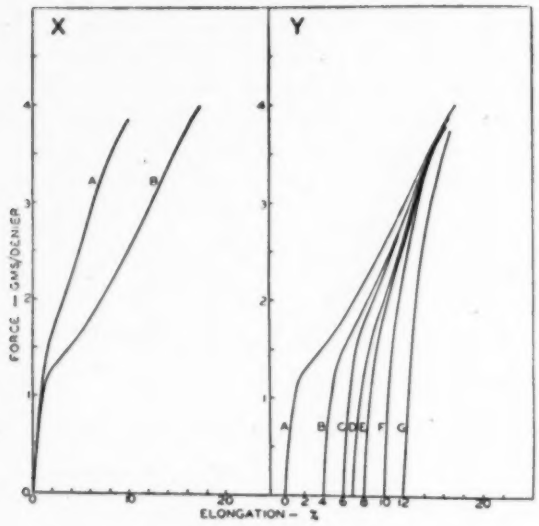

FIG. 6. Elongation to break curves for normal and slashed yarns.

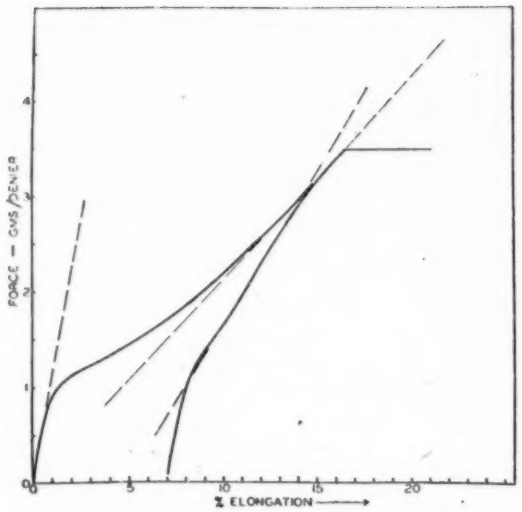

FIG. 7. True relationship between normal and slashed yarns.

five turns per inch and also that the data obtained from constant rate of elongation experiments on the same yarn agree just as well.

In applying this method to a study of new textiles, a careful study of the initial stress-strain curves and data must be made to prevent two errors, the causes of which are not always obvious, from entering the experiments.

The first of these errors comes from the slight leveling off of the stress-strain curve just after the yield point is attained (see Fig. 2). This leveling off or hump has been explained on the basis of the three-element model by thixotropy[1] and on the basis of the two-state model as the start of the transition of the one state to another.[3] This leveling off occurs every time the yield point is attained in a thixotropic substance. Examination of a normal elongation to break stress-strain curve will reveal this hump and also give the straight upper slope which should be used to determine the value of k_2.

The second error is more insidious, namely, that the upper envelope must be attained before any creep or relaxation measurements are made. This is shown in Fig. 5, which depicts a stress-strain curve in a constant rate of loading experiment. The lines AC and $A'C'$ represent the amount of creep in time Δt from the envelope.

TABLE II. 1100/490 yarns.

No.	Denier / filament	Sample length (cm)	Rate of loading $\left(\frac{\text{dynes}}{\text{cm}^2\ \text{sec.}}\right)$	Rate of elongation (sec.^{-1})	Breaking strength average $\left(\frac{\text{g}}{\text{denier}}\right)$	Breaking strength sample $\left(\frac{\text{g}}{\text{denier}}\right)$	k_1 $\left(\frac{\text{dynes}}{\text{cm}^2}\right)$	k_2 $\left(\frac{\text{dynes}}{\text{cm}^2}\right)$	Δt	Stress $\left(\frac{\text{g}}{\text{denier}}\right)$	α_∞ $\left(\frac{\text{cm}^2}{\text{dyne}}\right)$
Value of k_2 uncorrected—upper envelope not yet attained											
23	1100/490	100	1.172	—	3.5	3.20	0.94	3.86	30	1.10	1.23×10^{-5}
										1.76	1.05
										2.01	0.89
										2.54	0.62
6	1100/490	100	1.172	—	3.5	3.26	1.18	3.95	30	1.47	1.18
										2.01	1.10
										2.76	0.405
Value of k_2 corrected—upper envelope attained											
23	1100/490	100	1.172	—	3.5	3.20	0.94	2.15	30	2.54	1.27×10^{-5}
6	1100/490	100	1.172	—	3.5	3.26	1.18	2.18	30	2.76	1.02
20	1100/490	100	1.172	—	3.5	3.32	1.14	2.18	30	2.71	0.925

[3] H. Burte and G. Halsey, "A new theory of non-linear viscous elasticity," Textile Research J. **17**, 465 (1947).

If a creep measurement is made before the envelope is reached on a return loop of a recycling curve, the amount of creep in time Δt will be only that represented by lines BC and $B'C'$. At first examination it would appear that this is not hard to detect; one only has to make an elongation to break curve and compare it with the curve from which the creep measurement is made. This is not always the case, however, as is evidenced in the relationship between a normal and a slashed yarn. In fact, it was the presence of an increase in the values of the creep obtained as the force increased for a slashed yarn that lead to an understanding of the true relationship between normal and slashed yarns. Figure 6-X shows elongation to break curves of a normal (curve B) and a slashed (curve A) yarn. The slashed yarn is actually a sample of the normal yarn which has been stretched while wet and dried in the stretched state, and there is no doubt that the two curves look quite different. Figure 6-Y shows a family of elongation to break curves ranging from the curve for a normal yarn (curve A) to curve G for a sample of the same yarn after it has been stretched while wet to 12 percent and then dried in the stretched state. Each of the yarns has been stretched 2, 4, 6, 8, 10, and 12 percent, respectively. It can be seen that each of the curves, as one goes from A to G, approaches the envelope of the normal yarn at a larger force until one arrives at curve G which does not quite reach that envelope before it breaks. It is also interesting to note that curve D is really curve A of Fig. 6-X placed in its proper place with origin at 7 percent elongation. It is seen that curve D fits in with the family of curves A, B, C, E, F, and G very well.

Figure 7 is another representation of actual elongation to break curves for normal and slashed yarns in their proper orientation. The dotted lines show the slopes that one would normally take for determination of the spring constants. It is seen that there is a straight portion of the slashed curve that could be used; however, it is also obvious that the true second slope is not attained until quite late in the curve. Thus there are two errors that might arise if it is not realized that the normal envelope has not been obtained. The first, an error in the value of α_∞, the other, an error in the value of k_2. Further aid to this view might be supplied in the phenomena, that slashed yarn, if wetted and dried, approaches the original normal yarn.

Consideration of the curves show that as one approaches the envelope, the extent of the creep obtained increases in value, leading to a decrease in the value of α_∞. Table II shows values of the spring and viscous constants of a slashed yarn. The top values are those obtained when a slashed yarn is considered as a separate entity, the lower ones when it is realized that the normal envelope has not been attained. Both sets of values show

TABLE III. Values of $e^x - 1/x$ *versus* x.

$\frac{e^x-1}{x}$	x	$\frac{e^x-1}{x}$	x
1.0	0.0000	4.75	2.588
1.01	0.0190	5.00	2.658
1.02	0.0395	5.25	2.722
1.03	0.0596	5.50	2.795
1.04	0.0792	5.75	2.855
1.05	0.0986	6.00	2.915
1.06	0.1150	6.25	2.975
1.07	0.1340	6.50	3.030
1.08	0.1520	6.6	3.050
1.09	0.1700	6.8	3.092
1.10	0.1878	7.0	3.132
1.11	0.2046	7.2	3.170
1.12	0.2210	7.4	3.208
1.13	0.2400	7.6	3.244
1.14	0.2560	7.8	3.280
1.15	0.2735	8.0	3.315
1.16	0.2890	8.2	3.349
1.17	0.306	8.4	3.380
1.18	0.325	8.6	3.413
1.19	0.340	8.8	3.443
1.20	0.355	9.0	3.474
1.25	0.432	9.2	3.504
1.30	0.504	9.4	3.532
1.35	0.575	9.6	3.561
1.40	0.638	9.8	3.588
1.45	0.702	10.0	3.617
1.50	0.763	15	4.140
1.55	0.821	20	4.510
1.60	0.876	25	4.790
1.65	0.930	30	5.020
1.70	0.980	35	5.210
1.75	1.030	40	5.375
1.80	1.082	45	5.518
1.85	1.125	50	5.640
1.90	1.170	55	5.762
1.95	1.206	60	5.862
2.00	1.250	65	5.960
2.25	1.447	70	6.050
2.50	1.615	80	6.208
2.75	1.765	90	6.351
3.00	1.908	100	6.474
3.25	2.028	110	6.586
3.50	2.140	120	6.690
3.75	2.242	130	6.782
4.00	2.335	140	6.870
4.25	2.420	150	6.950
4.50	2.510	160	7.025

one common feature: the values of α_x decrease as the force and elongation increase. The important point, however, is that the only true value of α_x for a slashed yarn is that obtained quite late in the curve just before the yarn breaks.

V. CONCLUSION

A method has been derived for applying the Eyring theory of the three-element model to textiles which, although employing the conventional spring constants, does not necessitate the location of the basic spring line for the determination of the viscous constants. Instead the method involves the magnitude of the creep in constant rate of loading experiments or the magnitude of the relaxation in constant rate of elongation experiments. This simplification of the experimental technique makes the method available for the characterization of textile yarns in routine laboratory tests on the normal commercial yarn testers.

In addition, the apparent relationship between normal and slashed yarns has been brought forth, namely, that slashed yarns are merely normal yarns which have been kept in an apparently metastable stretched state by having been stretched while in a wet state and then dried.

The authors wish to thank Dr. J. H. Dillon, under whose direction the work described in this paper was carried out; The Office of the Quartermaster General, Research and Development Branch, who sponsored the work in part; the American Viscose Corporation, Front Royal, Virginia, who sponsored the experimental work on the yarns in their Research and Development Laboratory at Front Royal, and the technicians there who carried out the experimental work.

Errata: Infra-Red Spectra of Hydrocarbons. II. Analysis of Octane Mixtures by the Use of Infra-Red Spectra Obtained at Low Temperatures

[J. App. Phys. 18, 960 (1947)]

W. H. Avery and J. R. Morrison

THE following errors occurred in the above-mentioned article:

1. The statement was omitted that the work was a contribution of the Research Laboratories, Houston Refinery, Shell Oil Company, Inc.
2. In the abstract, "spactra" should be "spectra" in line 2, paragraph 2.
3. The second method of representing Eq. (11), page 965, should be deleted.

Method for the Absolute Measurement of Dynamic Properties of Linear Structures at Sonic Frequencies*

W. James Lyons and Irven B. Prettyman
Chemical and Physical Research Laboratories, The Firestone Tire and Rubber Company, Akron 17, Ohio
(Received January 20, 1948)

A full account, including the theoretical basis, is given of a method whereby the dynamic stretch modulus, coefficient of internal friction, and hysteretic energy loss of textile yarns and cords, composed of either continuous filaments or staple fibers, can be accurately determined at longitudinal vibration frequencies above 100 cycles/sec. The method, which employs electromagnetic excitation, is applicable also to glass cords, and metallic wires and cables. Results have been obtained at frequencies extending to above 300 cycles/sec. A concise description is given of the improved stretch vibrometer. Results on a typical cotton cord show that energy absorption by this instrument is negligible, permitting the calculation of an accurate internal friction coefficient, and absolute hysteretic loss. Measurements on eight natural and synthetic textile fibers reveal that the dynamic moduli range from 6.4×10^{10} dynes/cm^2 for Velon monofil to 32×10^{10} dynes/cm^2 for a ramie cord. The dynamic moduli of Fiberglas and steel cords are found to be 54 and 106×10^{10} dynes/cm^2, respectively. The internal friction coefficients are found to vary hyperbolically with frequency: in a 11/4/2 cotton cord, for example, from 16 to 3×10^6 poises between frequencies of 60 and 320 cycles/sec.

INTRODUCTION

NUMEROUS investigations of the elastic and hysteretic behavior of a wide range of materials under the influence of cyclic stresses have been reported. Appreciably less copious however, is the literature on the dynamic properties of high polymeric materials under controlled conditions, particularly at sonic frequencies of cyclic stressing. The application of dynamic methods to the study of the properties of the organic high polymers is particularly fruitful, for the relatively large strains which are attainable are accompanied by technologically significant energy dissipation at the frequencies encountered in use. Thus, unlike the case of metals, where generally only small strains are tolerable for practical study, static measurements on high polymers have poor, or no predictive value for behavior under dynamic service conditions.

Of particular interest from the standpoint of dynamic elasticity and hysteresis are the textile yarns and cords (and their component fibers or filaments) that go into the composition of the mechanical fabrics. The outstanding example of this class of textiles is tirecord.

It is estimated that size 6.50×15 tires, on a typical passenger car traveling at 50 mi./hr., turn at the rate of about 11 rev./sec. This is the frequency with which the component cords are subjected to a cycle of loading, recovery, and compression. A cord, however, is not deformed continuously at a uniform rate during a single revolution of the tire, but is rapidly flexed when the section of the tire of which it is a part comes into contact with the pavement, or strikes an obstacle. It will be seen that the momentary rate of loading in this process (in which the elasticity of the cord has its greatest importance) is much higher than would be simulated by harmonic longitudinal vibrations at a frequency equal to the rotary speed of the tire. Evidently, an adequately simulative laboratory test should employ cyclic loading at rates on the order of hundreds of cycles per second. This conclusion applies even more pertinently to tests on cords destined for use in high speed bus and truck tires, where the dissipation of mechanical energy as heat has considerable significance.

The earliest dynamic measurements on high polymers in linear form were made by Meyer and Lotmar.[1] They employed a method involving the classical relation between the velocity of sound in a material, and its modulus of elasticity (Young's). They were able to compute crude values for the moduli of various synthetic filaments and films at acoustical frequencies. Using

* Presented at the Fifth Meeting of the Division of High-Polymer Physics, American Physical Society, Chicago, Illinois, December 29–30, 1947.

[1] K. H. Meyer and W. Lotmar, Helv. Chim. Acta 19, 68 (1936).

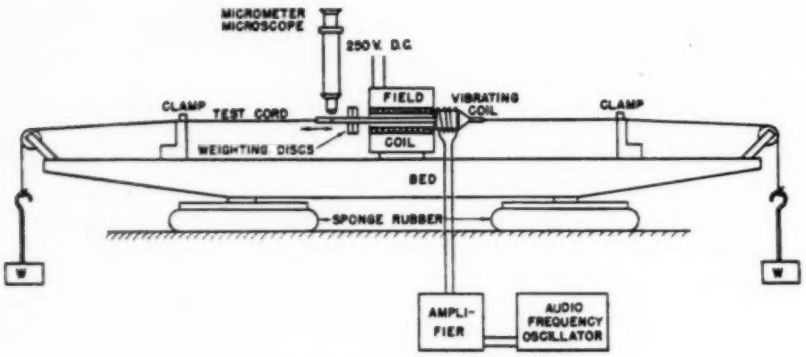

FIG. 1. Schematic diagram of stretch vibrometer and auxiliary equipment.

the same sound velocity principle, Ballou and Silverman[2] greatly refined the method by the introduction of piezoelectric driving and pick-up devices. They obtained the dynamic moduli of continuous rayon and Nylon filaments, and cellulosic films. Neither of these investigations contemplated in principle the measurement of concomitant hysteretic losses. More recently Nolle[3] has adapted the Ballou and Silverman technique to a theory which involves the measurement of acoustic attenuation. From the results he is able to compute the "viscous part of Young's modulus," as well as the conventional modulus, of thin rubber-like strips. Continuing work on the same technique, Ballou[4] has introduced attenuation measurements into the study of the dynamic properties of textile filaments.

While the foregoing method has been developed to the point where some measure of the dissipation of energy in high polymeric filaments and strips, longitudinally vibrated at sonic frequencies, is possible, the method is restricted to continuous test specimens and to yarns of very low twist. A method adaptable to staple fibers, and to high twist yarns and cords was, however, employed by Wakeham and Honold,[5] but with a low frequency: 1 cycle/sec. They measured the dynamic stretch modulus and hysteresis in cotton, rayon, and Nylon tirecords.

In June, 1947 the present authors[6] announced a method by which successful measurements of the elastic moduli were made on cotton, rayon, and Nylon cords forcibly vibrated longitudinally at frequencies above 100 cycles/sec. by electromagnetic means. Measurements of relative indices of hysteresis loss in the three samples were also reported. The method is applicable to: (a) organic continuous filaments and film strips, (b) glass and metal wires and cords, (c) high twist yarns and cords, coated and uncoated, and (d) yarns and cords composed of staple fibers, e.g., cotton, spun rayon, etc. Further studies and modifications in the apparatus have been undertaken with a view to improving the confidence which could be placed in the measurements of the internal friction term and the hysteresis as genuine properties of the test sample. As will be shown, it is now possible by means of the present apparatus to obtain the *absolute* value of the energy absorption (hysteretic loss) and a reliable value for the coefficient of internal friction, as demonstrated by data on a cotton cord sample.

THEORY OF THE METHOD

From the standpoint of the pure dynamics the phenomena of major interest in this experiment is the behavior of the vibrating element in the apparatus. Cognizance is taken of the properties of the test specimen only because they exert a damping influence on the motion of this element. The equation of motion of the element is:

$$m(d^2s/dt^2)+b(ds/dt)+(E/q)s=F\cos\omega t, \quad (1)$$

where m is the vibrating mass; s is the displacement from the equilibrium position; b is the damping factor; E is the dynamic stretch modu-

[2] J. W. Ballou and S. Silverman, Textile Research **14**, 282 (1944); *ibid.*, J. Acous. Soc. Am. **16**, 113 (1944).
[3] A. W. Nolle, J. Acous. Soc. Am. **19**, 194 (1947).
[4] J. W. Ballou, The Fiber Society Meeting, Princeton University, September 5, 1947.
[5] H. Wakeham and E. Honold, J. App. Phys. **17**, 698 (1946).
[6] W. J. Lyons and I. B. Prettyman, J. App. Phys. **18**, 586 (1947).

lus; q is the shape factor of specimen; F is the amplitude of applied force having frequency $\omega/2\pi$. Equation (1) has been applied to high polymers at sonic frequencies by Gehman, Woodford, and Stambaugh,[7] who studied compressive vibrations in flat cylinders of rubber, and by Dillon, Prettyman, and Hall,[8] who studied shear vibrations in similar specimens. The assumption in Eq. (1) is that the damping forces are proportional to the velocity.

The dissipative forces represented by the factor b may, *a priori*, be considered as arising in the vibration of the instrument, in the turbulence of the air about the vibrating coil, etc., as well as in the internal friction of the test specimen. It is important that the latter be identified, for the numerical values which are finally computed should be preferably physical constants of the test specimens only. To facilitate the analysis of the distribution of dissipated energy between specimen and external elements, a binomial damping factor has been introduced. Equation (1) thus becomes

$$m(d^2s/dt^2)+[(\mu/q)+J](ds/dt)+(E/q)s=F\cos\omega t, \quad (2)$$

where μ is the coefficient of internal friction in the test specimen,[9] and J is the coefficient of instrumental damping. The shape factor q is equal to $L/2A$, where L is the free length of each matched piece of filament or cord, and A is the cross-sectional area (exclusive of interstices between fibers in yarns and cords).

For the steady-state solution of Eq. (2), well-known conventional methods lead to:

$$s=\frac{qF}{[(E-qm\omega^2)^2+\omega^2(\mu+qJ)^2]^{\frac{1}{2}}}\cos(\omega t-\phi), \quad (3)$$

where ϕ is the phase angle. Differentiation of the denominator in the right-hand side of this equation yields, for the conditions of maximum amplitude which defines resonance,

$$E=qm\omega_0^2+\frac{(\mu+qJ)^2}{2qm}, \quad (4)$$

where ω_0 is the resonant angular velocity. Numerical results indicate that $(\mu+qJ)^2/2qm$ is negligible in comparison with $qm\omega_0^2$. Thus we may place

$$E=qm\omega_0^2, \quad (5)$$

and obtain for the maximum amplitude of resonance:

$$s_m=\frac{qF}{\omega_0(\mu+qJ)}. \quad (6)$$

Now, integration of the work of the damping or frictional forces over a complete cycle, yields for the total damping energy per cycle in the *system*:

$$R=[(\mu/q)+J]s_m^2\omega_0\pi. \quad (7)$$

From Eq. (6):

$$(\mu+qJ)/q=(\mu/q)+J=F/\omega_0 s_m. \quad (8)$$

Accordingly, R may be expressed independently of the damping factor:

$$R=F/(\omega_0 s_m)\cdot s_m^2\omega_0\pi=Fs_m\pi. \quad (9)$$

It is to be noted that, as a mathematical function, R here is independent of the length L, but

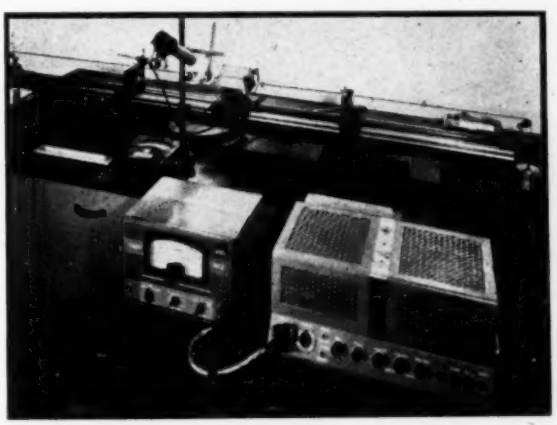

FIG. 2. General view of stretch vibrometer assembly, showing oscillator and amplifier in foreground, with vibrometer proper and micrometer detecting unit in background.

[7] S. D. Gehman, D. E. Woodford, and R. B. Stambaugh, Ind. Eng. Chem. **33**, 1032 (1941); *ibid.*, Rubber Chem. Tech. **14**, 842 (1941).

[8] J. H. Dillon, I. B. Prettyman, and G. L. Hall, J. App. Phys. **15**, 309 (1944); *ibid.*, Rubber Chem. Tech. **17**, 597 (1944).

[9] The quantity represented by μ has been called the "coefficient of viscous traction" by F. T. Trouton, *Proc. Roy. Soc.* (A), **77**, 426 (1906), "normal coefficient of viscosity" by W. Rosenhain, *Int. Crit. Tables*, **5**, 6 (1929), and "longitudinal viscosity" by Wegel and Walther, Physics, **6**, 141 (1935). However, while μ has the dimensions of "viscosity," there appear to be objections to its being identified as such.

depends on the displacement s_m (which has the dimensions of *length*). Energy considerations permit R to be written also:

$$R = R_i + H, \tag{10}$$

where R_i = energy loss/cycle in the instrument, etc., and H = total hysteretic loss/cycle in the whole test specimen. It is to be expected that H is directly proportional to the vibrating length of filament or cord L, since, on the average, the *strain* in each unit length is duplicated by that in every other unit length. Thus, from the physical point of view R is a linear function of L, and a graph of $R = Fs_m\pi$ against L should yield a straight line intercepting the R axis. Anticipating a possible frequency dependence in the response of all the damping agents, the graphing is to be done at a selected fixed frequency. The R intercept ($L = 0$) will give the value of the energy loss per cycle in the apparatus, i.e., R_i, at the particular frequency.

From the definitions and Eqs. (7) and (10) it is apparent that

$$R_i = Js_m^2\omega_0\pi, \tag{11}$$

and thus, at any selected L, the hysteretic energy of the specimen can be calculated from observed quantities by means of the relation:

$$H = (\mu/q)s_m^2\omega_0\pi = Fs_m\pi - R_i. \tag{12}$$

The energy loss per cycle per unit volume, the so-called *hysteretic constant* of the test specimen is given by:

$$H_c = H/2AL = (Fs_m\pi - R_i)/2AL. \tag{13}$$

From Eq. (12) we obtain also the relation for the coefficient of internal friction:

$$\mu = \frac{q(Fs_m\pi - R_i)}{s_m^2\omega_0\pi}. \tag{14}$$

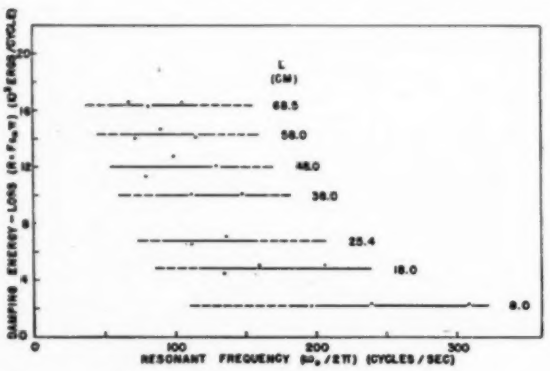

FIG. 3. Total damping energy loss per cycle for various resonant frequencies, with 11/4/2 cotton cord on vibrometer.

While the development in the foregoing paragraphs has been generalized to embrace the calibration of extraneous damping losses, and thereby lead to absolute values for the physical constants of the test specimens, in actual experiments thus far conducted with the improved apparatus, the instrumental energy loss R_i has been found to be immeasurably small compared to H. The equations for H, H_c, and μ remain applicable, with the condition that, for these experiments, $R_i = 0$.

EXPERIMENTAL METHOD

The apparatus has remained essentially as originally described.[6] The bed which was used on the stretch vibrometer proper in the preliminary experiments has been replaced by a heavy, iron, optical bench, 2 meters in length. This is securely bolted at points midway between the center and the ends of the bench to steel plates 30.5 cm by 61.5 cm by 1.3 cm thick. Each plate rests upon a sponge rubber pad. The supports, in which the two pieces of the specimen are securely clamped at the outer ends of their vibrating lengths, have also been made more massive and are rigidly fastened to the bed. These steps were taken to increase the inertia of the instrument, and thereby minimize its contribution to the damping. The vibrometer in its present form is shown schematically in Fig. 1, while a photographic view appears in Fig. 2.

The electromagnetic field coil, obtained from an early model radio loud-speaker, is mounted at the middle of the top face of the bed. Through an axial hole in the core passes a phenolic plastic rod on one end of which is mounted a lightweight coil 3.5 cm in mean diameter, and having 50 turns of No. 27 (B. and S. ga.) copper wire. The rod is supported freely in the core by the pieces of test cord attached coaxially at each end. Each piece of cord passes over the clamp support and thence to a pulley, from which it supports a load of weights. The static loads balance each other and allow the cords to be placed under tension without displacing the rod and attached coil. Before vibration is started the

clamps are tightened on the test pieces while they are still under tensile stress. This feature of the preparation for an experiment was adopted for positive avoidance of motion in the test cords beyond the outer ends of their *free* lengths.

With a direct current passing through the electromagnetic unit, the small coil is in a strong magnetic field, so that when an alternating current is sent through the latter coil the axial rod vibrates longitudinally as a unit, producing, in phase, periodic extensions and contractions in the test pieces. A static calibration, using known weights attached to the axial rod, established the relationship between the impressed force F and the current through the vibrating coil. This relationship, as in similar calibrations by others,[7,8] was found to be accurately linear. A calibrated micrometer, focused on a mark on the vibrating rod, has been used exclusively in the improved instrument to measure the amplitude of vibration s_m, which, in the present experiments, ranged from ± 0.01 to ± 0.08 cm. By means of circular plastic disks, which can be slid over one end of the rod, the vibrating mass may be varied, thus permitting alteration of the resonant frequency without changing the specimen length.

The vibrating coil is energized by a 50-watt power amplifier, controlled by a conventional oscillator unit providing a wide, continuous selection of audiofrequencies. Observations on a cathode-ray oscillograph, connected into the circuit periodically, established the essentially sinusoidal character of the voltage applied to the vibrating coil.

RESULTS

The technique outlined in the theoretical section above has been applied in an extensive study of typical performance of the improved stretch vibrometer, using a raw cotton tirecord of 11/4/2 construction. Static tests on this sample (conditioned at 65 percent R.H., 70°F.) indicated a breaking load of 8.5 kg (18.7 lb.) and an ultimate elongation of 14.3 percent. The present experiment was conducted with the test pieces under an initial tension of 2.0 kg, with an ambient temperature of 25°C (76–78°F) and relative humidity of 50–53 percent.

The cross-sectional area of the sample was determined from the weight of a 200-cm specimen and the bulk density of cotton: 1.5 g/cm³. Included as part of the vibrating system in the calculations was half the mass of the free length of each test piece. It has been repeatedly found that the uniformity of this cord sample is such that replacement of one specimen length by another yields, under identical experimental conditions of load, length, etc., the same response as to frequency and amplitude, within the limits of precision of the instrument.

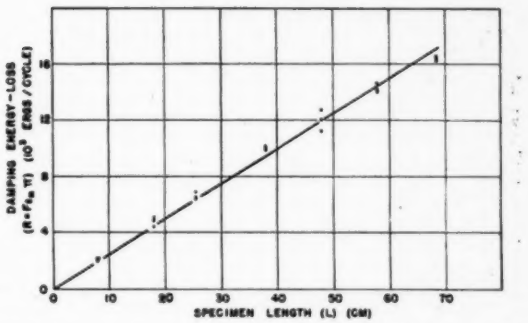

FIG. 4. Total damping energy loss per cycle as a function of free length of a single specimen. Data are from graph of Fig. 3.

Instrumental Damping

Measurements were made with seven different free lengths L and, with each length, 3 different masses for the vibrating system (except for two cases: $L = 25.4$ and 38.0 cm, where data involving only 2 masses were obtained). In accordance with Eq. (5) the resonant frequency $\omega_0/2\pi$ was found to change with changes in cord length and vibrating mass. However, when R was calculated according to Eq. (9) it was found that R was independent of frequency within the limits of experimental error. The results are shown graphically in Fig. 3. The fact that in the frequency range of this experiment R is substantially independent of frequency is in accordance with the ideal case, as summarized by Eq. (9). This could not, however, have been anticipated without prior information on the vibration characteristics of the instrument. The independence of R and ω_0, shown in Fig. 3, implies that the present vibrometer is not responding perferentially to any of the frequencies employed.

In Fig. 4 values of R which appeared in Fig. 3 for the various cord lengths are plotted against

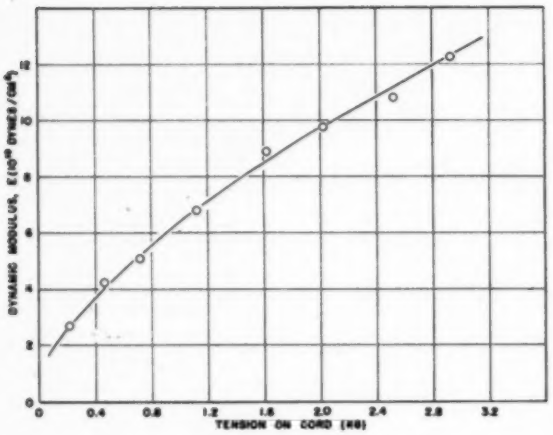

FIG. 5. Effect of initial static tension in cord on the dynamic modulus of 11/4/2 cotton cord at 76°F and 21 percent R.H.

these lengths. Had R shown frequency dependence it would have been necessary to take interpolated values of R at some selected frequency, but in view of the present data, the relation represented by Fig. 4 may be said to hold over the frequency range 60 to 320 cycles/sec. The graph confirms the expectation that R is a linear function of L, and reveals furthermore that the extraneous damping energy R_i is immeasurably small, for the graph practically passes through the origin. The various values of R at each L are insufficiently concentrated to permit reliable extrapolation to zero length to evaluate R_i precisely. The data do, however, indicate that R_i may be placed equal to zero without introducing into the calculations of H_e and μ an error of more than 1 percent for the greater cord lengths or more than 2 percent for

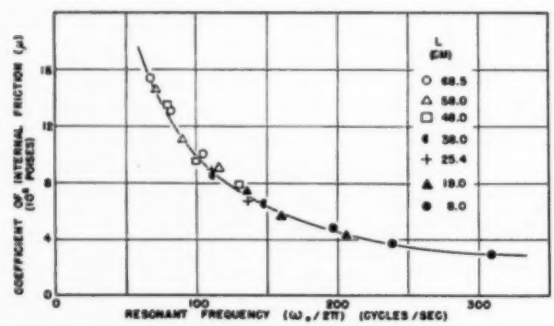

FIG. 6. Coefficient of internal friction of 11/4/2 cotton cord as a function of the frequency of longitudinal vibration, for seven different free lengths of cord.

the shorter cord lengths, for samples similar to the present cotton cord in hysteretic properties.

Hysteresis in Sample

From the data of Fig. 4, taking $R=H=Fs_m\pi$, and remembering that the total length of cord is $2L$, we obtain for the hysteretic energy loss per unit length of cord per cycle: 125 ergs/cm-cycle. Applying Eq. (13), with $A=3.15\times10^{-3}$ cm², we obtain the corresponding loss for unit volume: $H_e=4.0\times10^4$ ergs/cm³-cycle. Referred to unit mass of cord this hysteretic loss amounts to 2.6×10^4 ergs/g-cycle. For a dry 18/4/3 cotton cord after 1000 cycles, Wakeham and Honold[5] found for this quantity the value 2.12×10^5 ergs/g-cycle. Each of these values, however, is descriptive only of the particular experiment under which it was obtained. The hysteresis loss may be expected, on quite general grounds, to depend on the strain amplitude; this inference is confirmed by Eq. (12). Evidently hysteresis values for different samples (or even different specimens of the same sample) are comparable only if obtained under uniform conditions of, at least, strain and frequency range.

Dynamic Stretch Modulus

For each of the 19 different combinations of specimen length and vibrating mass involved in the foregoing experiment, values of the dynamic modulus E were calculated, ranging from 9.6 to 10.7×10^{10} dynes/cm². The dispersion of values cannot be correlated with any known quantity; the results confirm E as a property sensibly independent of L and m, as should be required of a material constant. The mean value of E is 10.2×10^{10} dynes/cm², which is to be associated with the previously mentioned tensile load of 2.0 kg.

That the modulus is dependent on the tension in the test specimen is shown by the graph of Fig. 5. These data were obtained with a constant vibrating mass m and cord length L (25.4 cm), but with various initial static loads. The change in load is reflected in a change in resonant frequency $\omega_0/2\pi$, with the result that E as given by Eq. (5), varies. It is seen that the modulus E increases with load, as was found by Meyer and Lotmar for continuous filaments.

In the vicinity of 1.2-kg load, E has a value of 7×10^{10} dynes/cm². This value differs by 10 percent from that obtained in our previously published experiment[6] on the same sample under the same tensile load. Wakeham and Honold found cotton cords of other constructions to have moduli lying in the range 2.5 to 5×10^{10} dynes/cm², the higher values being attained gradually as vibration was prolonged into thousands of cycles.

Coefficient of Internal Friction

Taking $R_i=0$, Eq. (14) reduces to

$$\mu=qF/s_m\omega_0. \tag{15}$$

Using this equation, and the data obtained in the study of damping effects at 7 different specimen lengths, coefficients of internal friction have been calculated. In Fig. 6 these values are plotted as functions of resonant frequency $\omega_0/2\pi$.

TABLE I. Dynamic properties of various cords, yarns, and filaments as measured on stretch vibrometer.

Fiber	Sample Construction	Dynamic measurements: Dynamic modulus, E (10^{10} dynes/cm²)	Internal friction, μ at 180 cycles/sec. (10^6 poises)	Temperature (°C)	Relative humidity (%)
Cotton	11/4/2	10.2	5.2	25	51
Viscose rayon	1100/2	15.2	4.0	21	52
Nylon	210/3/3	8.7	2.3	23	51
Du Pont Fiber V	75/16/2	10.9	3.1	21	69
Du Pont Fiber A	300-den. yarn	16.4	8.9	21	68
Vinyon N	300-den. yarn	10.6	4.0	22	64
Velon	0.012-in. monofil	6.4	10.0	21	64
Ramie	3-ply cord	31.9	7.5	21	64
Fiberglas	7-ply cord	53.9	11.3	21	65
Steel cord	6×3×0.0058 in.	106.2	—	21	50

It will be seen that (a) the μ-*vs.*-ω_0 relationship is independent of L, and (b) the coefficient μ is a hyperbolic function of ω_0. The latter relation, which is not anticipated by dynamic theory, may be expressed

$$(\mu+\alpha)(\omega_0+\beta)=\text{constant}, \tag{16}$$

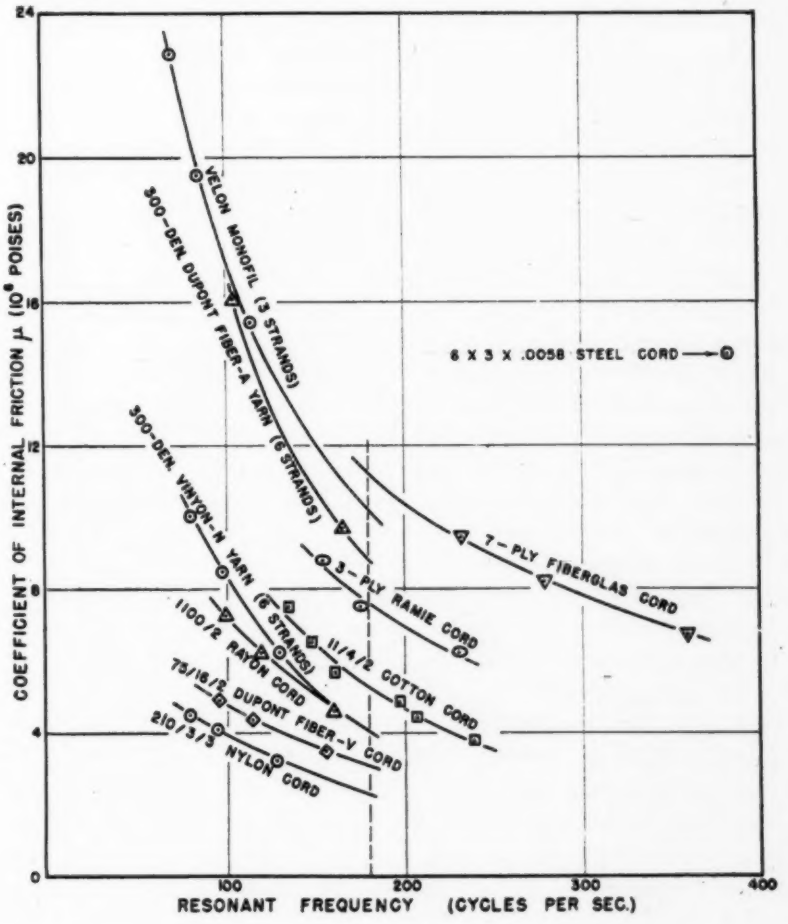

FIG. 7. Coefficient of internal friction of various linear structures as a function of frequency; all, except the steel cord, under a tension of 2.0 kg. The free length of specimen was 25.4 cm.

where α and β are empirical constants. The product $(\mu+\alpha)(\omega_0+\beta)$ has the dimensions of the *hysteresis index* which has been used to characterize the internal friction of elastomers.[8]

Other Filamentous Materials

Following the above study of the improved model of the vibrometer, using the cotton sample, dynamic measurements were repeated on the same rayon and Nylon samples for which results were previously published,[6] and have been extended to a number of other materials in linear forms. The general techniques described for the cotton cord experiments were employed here also. In Table I are given mean dynamic moduli E determined at two or more frequencies on each of nine textile samples and at a single frequency on a steel-wire sample. The frequencies are indicated in Fig. 7. As in the case of cotton, no consistent dependence of the modulus on frequency was detected in the frequency range employed. A uniform tensional load of 2.0 kg was applied to all samples except the steel cord, on which 2.9 kg was used. The difference in tension in the test pieces in the two sets of experiments is believed to account (as in the case of cotton) for the differences between the present moduli for rayon and Nylon and those previously reported.

In Fig. 7 are shown the coefficients of internal friction μ of the samples listed in Table I as a function of resonant frequency. In order to facilitate comparison at a single centrally located frequency, interpolated or extrapolated values of μ at 180 cycles/sec. have been read from Fig. 7 and entered in Table I. The present internal friction coefficients derived for cotton and rayon differ from those found previously, while that of Nylon is in good agreement. The differences are accounted for quite well by introducing the dependence of internal friction on frequency, tension, and strain-amplitude.

The value of E in Table I for viscose rayon cord falls between those for air-dry (11.5×10^{10} dynes/cm^2) and oriented (33×10^{10} dynes/cm^2) viscose filaments, reported by Meyer and Lotmar, and is within the range (9 to 18×10^{10} dynes/cm^2) reported by Ballou and Silverman for textile viscose. It is lower by from 25 to 50 percent, than that found by the latter workers for "Cordura" tirecord yarn, though the filaments in both rayons are presumably oriented viscose. The difference, however, is in the sense which would be expected as a result of the twisted construction of the cord. The present dynamic value of E for Nylon is in excellent agreement with those of Ballou and Silverman on drawn Nylon at low elongations. The relatively high value for E for ramie cord, in Table I, reflecting the intrinsic stiffness of the component fiber, is in agreement with Meyer and Lotmar's findings on ramie single fibers. As between similar textile forms no comparisons of the present results on ramie or cotton at sonic frequencies can be made, since previous methods have not allowed measurements at such frequencies on yarns or cords composed of staple fibers.

CONCLUSIONS

The method described herein appears to be readily adaptable also to the study of the dynamic properties of high polymer films if these can be obtained in strips. While exploratory tests indicate that the highly extensible elastomers of low modulus present special problems, these do not appear insuperable. Observations have been made on a solid steel wire, but repeated rupture of the test specimen at resonance has precluded thorough measurements being made. It is expected, however, that the problem is one of a mastery of sufficiently refined technique. When this is achieved, the method may be applicable to the study of the longitudinal dynamic properties of metals and alloys, in the form of wires or ribbons. The method is, however, especially suitable to the study of textile yarns and filaments. The ultimate application of results in this field, to the elucidation of structure, mechanical behavior, and energy relations at the molecular level, in new as well as old linear high polymers, is foreseen.

The cooperation of numerous members of the Firestone Research Staff, and in particular Dr. J. W. Liska, in facilitating execution of this project, is gratefully acknowledged.

Regular Contributed Original Research

Electric Field Intensity Inside of Natural Clouds

Ross Gunn
Division of Physical Research, U. S. Weather Bureau, Washington, D. C.
(Received November 10, 1947)

Measurements of the electric field on the surface of aircraft flying through all types of weather and clouds are summarized. The measured electric field inside a thunderstorm just prior to a lightning strike at 12,900 feet was 3400 volts/cm. The average maximum field for 9 different thunderclouds was 1300 volts/cm. It is noted that large fields usually occur only inside the cloud and at altitudes somewhat comparable to the freezing level. Frequent reversals of the field are observed in these areas. The electric field measured inside a stable non-precipitating cloud is less than 10 volts/cm.

DURING the war years radical ideas and surprising data have been presented concerning the electrical fields to be expected inside of various types of natural clouds. For example, as a result of numerous sounding balloon flights in thunderstorms, G. Simpson and G. D. Robinson[1] "are led to the conclusion that the fields in a thundercloud are of the order of 100 volts/cm except in relatively small regions where there is great electrical activity in which lightning discharges originate." On the other hand, an interesting theoretical paper by J. Frenkel[2] concludes that in an ordinary quiescent cloud; "The sinking of the drops under the influence of gravity leads to a polarization of the cloud (producing a) steady field . . . of the order 30–150 volts/cm."

In view of the mass of earlier data concerning the characteristics of lightning, it is somewhat disturbing to learn that thunderstorm electric fields are small compared to the dielectric strength of air, while the fields in a simple cloud are expected to be of the same order of magnitude. It seems evident that further reliable observational data on the electric fields measured inside various clouds are necessary. It may be stated in advance that neither of the conclusions above cited is consistent with the experience of the research team of the Army-Navy Precipitation Static Project. This project was organized during the war to investigate an unusually serious aircraft operating problem occurring only in bad weather. Its air operations team made hundreds of flights with well instrumented aircraft through all types of clouds and thunderstorms. That these flights encountered a fair sample of all types of weather is attested by the fact that the project airplanes were struck by lightning three times in the course of the investigations.

The flying laboratories of the project, consisting of a B25 medium bomber and a B17 heavy bomber, carried numerous instruments especially developed for the study of atmospheric electric phenomena. The most valuable instrument used in the interpretation of the electrical state surrounding the aircraft was found to be an electric field meter that was designed to measure the electric field on the belly of the airplane just aft of the main wing.[3] This meter measures the sign of the electric field and is calibrated to give a full-scale deflection for 100, 400, 1000, and 4000 volts/cm according to the position of a selector. With two of these electric field meters mounted, for example, one on the belly and one on the top of the fuselage immediately above, it is possible to determine the magnitude of the vertical electric fields produced by clouds outside the airplane (exogenous fields) as well as the electric field caused by the accumulation of free charge on the airplane itself (autogenous fields). It is evident

[1] G. Simpson and G. D. Robinson, Proc. Roy. Soc. **A177**, 281 (1941).
[2] J. Frenkel, J. Phys. U.S.S.R. **8**, 285 (1944).
[3] (a) Ross Gunn, Phys. Rev. **40**, 307 (1932); (b) Waddel, Drutowski, and Blatt, Proc. Inst. Radio Eng. **34**, 161 (1946).

that a positive free charge deposited on and carried by the airplane will produce a radially outward field both on the top and bottom of the fuselage, while an exogenous vertical field produced by charges in adjacent clouds will be radially inward at the belly position and outward on top. Thus, the relative contributions of the autogenous and exogenous electric fields may be determined. For a discussion of the mechanisms responsible for the accumulation of free charge of a single sign on aircraft in flight and data exhibiting both types of electrification, the reader is referred to a summary report of the Precipitation Static Project.[4] It may be noted here that the unipolar charging of the airplane by its engine will build up surface fields of -7 volts/cm, while the particles in a haze layer over a city will frequently generate fields of -25 volts/cm, and dry crystalline snow occasionally produces fields up to -450 volts/cm by triboelectric action.

ORDINARY CLOUDS

It has been observed in clouds producing steady rain and showing inappreciable convective activity that the electric field produced within the cloud itself is *less* than 40 volts/cm.

In normal stable clouds without precipitation, the cloud electric field is *less* than 10 volts/cm.

In each case the value of the electric field is determined from simultaneous readings of the field meters mounted both on the top and bottom of the fuselage so that the values are independent of free charges carried by the airplane itself. It is seen, therefore, that flight observations do not support the theoretical estimates of Frenkel[2] but indicate rather, that quiescent clouds, considered as a whole, are substantially neutral.

THUNDERCLOUDS

In Fig. 1 is plotted the electrical field measured on the belly of the B25 airplane during a flight through an active thunderstorm on August 5, 1944, when it was struck by a bolt of lightning that produced considerable burning at its point of entry on the right wing tip and left the airplane at its nose. It is seen that the electrical field just prior to the instant of discharge was 3400 volts/cm. Two other peaks having opposite signs and of magnitude 2000 volts/cm were also observed. The field, averaged over a distance of 13 kilometers, approximated 700 volts/cm. In a thunderstorm explored on July 24, 1945, complete measures of the electrical field and charges

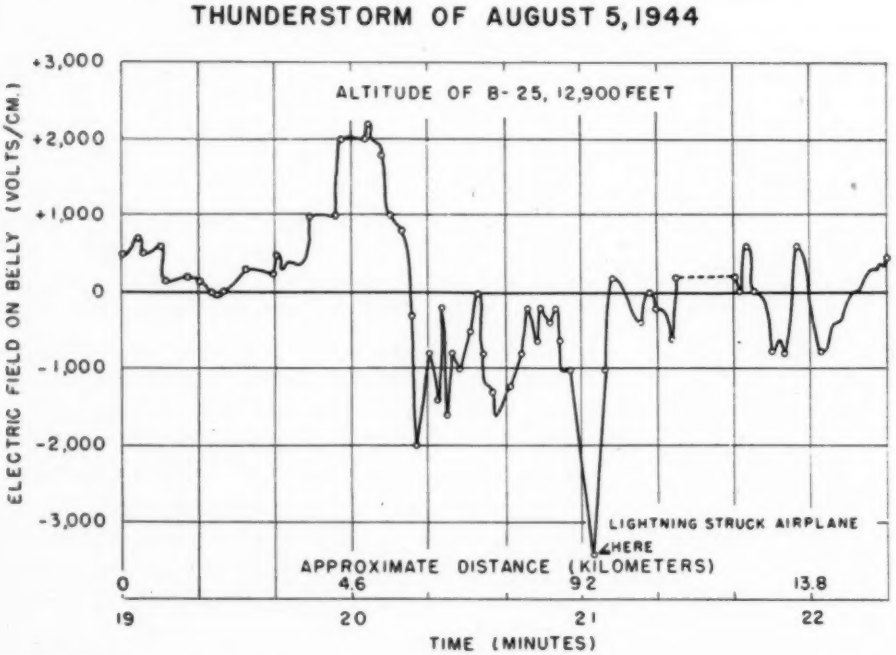

FIG. 1. Electric field intensity on the belly of a B25 airplane inside an active thundercloud.

[4] Ross Gunn, G. D. Kinzer, R. G. Stimmel, *et al.*, Proc. Inst. Radio Eng. **34**, 156 and 234 (April-May 1946).

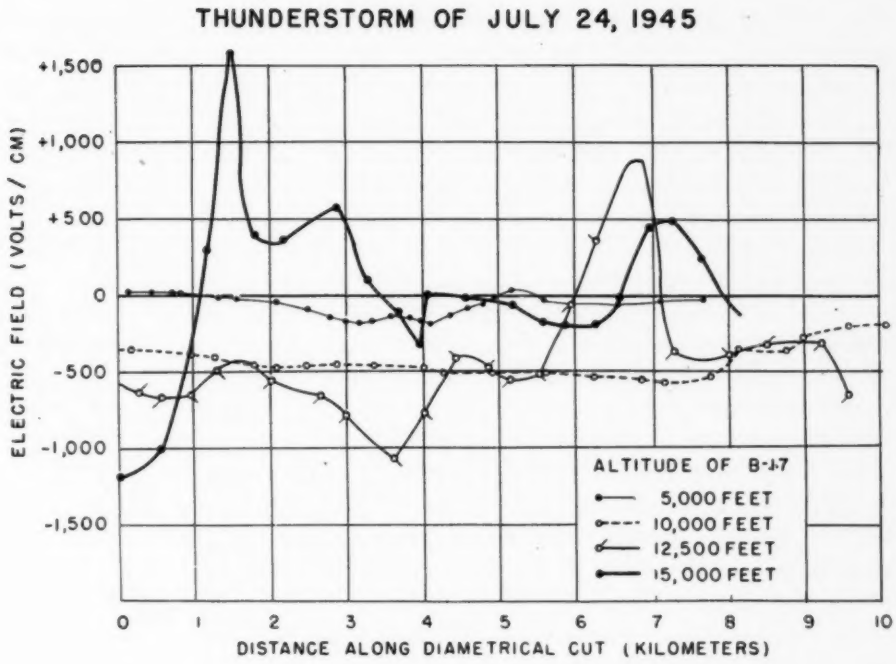

FIG. 2. Electric field intensity at various altitudes inside an active thundercloud.

on the precipitation droplets were made. The electrical field measured in successive traverses at 15,000, 12,500, 10,000, and 5000 feet is shown in Fig. 2. The freezing level was at 14,000 feet. These curves are thought to be reasonably typical and do not represent regions of unusually large electrical field because no lightning strikes were encountered. The data show that the electrical fields, particularly at altitudes near the freezing level, frequently approximate or exceed 1000 volts/cm. In a total of nine thunderstorms examined in 1944 by repeated flights through each one of them, the average maximum measured field was 1300 volts/cm. The laboratory airplane was struck in only one of these storms so that the numerical values may be thought of as representative.

The curves of Fig. 2 show that the electrical fields encountered are a maximum somewhere near the freezing level and decrease toward the ground. In evaluating the significance of this decrease of electrical field as the altitude becomes less, it should be emphasized that the research team has noticed in numerous flights through isolated thunderstorms that the electrical field from the towering cumulus cloud almost overhead does not extend much beyond the cloud itself, and large electrical fields are rarely measured until the airplane actually enters the cloud. Since the change in geometry from a position just outside and just inside the cloud is not great, we are led to the conclusion that during the period of charge accumulation the free charges are largely confined to the cloud itself or to its boundaries. This limitation of the largest electrical fields to actual cloud areas has been noticed and checked on several occasions. This shows that the free charge in a cloud is characterized for the most part by bipolar distributions. However, due to the difference in conductivity and discharge rates of free charge at high and low altitudes and to the intervention of lightning, residual free charges and electric fields necessarily co-exist.[5]

The alternating character of the electric field, as exhibited by Figs. 1 and 2, is of theoretical importance and emphasizes the hazards involved in drawing conclusions about the distribution of free charge in the atmosphere from electric field data collected at a single point.

The measured fields cited above may be converted to the electric fields existing within the cloud proper, but these values are subject to some uncertainty because the presence of the airplane distorts the electrical field within the cloud. It

[5] R. Gunn, Quart. J. Terr. Mag. and Atmos. Elec. **40**, 79 (March 1935).

may be recalled that the introduction of a conducting sphere oriented with its axis parallel to the original direction of a uniform electrical field, E_0, concentrates the lines of force in such a way that the field E on its surface is given by $E=3E_0\cos\varphi$, where φ is the colatitude. Thus, fields measured at the surface must be multiplied by factors ranging from $\frac{1}{3}$ upward in order to obtain the undistorted electric field intensity existing nearby. An airplane distorts the field in the same manner, but, because of its complicated geometry, the angular position between the original electrical field outside and the axis of the airplane must be precisely known before the correction factor can be specified. Model experiments have shown that if the electrical field is vertical and the airplane is in a normal flying attitude, the measured electrical field on its belly is 2.1 times the undisturbed electric field, but if the field has strong horizontal components, the measured value on the belly is considerably lower than the actual cloud field. With the object of determining the approximate magnitudes of the horizontal field intensity, each aircraft was provided with wing tip and tail dischargers,[4] insulated and connected through microammeters to the body of the airplane. The sign and magnitude of the current to each discharger was recorded simultaneously with the electric field meter data, and these permitted an estimate of the approximate direction of the external field intensity. As might be expected, the direction of the thunderstorm fields were seldom vertical, so that the field intensity values plotted in Figs. 1 and 2 may be considered as being generally less than the undisturbed field some distance away from the aircraft. For example, in the case of the lightning strike mentioned above the current to the right wing, one second before the strike, was -200 microamperes, while that to the left wing was $+200$ microamperes. This showed that strong horizontal components existed which directed the stroke into the right wing and out the nose. Thus, although the measured belly field intensity was 3400 volts/cm, its actual value in space was probably considerably greater.

It may be seen from the above data that the observed electric field intensities just prior to a lightning discharge are an appreciable fraction of the dielectric strength of air and of the order of 3000 volts/cm. There is no evidence to suggest that the electric fields approximate only 100 volts/cm or that they are limited to relatively small regions as suggested by Simpson and Robinson. Their method of measurement has already been criticized by S. K. Banerji[6] who thinks their electric fields should be multiplied by a factor of at least 20. The present observations are consistent with Banerji's point of view.

The author takes this opportunity to express his thanks and appreciation to the Army-Navy Precipitation Static research team for its excellent performance and devotion to the hazardous work partly outlined here.

[6] S. K. Banerji, Quart. J. Roy. Meteor. Soc. **64**, 221 (1938).

Apparatus for Weighing in Vacuum*

G. W. Monk
*Carbide and Carbon Chemicals Corporation,** Oak Ridge, Tennessee*
(Received October 22, 1947)

An apparatus is described which can be used to measure the weight of a sample in a vacuum (0.01 micron) at temperatures up to about 700°C. Typical preliminary results are given for the outgassing of aluminum, carbon, and "Teflon."

APPARATUS

THE weight of the test sample while under vacuum and at elevated temperatures is measured by means of an electrically operated chemical balance mounted in the same vacuum system. Figure 1 is a diagram of the apparatus used except for the pumps, valves, and gauges. A chain type balance with a maximum load of 200 grams and a sensitivity of 0.05 milligram is remounted so that the chain, rider, and beam-clamping mechanism can be driven by small 110 v reversible induction motors with gear boxes giving a shaft speed of about 6 r.p.m. The cam to operate the beam clamping mechanism and the tape pulley are coupled to their motors by means of short uncased flexible shafts while the rider moving fork is mounted on a balanced arm driven directly by the third motor. All grease was washed out of the gear boxes and from the moving parts of the balance mechanism so that a pressure of 0.01 micron was easily reached in the vicinity of the balance by means of a 4-inch oil diffusion pump. The motor leads were brought out through "Teflon" seals to a control box. When a weighing is desired the beam is brought to balance by means of the motors while observing the indicator and tape through the bell jar.

The sample is suspended on a platinum wire within the radiation furnace in the second vacuum system below. The two vacuum systems are separated by the high impedance baffle which contains a long hole just large enough to clear the support wire. This arrangement allows large pressure and temperature differences to exist between the two systems. Temperature measurements on dummy samples show that the temperature of the sample can be easily controlled up to about 800°C. The water-cooled baffle condenses the vaporized material from the sample and acts as a heat shield. With samples such as carbon or aluminum, the 8-inch diffusion pump maintains the pressure near the sample below 0.01 micron during operation. The samples are usually 5- to 10-gram cylinders with a small hole drilled near the top for the support wire.

PRELIMINARY RESULTS

To indicate one application of the apparatus and its sensitivity, some typical preliminary

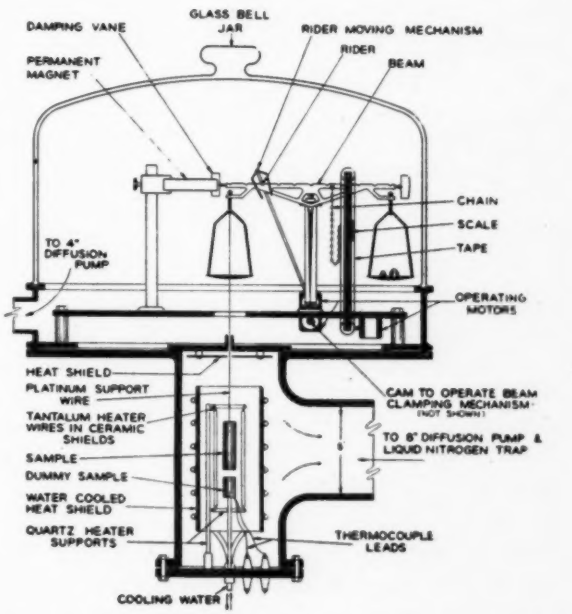

FIG. 1. Diagram of the equipment used in measuring the weight of materials under vacuum at elevated temperatures.

* This document is based on work performed under Contract No. W-7401-eng-23 for the Atomic Energy Project, and the information covered therein will appear in Division I of the *National Nuclear Energy Series* (Manhattan Project Technical Section) as part of the contribution of the Tennessee Eastman Corporation, Oak Ridge, Tennessee.
** Formerly with Tennessee Eastman Corporation, Oak Ridge, Tennessee.

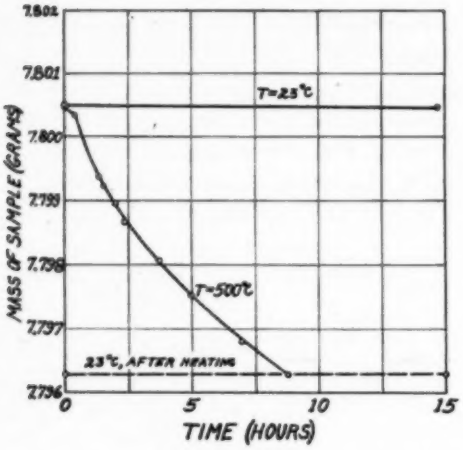

FIG. 2. Mass of an aluminum sample as a function of the time of outgassing at various temperatures. The cylindrical sample had a surface area of 1.96 in.²

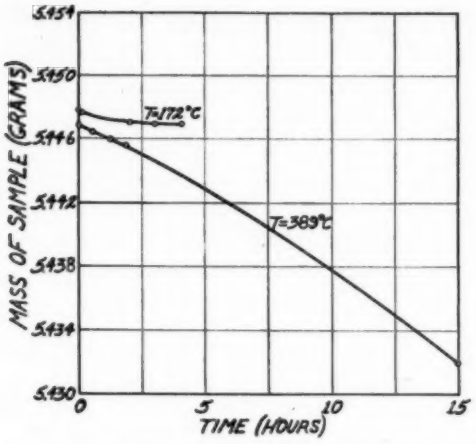

FIG. 4. Mass of a "Teflon" sample as a function of the time of outgassing at various temperatures. The rectangular strip had a surface area of 3.2 in.²

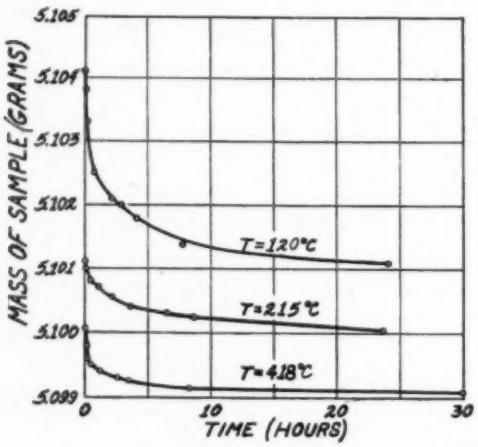

FIG. 3. Mass of a carbon sample as a function of the time of outgassing at various temperatures. The cylindrical sample had a surface area of 2.18 in.²

outgassing results are plotted in Figs. 2–4 in which corrections have been made for the buoyancy of the air. In all the curves time is measured from the start of evacuation or from the time of temperature change. Figure 2 shows the variation in weight of an aluminum cylinder at room temperature, 500°C, and again at room temperature after having cooled in vacuum. The sharp break in the 500° curve is due to an adjustment in the temperature after the run started. Figure 3 indicates the results for carbon in which case the vaporized material was apparently a surface contamination. The curves are not expotential, being of a much too rapid descent during the first few minutes. Cooling the carbon in air or vacuum, then reheating did not result in appreciably more outgassing until the original temperature was exceeded. Polytetrafluoroethylene (C_2F_4) or "Teflon" shows (see Fig. 4) no appreciable outgassing below 100°C but is objectionable above 200°C, and at 389°C chemical changes are occurring and large quantities of material are given off. At about 450°C the sample literally exploded and the rate of loss of weight became too great to measure. After about 30 seconds at this temperature, the sample was swollen to twice its normal size because of the many internal "explosions" and was apparently flecked with carbon throughout.

There are many other applications of this type of equipment since it is so rugged and easily operated. Absolute pressure measurements can be made by directly measuring the force between the hot and cold plates in a Knudsen type gauge. Pressures of 0.01 micron could be easily measured this way. The rate of flow of gases and vapors under very low pressures can be obtained by measuring the difference in pressure on the ends of a cylinder suspended in the stream. The vapor pressure of a great many materials could be studied at high temperature by observing their rate of loss of weight per unit area.

The work reported here was done during 1945 and declassified by the Atomic Energy Commission on September 12, 1947.

Ionosphere Reflections Recorded Mechanically by Means of a Repetition Frequency Converter

W. STOFFREGEN
Norwegian Defense Research Establishment, Bergen, Norway
(Received November 3, 1947)

A method of converting the high repetition frequency used by echo sounding to a lower value by means of a converter between the receiver and the recorder is described. The method is adapted to recordings of radio-echoes from the ionosphere, in which case the repetition frequency of 50 c/sec. of the pulse transmission after reception is converted into a repetition frequency of $\frac{1}{2}$–$\frac{1}{3}$ c/sec. before being supplied to the recorder. Ionosphere echoes having a delay of the order of milliseconds and a pulse width of about 20–100 μsec. may thus be recorded mechanically.

The principle of repetition frequency conversion described here may also find applications in recording ultrasonic or radar reflections.

WHEN recording echo reflections of radio waves, either ionosphere echoes in the h.f. band or echoes in the u.h.f. region ordinary in radar technique, one has to use cathode-ray oscillographs in order to delineate the echo pattern.

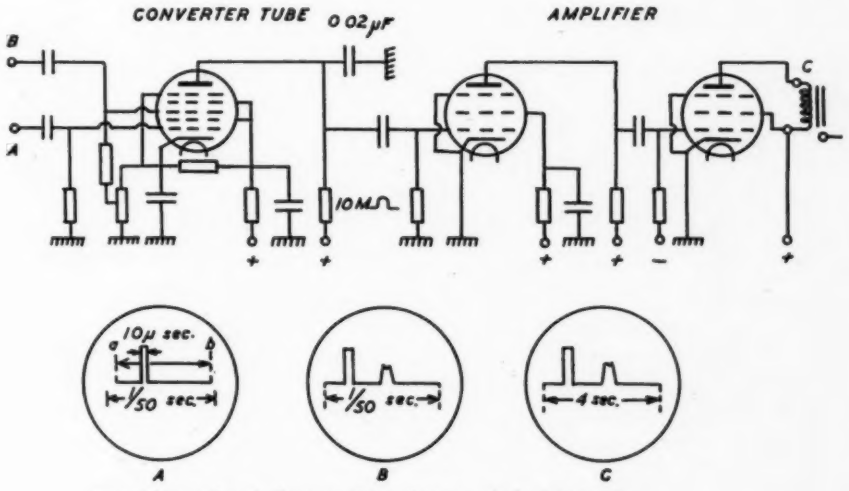

FIG. 1. Principle of frequency conversion.

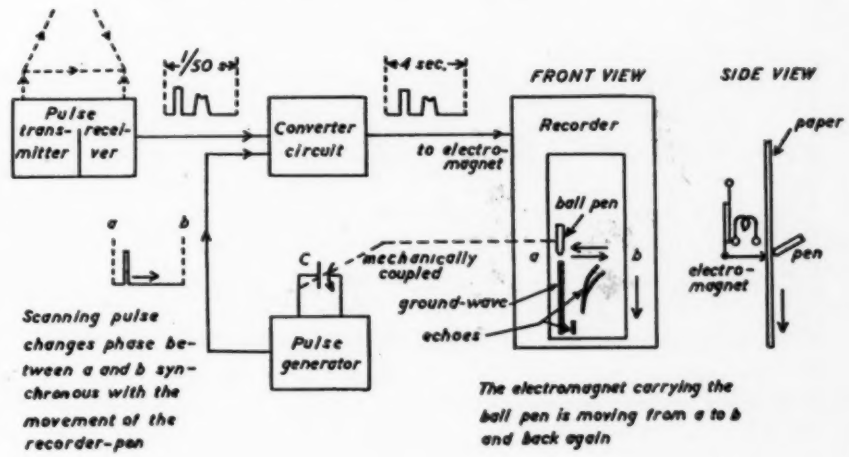

FIG. 2. Automatic ionospheric echo recorder supplied with repetition frequency converter. The mechanical echo recorder is shown to the right.

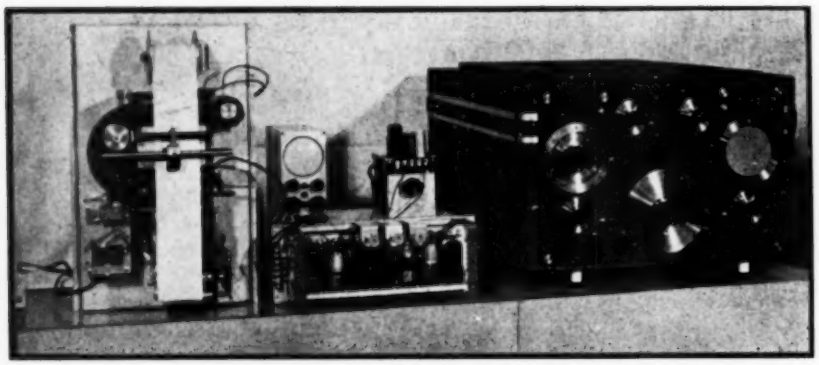

FIG. 3. The experimental arrangement.

In the routine work of ionospheric research the continuous photographic recording of echoes is of considerable importance. In order to obtain an instantaneous survey of the conditions of reflection it would be of value, however, to have available a method of recording the echoes directly, thus avoiding the process of photography. This would be possible if, by means of a suitable conversion process, one could reduce the high repetition frequency of the echo sounding to a lower value, thus making the use of a mechanical recorder possible.

It would seem obvious that such a frequency conversion method must be based on some application of the stroboscopic principle. The method here described is based on the principle

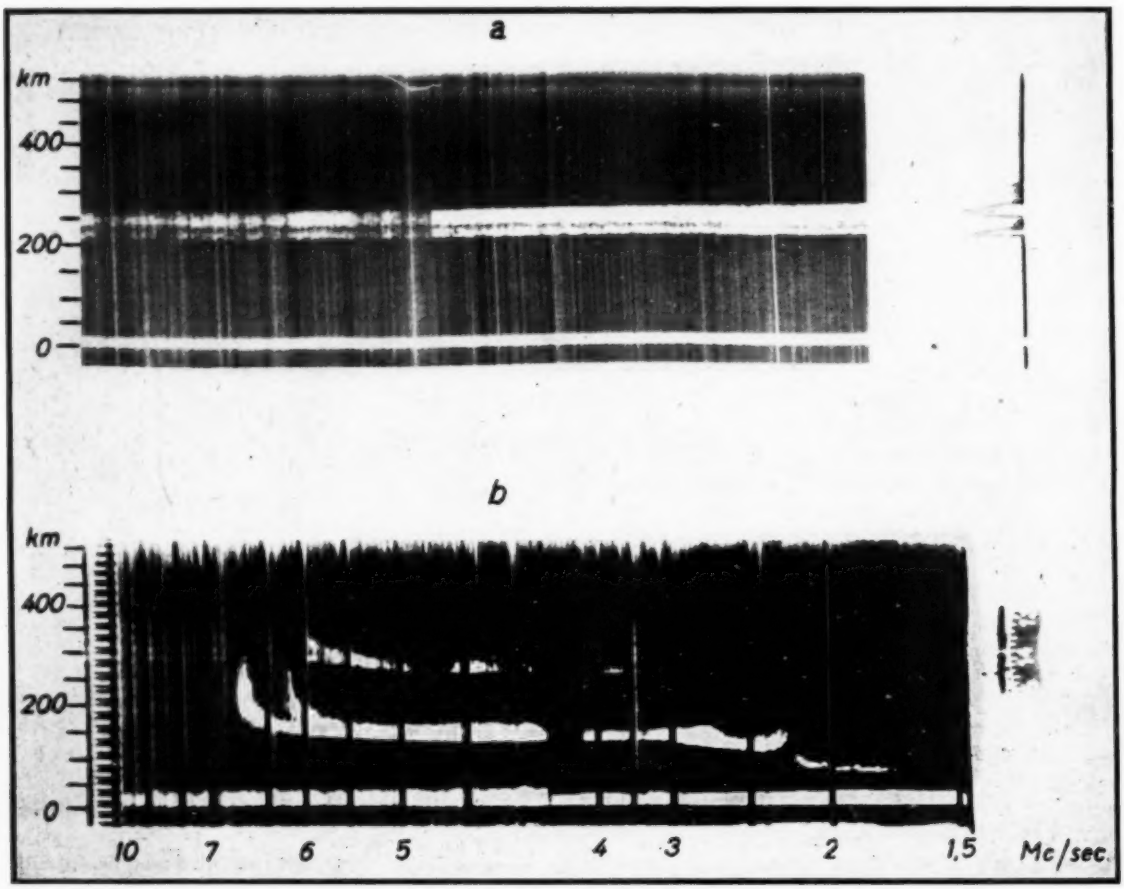

FIG. 4. Usual photographic records.

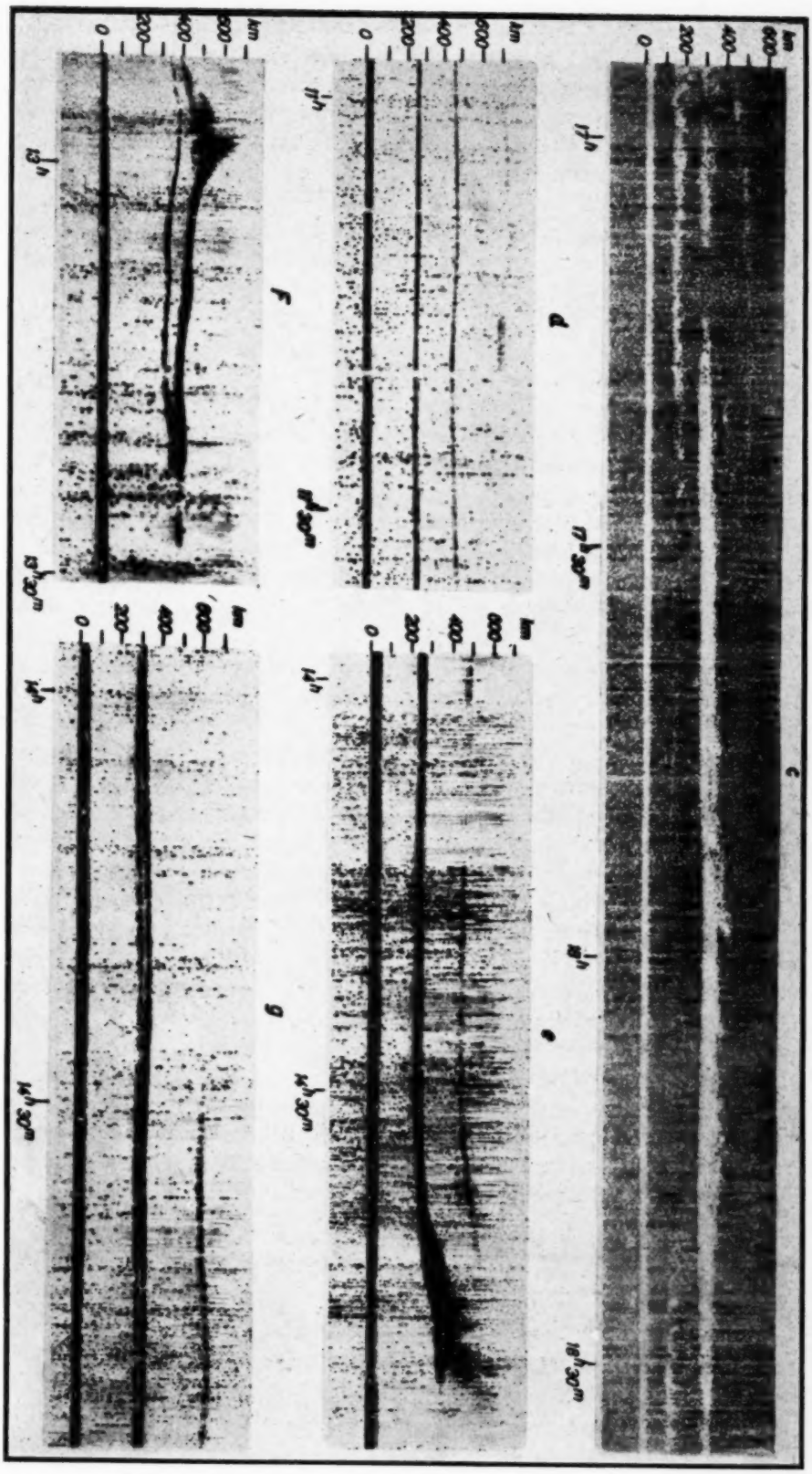

FIG. 5. Records produced by means of repetition frequency converter.

of scanning the echo pattern of a high repetition frequency by means of short pulses. The scanning pulse is periodically displaced along the sweep by means of a phase-adjusting device.

In order to obtain a detailed analysis of the echo pattern by means of the scanning pulse, it is of importance that the repetition frequency of the phase change is low compared with that of the pulses. The repetition frequency of the phase change, however, must not be so low that an appreciable change in the echo structure occurs during any single period. In the experiments described in the following, we have a repetition frequency of 50 c/sec. commonly used for ionosphere echo soundings. The period for scanning the sweep with the artificial pulse was 4 sec. According to this, 200 successive points along the sweep will be scanned. For a detailed analysis of the echo structure it is further evident that the width of the scanning pulse must be considerably narrower than the echoes appearing. In Fig. 1 the principle of the converter is shown. The echoes and the scanning pulse are coupled to the converter tube at A–B. The grid bias is sufficiently negative to prevent anode current when echo amplitudes or the scanning pulse appear separately. When echoes and scanning pulses coincide, the converter tube is operating. By means of the values of R and C indicated in Fig. 1 the converted pulses are smoothed. After amplification we thus obtain the ionospheric echo pattern indicated on B, this having a primary repetition time of 1/50 sec., slowed down to 4 sec. The phase variation of the scanning pulse is synchronized with the movement of the pen on the recorder, the scanning pulse thus being continuously displaced along the echo pattern during 4 sec.

In Fig. 2 is given a block diagram of an ionospheric echo recording apparatus with a repetition frequency converter unit attached.

The Institute's automatic echo recorder was used and supplied with a separate pulse generator and converter unit. The phase displacement of the scanning pulse was made by the condenser C, which was mechanically coupled to the horizontal displacement of the ball pen of the recorder (the latter being uniformly displaced from a to b in 4 sec.). The voltage pulses appearing when the scanning pulse slowly passes the echo amplitudes operate the electromagnet which presses the paper strip against the ball pen.

Figure 3 shows the experimental arrangement. To the left is shown the mechanical recorder, and in the center of the picture the converter circuit is seen, with monitor-oscilloscope and rectifier. To the right the portable automatic ionosphere recorder of the Institute is shown.

Figure 4 shows as a comparison two usual photographic records taken with the automatic ionosphere recorder. Figure 4a shows a record on fixed frequency; to the right of the record is a photograph of the pattern on the cathode-ray tube, showing the transmitter signal and reflections from the F layer. Figure 4b is a photographic P', f record taken with the same recorder.

Figure 5 shows examples of records made, with the new method, directly on ordinary writing paper. Figure 5c shows reflections from the E and F layers made on fixed frequency. The polarity on the pen-recorder is chosen so that the echoes appear white on a black background. The records shown in Fig. 5d–g are made with changed polarity so that echoes appear black on a white background. The reflections are from the F layer, and it will be seen that the records show well the details of the echo structure. The noise level was especially very high in Fig. 5e without distorting the record.

The author wishes to express his sincere thanks to Dr. Leiv Harang for facilities given during the development work.

Quantitative X-Ray Investigations on the Crystallinity of Cellulose Fibers. A Background Analysis

P. H. Hermans and A. Weidinger
*Laboratory for Cellulose Research of the AKU and Affiliated Companies, Utrecht, Netherlands**

(Received November 4, 1947)

A quantitative investigation of the intensity of scattered radiation in a series of native and regenerated cellulosic objects, including bacterial cellulose and fibers transformed into cellulose IV, is offered. The technique used involves the use of copper radiation monochromatized by reflection, specimens with randomized orientation of equal size and density, rotation of the plane film, and measurement of primary beam intensity by means of a device introduced by Goppel.

The procedure of evaluation consists of measuring integrated intensities of the crystalline peaks and that of the diffuse background. After correction of the latter for radiation scattered by air and for the background components due to Compton radiation and thermal scattering, as derived from exposures of sugar crystals and diamond, the diffuse background is represented by a curve exhibiting a flat maximum.

The height of this maximum was assumed to be a correct relative measure of the disordered portion and the total intensity of the coherently diffracted radiation of the crystalline peaks as a relative measure of the crystalline portion.

Within the series of native specimens the ordered and disordered fractions are found to be equal in cotton, cotton linters, ramie, and flax fibers. In woodpulp the disordered fraction is slightly higher and in bacterial cellulose considerably higher.

Within a series of rayons, including slightly and highly orientated viscose rayons, Cellophane, Lilienfeld rayon, and cuprammonium rayon, the ordered and disordered fractions were also found to be equal. Slightly less disordered substance is found in Fortisan, in mercerized ramie and in specimens where cellulose II has been transformed in cellulose IV by a heat treatment.

It is shown that the relative proportions of the fractions of disordered substance, for all objects investigated, are in satisfactory quantitative agreement with those deduced from the sorptive capacity for water vapor.

The absolute percentage of the crystalline portion calculated from the experimental data is 70 ± 2 percent for the native fibers and 39 ± 3 percent for the rayons. These figures are in reasonable agreement with those previously estimated from sorption isotherms (68 percent and 35 percent), from density determinations (60 percent and 25 percent), from birefringence and x-ray orientation measurements in regenerated fibers ($\lesssim 40$ percent for rayon), and from recrystallization of amorphous cellulose powder (~ 35 percent for rayon).

The observed relative intensities of the principal crystalline interferences give rise to a discussion of the limited scope of the concept "crystallinity" in cellulose fibers, and it is argued that the concept "degree of lateral order" may be preferable.

Comparison of observed relative line intensities with the theoretically calculated ones, reveals another marked difference between native and regenerated fibers, pointing to the fact that certain states of lateral order prevalent in the latter may be absent in the former.

1. INTRODUCTION

THIS paper is an attempt to contribute to the much discussed problem of the crystalline-amorphous ratio in native and regenerated cellulose fibers through x-ray diffraction experiments on a quantitative basis.

In previous work[1] it has been shown that cellulose fibers like ramie and woodpulp, when transformed into an amorphous powder by dry grinding in a vibrating ball mill, yield x-ray diffraction photographs resembling those exhibited by liquids. A broad diffuse band, having its maximum near the location of the (002) interference of crystalline cellulose, is observed. If the powder is allowed to recrystallize partially, by being heated for a few minutes in the water-wet condition, crystalline interferences reappear superimposed on a diffuse background of lower intensity but having the same shape and location. From the decreased intensity of the maximum that resulted after crystallization, it was concluded that about 30–35 percent of the substance recrystallizes, a figure which could be given additional support from measurements on sorption and heats of wetting.

It also has been shown previously that a diffuse background of this character is invariably found in the x-ray diffraction pattern of all natural and artificial cellulose fibers when duly corrected for radiation scattered by the air and for that due to

* Communication No. 52.

[1] P. H. Hermans and A. Weidinger, J. Am. Chem. Soc. 68, 2547 (1946).

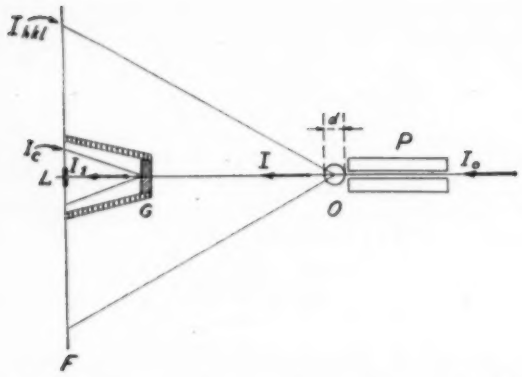

FIG. 1. Diagram of set-up for exposures; P pinhole system; O fiber pellet; G auxiliary miniature Goppel camera; F film.

the non-monochromatic components of the Ni-filtered copper radiation used.[2]

Hence, the disordered or "amorphous" cellulose component exhibits a similar behavior with regard to x-ray diffraction as does amorphous rubber, the difference being that in cellulose the amorphous band tends to be more masked by the superimposed interferences of the crystalline component than in rubber, where its presence shows up right away.

The present paper is concerned with quantitative measurements of this background intensity and that of the crystalline interferences superimposed thereon, carried out with an improved technique developed for the purpose.

The fiber samples were x-rayed in the form of pellets of definite shape and dimensions in which the single fibers were orientated at random. The preparation of these pellets is described in Section 2E. To measure the intensity of the radiation incident on the film in subsequent exposures, a device first introduced by J. M. Goppel was used. Corrections were applied for radiation scattered by air and for background components due to Compton scattering and thermal agitation.

FIG. 2. Exposures of cellulose and air taken with the comparison camera.

[2] P. H. Hermans and A. Weidinger, Rec. trav. chim. **65**, 620 (1946).

2. EXPERIMENTAL PROCEDURE

Reflected monochromatic copper radiation from a pentaerythrite monochromator was used throughout this investigation. As a source of x-rays, a tube with rotating anode was employed operating at 25 kv and 100 ma.

A. Measurements of Incident Radiation

A beam of monochromatic radiation (see Fig. 1) falls through the pinhole system P on the object O, which consists of a fiber pellet orientated at random and large enough to cover entirely the diaphragm. A pencil of x-rays of original intensity I_0 traverses d cm of the object and its intensity is thereby reduced to I, owing to absorption. We then have

$$I = I_0 e^{-\mu d} \quad \text{or} \quad \ln I_0 - \ln I = \mu d, \tag{1}$$

where μ is the absorption coefficient of the object.

The intensity of the diffracted radiation giving rise to an x-ray pattern on the film F is proportional to I. In order to measure I, the technique introduced by Goppel[3] is applied. The transmitted primary pencil of x-rays is directed toward the center of the front plane of a small brass cone G, which serves as a miniature second camera. At the front of G a thin layer of a microcrystalline preparation of a suitable inorganic substance is located, giving rise to a diffraction pattern consisting of Debye-Scherrer circles on the small circular section of the film inside G. The primary beam transmitted by the inorganic comparison substance is finally intercepted by a little lead plate L before reaching the film. Its intensity I_1 is given by

$$\ln I - \ln I_1 = \mu_1 d_1, \tag{2}$$

where μ_1 and d_1 are the absorption coefficient and the thickness of the comparison preparation placed on top of G. Since the same comparison preparation is used throughout, $\mu_1 d_1$ remains constant and, consequently, $I/I_1 = \text{constant}$.

In photometric measurement of the intensity I_e of the comparison interferences inside the

[3] J. M. Goppel, Thesis, Delft 1946. Also see App. Sci. Res. **A1**, 3 (1947).

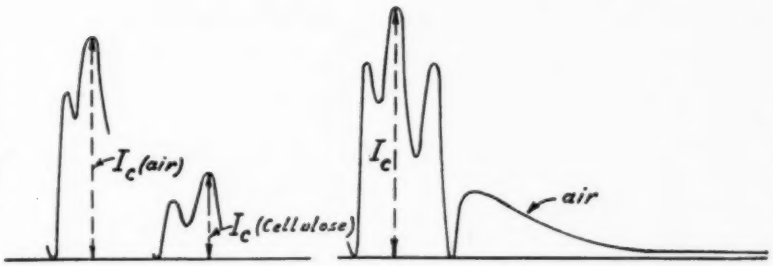

FIG. 3. Photometer traces of the comparison interferences I_c corresponding to the central part of Fig. 2 (with and without absorption in cellulose).

FIG. 4. Photometer curve showing intensity distribution of radiation scattered by the air in the camera.

Goppel cone, this intensity will be proportional to I and, consequently, also to the intensity of the cellulose interferences I_{hkl} on the film outside G.

The cellulose interferences I_{hkl} are, in their turn, proportional to the quantity of cellulose irradiated. When the pinhole system is kept constant, this quantity is proportional to d.

From the foregoing it follows that for a given substance in O (Fig. 1) the quantity

$$I_{hkl}/I_c \cdot d = \text{constant}, \qquad (3)$$

independently of the amount of radiation I_0 falling through the pinhole system and, hence, independently of exposure time and possible fluctuations in the intensity I_0 during exposure. This is the principal equation upon which the computation of our experimental results is based.

The comparison interference in the miniature camera can be seen in Fig. 2 and in the central parts of Fig. 9A and B (where only two quadrants of the film are exposed, the other two having been covered by lead sectors for reasons to be explained below). Figures 3 and 5 show radial photometer curves taken from pictures of this kind.**

B. Check on the Thickness of the Preparations

In preliminary experiments (compare Section 3C) Eq. (1) was checked by taking diffraction pictures of layers of Cellophane several sheets thick, varying the number of sheets exposed, and thus varying d in a known way. The value of the absorption coefficient μ was calculated from theoretical data (Section 3G) and also experimentally determined from experiments with Cellophane of known absolute thickness.

In the final experiments the thickness and density of the pellets of randomly orientated fibers was kept constant as nearly as possible. In the majority of cases a check on the constancy of μd was applied in the following way.

When the first exposure (corresponding to Fig. 5) had been taken, the exposed film was replaced by a fresh one. Then a relatively short second exposure was taken, using Astbury's comparison principle. Keeping tension and current of the tube as constant as possible, the specimen O was alternatively exposed to or turned away from the beam every 5 minutes, using a device allowing one to readjust the specimen before the pinhole P in exactly the same position as before. At the beginning of each cycle the lead sectors covering two quadrants of the film were rotated 90° simultaneously with the movement of the specimen, thus giving free the other two film quadrants. Using an even number of equal exposure cycles, the total amount of incident radiation I_0 during the exposure of both sets of film quadrants could be considered as being equal.

A typical exposure of this kind is shown in Fig. 2. In two quadrants of the film inside the miniature camera the comparison interferences are weakened by the absorption in cellulose and air; in the other two they appear considerably stronger, since no cellulose has been in the path of the beam. Outside the miniature camera cellulose interferences appear in the former two quadrants (just visible in Fig. 2). In the other two quadrants only some radiation diffusely scattered by the air in the camera can be detected.

Figure 3 shows the corresponding photometer traces taken radially on two different quadrants inside the miniature camera. From the intensities

** The photometer used was constructed in the Laboratory for Technical Physics of the Technical University in Delft, and based on the principles indicated by Wheeler and Robinson. Hence, the intensity of blackening indicated on the photometer trace was independent of the characteristics of the film used and directedly proportional to the amount of incident radiation.

TABLE I. Survey of cellulose reflexions after Andress.

Cellulose I				Cellulose II			
hkl	syn	$2\sin\vartheta/2$ / λ	Intensity	hkl	syn	$2\sin\vartheta/2$ / λ	Intensity
101	A_1	0.168	83	101	A_0	0.136	75
$10\bar{1}$	A_2	0.187	57	$10\bar{1}$	A_3	0.225	240
002	A_4	0.257	360	002	A_4	0.242	180
021	—	0.232	82	021	—	0.230	57
				—	III^1	0.316	60
040	—	0.389	22	040	—	0.388	40

of the comparison interferences I_c in the cellulose and air quadrants, the value of μd can be computed from the equation

$$\ln(I_c)_{\text{air}} - \ln(I_c)_{\text{cellulose}} = \mu d. \tag{4}$$

If μ is known, the thickness d of the object can thus be determined from x-ray data, or, if d is known, μ can be calculated, with the convenient equation

$$d = -(2.30 \log r)/\mu, \tag{5}$$

where

$$r = (I_c)_{\text{air}} : (I_c)_{\text{cellulose}}.$$

The mass absorption coefficient for $C_6H_{10}O_5$ can be calculated from atomic data[4] to be 7.78. Multiplying this with the density ρ of rayon and Cellophane at 65 percent relative humidity (being 1.48) we find the linear absorption coefficient for our material $\mu = 11.3$ cm^{-1}. This figure could be shown to be in good conformity with experiments (Section 3C). For sugar $\mu = 12.6$ ($\rho = 1.5$g), for diamond $\mu = 15.9$ ($\rho = 3.51$).

C. Computation of Correction for Radiation Scattered by Air

In Fig. 4 a photometer curve of an exposure without cellulose is shown in full. The right-hand part of the curve, referring to the film outside the miniature camera represents the distribution of the radiation scattered by the air. (This curve is drawn on a vertical scale enlarged 3.5 times as compared to that of the comparison interference I_c.) Such curves, if once known for a given value of I_c, permit computation of the background component due to the air scattering for any value of I_c.

[4] A. H. Compton and S. K. Allison, *X-Rays in Theory and Experiment* (D. van Nostrand and Company, New York, 1935).

D. Evaluation of Radiation Diffracted by Cellulose

The crucial point in work of this kind is to separate correctly the radiation selectively diffracted by the crystalline portion from the "diffuse background." Figure 5, reproducing the complete photometer curves of native ramie and of a rayon sample (reduced to equal values of I_c), shows how we endeavored to solve this question.

The broken line is assumed to represent the separation between the background and the "crystalline" interferences which are superimposed thereon in the form of peaks. The dotted line gives the background after correction for radiation scattered by the air.

In exposures of this kind only a few of the interferences characteristic for cellulose appear with appreciable intensity. They are listed in Table I for cellulose I (native modification) and cellulose II (mercerized modification) together with the respective values of $2(\sin\frac{1}{2}\vartheta)/\lambda$ after Andress as tabulated in Mark's book.[5] (The calculated relative intensities given in the last column will be referred to later.) The angles of diffraction of the reflections marked with a brace in the third columns are so near to each other that they appear as single peaks on our photographs (see Fig. 5a and b). This is partly caused by the natural width of the lines and partly to a slight extra broadening owing to the conditions of the exposure (large diameter pinhole system of 0.8 mm and thick objects, see below). The principal part of the radiation diffracted by the crystalline portion is, therefore, concentrated in two peaks, representing A_1+A_2 and A_4+021 in cellulose I and A_0 and A_3+A_4+021 in cellulose II. For simplicity, we shall designate the peaks in cellulose I with A_1 and A_4, those in cellulose II with A_0 and A_3.***

As indicated in Fig. 5, it has been assumed that in native cellulose the minimum between the A_1 and A_4 peaks lies well above the background, in other words, that there is a slight overlapping of the A_1 and A_4 peaks. In curves of regenerated cellulose, where the A_0 and A_3 peaks are farther apart, it has been assumed that the background

[5] H. Mark, *Physik und Chemie der Cellulose* (Julius Springer Verlag, Berlin, 1932).

*** In native cellulose the 040 line appears as a small peak behind A_4. In cellulose II this interference did not show up.

line touches the minimum. The course of the background line in its initial part (a) was taken as a guide and then leads to this assumption. This followed still more convincingly from photometer curves taken with a higher transmission ratio (12 times) in the horizontal direction. Such curves were always taken in addition to the normal ones (transmission ratio 3.9 times) reproduced in Fig. 5. In the case of regenerated cellulose this method of evaluation met with further support in that it was found that only in this way symmetrical A_0 peaks could be obtained. Other procedures led into unexplicable irregularities and it is therefore believed that the one chosen is correct.

The final downward boundary of the second peak was extrapolated as indicated in Fig. 5. As a measure of intensity, the surface of the two main peaks (integrated intensity) was determined.† In view of the overlapping of more than one interference and possible variations in actual line width in various objects, this seemed to be a better procedure than measuring the height of the peaks.†† Furthermore, the total intensity of the "crystalline" diffracted radiation above the background curve, including the weaker reflections beyond the second peak as well as the total of the diffracted radiation (crystalline plus amorphous), were computed in a similar way. We shall designate these quantities as "total crystalline radiation," symbol I_{cr}, and "total radiation," symbol I_{tot} (comprising the diffraction angles from 7° up to 42°).

Evaluation of the diffuse background consists of the following steps. First the intensity of the radiation scattered by the air in the camera is computed from a standard curve (accounting for the value of I_c, see Section 2C) and subtracted from the background. This correction was usually a relatively small one (area between broken line and dotted line in Fig. 5). The remaining background shows a flat maximum with the height A_m (see Fig. 5), located somewhere between the two main crystalline peaks. This background radiation is, for the main part, due to the scattering of the disordered fiber portion, but is still to be corrected for the radiation due to the thermal agitation of the atoms and to Compton radiation. Since the crystalline and the amorphous portion both contribute to these components (and if it may be assumed that they contribute equally per unit of mass), this portion of the background radiation has to be substracted in order to obtain a reliable measure of the quantity of the disordered or "amorphous" substance. In order to find this correction, exposures were made of several single crystal plates of cane sugar (with rotation of the film). The background curve was determined and corrected for radiation scattered by air (cf. Section 2C and Fig. 11).

It was assumed that the *Compton*-plus thermal components of the background for cellulose are equal to those of the sugar crystals. The hatched area in Fig. 5a and 5b corresponds to this correction, drawn on the correct scale.

The thus corrected height of the amorphous maximum A_m between the dotted line and the

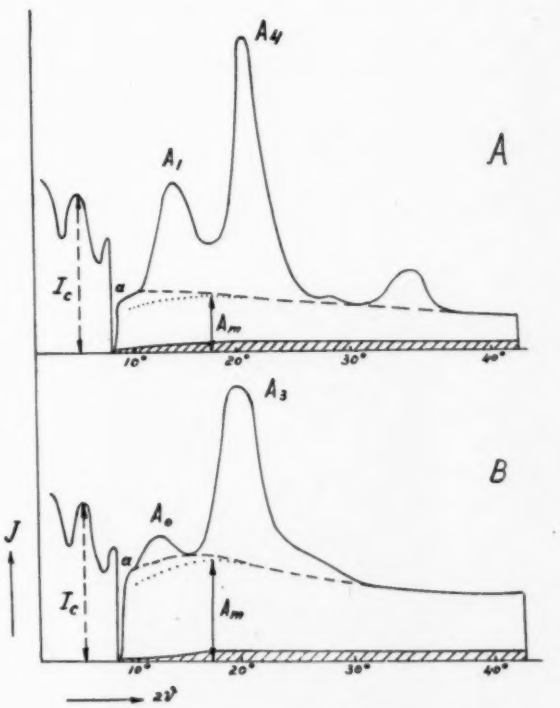

FIG. 5. Photometer traces: *A* for a native ramie pellet, *B* for a rayon pellet. I_c comparison interference. Broken line = background curve. Area between broken line and dotted line = correction for air scattering. Hatched area = correction for thermal and *Compton* components. (Scale 1:2.2).

† Integration was performed by copying the traces of the photometer curves in duplicate on transparent paper of known weight per unit surface, cutting the figures out, weighing them, and taking the average value.

†† It was found that the proportions were not very different if the heights of the peaks were used as a measure of intensity.

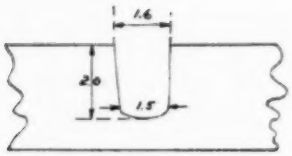

FIG. 6. Brass mold serving to prepare randomly orientated fiber pellets.

hatched area was considered to represent a relative measure of the disordered portion.

The background of diamond was also determined. It exhibited the same shape but its intensity was 0.59 times lower.

E. Elimination of Orientation Effects. Preparation of the Objects

Since it was our aim to obtain comparable quantitative measurements for various fibers of different kind and orientation, it was necessary to exclude any specific effects of orientation. Preferred orientation of any crystal plane may give rise to unpredictable changes in relative intensity of the corresponding interferences (see experiments with Cellophane in Section 3C). True, rotation of the orientated fibers in a plane perpendicular to the x-ray beam during exposure would yield an apparently "isotropic" diffraction picture on the film. However, effects of orientation are thus merely eliminated in two dimensions instead of in three as required. It was necessary, therefore, to realize random orientation of the fibrous objects themselves. This was done by weighing off exactly 3 mg of the air-dry fibrous material, carefully separating it into single fibers cut into pieces of $\frac{1}{2}$- to $\frac{5}{8}$-inch length, which were then dropped on top of each other in positions chosen at random on a glass plate wetted with a few drops of a 0.5 percent solution of arabic gum. Using two needles, a pellet was prepared by folding the wet fibers together, always taking care to conserve randomness of orientation as well as possible. The moist pellet so obtained was rolled between thumb and forefinger to almost spherical shape and laid on filter paper to drain off most of the liquid. After that, the pellet was carefully introduced into a mold, an accurately drilled hole in a brass plate (inside polished). The dimensions of this mold in millimeters are indicated in Fig. 6. Pressure was exerted on the pellet with a glass rod having a flat end just fitting the hole. The liquid was thus expelled and removed with a piece of filter paper. The amount of water then left in the pellet amounted to very nearly 3 mg. For 10 minutes the brass plate was laid on a hot plate with a surface temperature of about 100°C. The pellet, then dry, could be readily removed from the mold as a coherent object, very nearly maintaining the dimensions of the mold. (The amount of arabic gum left in the pellet (0.5 percent) is so small as to be negligible.) Finally, the pellet was mounted with its basis on a support made from a piece of brass wire flattened at one end and bent as shown in Fig. 7. A small drop of molten resin served as an adhesive. The diameter of the pellet at the middle of its height was measured under the microscope in two mutually perpendicular directions. The average value was accepted as being the thickness of the pellet. It very nearly corresponded to the dimensions of the mold.

FIG. 7. Micrograph of mounted fiber pellet ready for exposure.

X-ray test pictures of these pellets (three of which are reproduced in Fig. 8) showed that, with few exceptions, perfect isotropy is not reached. Numerous attempts to improve on this point failed. Quantitative evaluation of orientation according to the procedure elsewhere described[6,7] showed, however, that the orientation factor f (which has the value 1.0 at perfect orientation) was usually around 0.10 and only in one case reached the value 0.24.

[6] J. J. Hermans, P. H. Hermans, D. Vermaas and A. Weidinger, Rec. trav. chim. **65**, 427 (1946).

[7] P. H. Hermans, *Contribution to the Physics of Cellulose Fibers* (Elsevier Publishing Company, Amsterdam and New York, 1946).

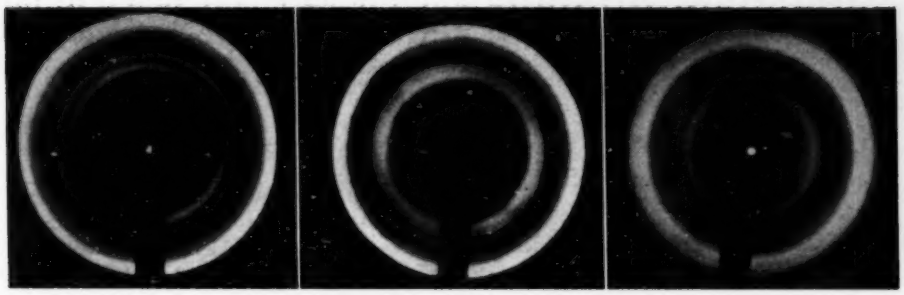

A B C

FIG. 8. X-ray test exposures of pellets, taken with 0.5-mm pinhole (film not rotated), showing that isotropy is almost—though not entirely—reached; *A* bacterial cellulose, *B* native ramie, *C* Fortisan.

Some of the orientation factors measured for pellets are listed below:

Native ramie	$f=0.093$
Standard cotton	$f=0.24$
Bacterial cellulose	$f=0.11$
Cord rayon	$f=0.115$
Fortisan	$f=0.10$

Mathematical analysis shows that for f-values below 0.25 the intensity of the circle obtained by rotating the pellet around the primary beam may be regarded as the intensity which would have been found if the cellulose itself had been perfectly isotropic, without introducing an appreciable error (which is *not* allowed at higher degrees of orientation, as already stated).

For reasons outlined below, we have not applied rotation of the pellet during exposure, but rotation of the film, using a Sauter camera with a motor-driven rotating film holder. In this way, x-ray patterns were obtained that showed no angular variations in intensity and corresponded closely to those of the truly isotropic objects.

F. Pinhole System and Definition of Irradiated Thickness

The beam leaving the pentaerythrite crystal monochromator exhibited the shape of a very narrow band rather than that of a circular pencil of rays. When using the usual pinhole system of 0.5-mm diameter and a stationary film, a texture was obtained in the diffraction pattern which had to be avoided. (This texture was due to unequal illumination of the pinkole by the narrow beam, and consisted in unequal widths of the Debye-Scherrer lines at various angular distances from the equator. Since further reduction of the diameter of the pinhole system led to very long times of exposure, another solution had to be found. Rotation of the film, as applied for the reasons previously discussed, automatically provided this solution since it equalized the texture. A further important advantage was that now even a pinhole system with a diameter as large as 0.8 mm could be used. Very reasonable exposure times amounting to $1\frac{1}{2}$–2 hours were thus made possible.

The additional broadening of the lines resulting from this procedure was immaterial with regard to the aim of this investigation, since it did not affect the ratios between the integrated intensities.

Two x-ray pictures of the kind finally used for the computations are reproduced in Fig. 9. The comparison interferences of the miniature camera are seen in the center.

The dimensions of the pinhole system used, and the location of the pellets in front of it are shown in Fig. 10 (top view). The maximum width of the pencil of x-rays, when traversing the specimen, is 1.2 mm. Since the diameters of the pellets were around 1.6 mm, all radiation passed through the latter, this being a necessary condition in order to define the absorption in the cellulose, and to justify the use of the equations given in Section 3A. The irradiated "thickness" (not used in the final computation since all the pellets could be considered as being of constant dimen-

TABLE II. Values of $I_\alpha/I_{\alpha=0}$ for various angles of deflection.

	Circular case	Flat plate	Cylinder (average)
0°	1	1	1
10°	1.002	0.986	0.994
20°	1.009	0.963	0.986
30°	1.021	0.926	0.974
40°	1.037	0.876	0.957

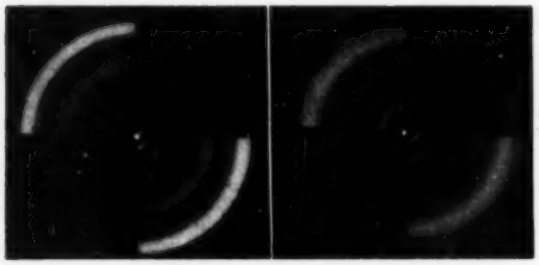

A B

FIG. 9. X-ray exposures of pellets as finally used for computation; *A* native ramie; *B* Cellophane shavings. Pinhole 0.8 mm; rotating film. The black sectors correspond to unexposed film and by their contrast demonstrate the presence of a diffuse background scattering on the exposed sectors.

sions and density) may be taken as practically equal to the pellet diameter d.

In the experiments with Cellophane sheets, carried out as a general check on the method applied, the thickness d is equal to the sheet thickness times the number of sheets placed on top of each other. However, in order to compare Cellophane with pellets, the densities must be taken into account. (See Section 3A.) As will be seen from Table VI, the thickness of the pellets as computed from absorption was constant within experimental error and always nearly corresponded to the calculated figure.

H. Dependence of Absorption on Angle of Deflection

Since integrated intensities and not the heights of peaks were measured, no correction for the use of a plane film was necessary. However, the dependence of absorption upon the diffraction angle has to be considered. As the pellets are cylindrical, the angular dependence for rays deflected in the horizontal plane can be taken from tables published by Kratky and Worthmann[8] for the circular case. Rays deflected in the vertical plane follow the case of absorption in a flat plate for which the equation

$$I_\alpha/I_{\alpha=0}=(1/\varphi)(1-e^{-\varphi}) \qquad (6)$$

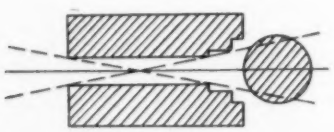

FIG. 10. Diagram of pinhole system and location of pellets in the x-ray beam. (Horizontal dimensions reduced sixfold.)

[8] O. Kratky and W. Worthmann, Monatshefte **76**, 263 (1947).

was calculated, where $\varphi=\mu d(1-\cos\alpha)/(\cos\alpha)$. For the value of $\mu d=0.9$ corresponding to that of the pellets, the values of $I_\alpha/I_{\alpha=0}$ hold, which are shown in Table II. For rays deflected in an arbitrary direction, the absorption in the cylinder is intermediate between those for the horizontal and the vertical deflections and we shall not make an appreciable error if we assume that the average value obtained on rotating the film is simply the average of the two figures (last column in Table II).

Since the amorphous maixmum A_m lies at about $\alpha=15°$ and the second crystalline peak A_3 or A_4 at 20°–21°, the correction is so small as to be negligible in comparison to experimental error. As the total width of our photometer traces extended to 42° (see Fig. 5) where the correction is still not greater than 5 percent, it was even permissible to discard the correction with regard to the surfaces I_{tot} and I_{Am}, since the areas to be compared roughly showed the same shape. Their proportion is, therefore, hardly affected by the correction.

I. Integration Along Debye-Scherrer Circles

In order to compute correctly the integrated intensity of scattered radiation from photometer traces taken radially, integration should be extended also from 0 to 2π along the Debye-Scherrer circles. This means that the ordinates of the photometer curves should be multiplied with the radius r of the Debye-Scherrer circle to which they correspond.

Of course, if merely relative measurements are required, this integration can be omitted if congruent curves or linear peak heights, having equal values of r, are involved. Since the peak heights Am of the background curves have the same r-value, and since the background curves to be compared are nearly congruent, the integration has, as a rule, not been carried out for these quantities, except in one case which shall be mentioned later.

Since crystalline intensity curves are also congruent in groups of specimens with identical crystalline modification, the integration could also be omitted within such a group. Only when comparing cellulose I with cellulose II was the necessity of this additional integration accounted for by multiplying the surfaces of the peaks with the radius r corresponding to the centers of the peak (see Section 4B). Since the r-values of the most intense peaks are not very different from each other, this gives rise to only a relatively small change in the crystallinity figures. (See Section 3B.)

K. Inorganic Comparison Sample in Miniature Camera

A mixture of aluminiumhydroxide and pure gypsum was prepared in powder form, mixed with water to form a thick paste, and then kept between parallel glass plates until dry. A thin plate of this material (consisting of $Al_2O_3 \cdot 2H_2O$ and $CaSO_4 \cdot 2H_2O$) was used as the comparison sample.

3. EXPERIMENTS

A. Density of Fiber Pellets

Fiber pellets molded according to Section 2E were measured to be 2.0 mm high and on the average 1.60 mm in diameter, from which their volume is calculated to be 4.0 mm³. From their air-dry weight of 3.0 mg, their density is calculated to be 0.75.

Since the density of a massive filament or sheet of air-dry regenerated cellulose amounts to 1.48,[7] the x-ray absorption in a pellet will be equivalent to that in a massive sheet of 0.75/1.48 times 1.6 mm = 0.81 mm.

From x-ray absorption measurements on 16 different pellets the average value of 0.841 ± 0.006 was computed. (See Table VI.) From the absorption coefficient of 11.3, the equivalent thickness d of a layer of another substance with the absorption coefficient μ can be calculated from the equation $\mu d = 0.84 \times 11.3$.

B. Background Measurements of Sugar Crystals and Diamond

Three good sugar crystals of various sizes were picked out and x-rayed perpendicular to two parallel crystal planes††† with the technique given in Sections 2A and 2B. The same was done with a nearly plane-parallel diamond cutting. The thickness d of the layer exposed was calculated from absorption by Eq. (5). The results, as compared with the thickness measured with a micrometer, are listed in Table III (μ for sugar 12.6, for diamond 15.9). Figure 11 shows the photometer curve of the 2.2 mm sugar crystal (ordinate scale corresponding to $I_e = 290$). Fortunately, no more than four crystal-interferences, two intensive and two weak ones, appeared so that the background line (broken curve) could be drawn unambiguously. After the subtraction of air scattering the dotted curve S, representing the true background was obtained.

TABLE III. Thickness in mm of sugar crystals and diamond as calculated from absorption and measured directly.

	I_e	$\frac{I_e}{\text{air}}$	Ratio	d_{calc}	d_{obs}
Sugar crystal I	18.5	68.5	0.26[5]	1.08	1.2
Sugar crystal II	37.5	607.0	0.062	2.30	2.2
Sugar crystal III	18.5	44	0.42	0.71	0.75
Diamond	22	50	0.44	0.52	0.50

The integrated surface of this background expressed in the units below in Table VII amounts to 43 for $I_e = 100$. The other sugar exposures yielded exactly corresponding results.

In the exposure of the diamond splitter no crystal-interferences appeared at all, it merely showed a weak background scattering which, after subtraction of air scattering and reduction to the same scale, yielded the dotted curve marked d in Fig. 11.

According to expectation the diamond background lies at a lower level than the sugar background. Owing to the rigidity of the diamond lattice the thermal component will be smaller.

It has been assumed that the corresponding background of cellulose is equal to that shown by the sugar crystals.

In order to render the I_e values of the diamond exposure comparable with that of the cellulose pellets the former was multiplied by 1.49, being the ratio of the ρd values of the diamond splitter (0.182) and that of the pellets (0.122) where ρ and d are the respective density and thickness.

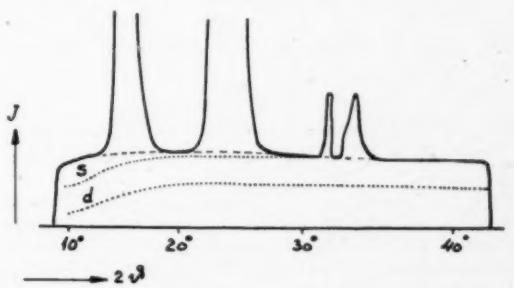

FIG. 11. Photometer trace of the diagram of a sugar monocrystal; S background curve corrected for air scattering. Curve d shows the corresponding background of diamond (on comparative scale).

††† The author is indebted to Mr. C. J. Asselbergs for a collection of cane sugar crystals.

TABLE IV. Control experiments with Cellophane.

Shape	(1) n	(2) I_c	(3) A_3	(4) A_m	(5) $(A_3/I_c \cdot n)$	(6) $(A_m/I_c \cdot n)$	(7) (A_3/A_m)
Sheets	5	172	217	41	0.24	0.048	5.0
Sheets	6	112	159	32	0.24	0.048	5.0
Sheets	8	93	178	37[b]	0.24	0.050[b]	4.7[b]
Sheets	8	140	280	52	0.25	0.046	5.4
Roll	~12	94	238	73	0.21	0.065	3.2
Pellet	9.3	34	37	19[b]	0.12	0.062	1.9[b]

TABLE V. Thickness of Cellophane piles calculated from absorption measurements.

	$(I_c)_{cell}$	$(I_c)_{air}$	$d_{(calc)}$	Actual d
4 sheets	32	48	0.35[b]	0.36
5 sheets	9[b]	16	0.46[b]	0.45
5 sheets	20	35	0.49	0.45
9 sheets	51	128	0.80	0.81

The ρd values used were found in dividing the experimentally found μd values by the mass absorption coefficient.

C. Control Experiments with Cellophane

Exposures were taken with uncoated Cellophane sheets of 0.09-mm thickness. A varying number n of such sheets were piled on top of each other.‡ The results are given in the first four horizontal lines of Table IV where the number of sheets n, the intensity of the comparison interference I_c, the height of the second peak (designated A_3), and the height of the background maximum (A_m; see Fig. 5) are listed. The first peak, A_0, does not appear on these photographs because of selective uniplanar orientation.‡‡ In the 5th and 6th column it is shown that Eq. (3) holds, and in the last column the ratio between A_3 and A_m is given, which is also constant as long as the pencil of x-rays is perpendicular to the plane of the sheets. (The experimental error is around 10 percent.) In the 5th line of Table IV figures are given for Cellophane rolled to form a little rod (consisting of about 12 layers in diameter). The 6th line, finally, refers to a pellet made by molding thin Cellophane shavings obtained by scratching a sheet with a sharp knife. The thickness of the single sheets was 0.09 mm, and the pellet corresponded to 0.84:0.09=9.3 sheets (see Section 3A).

Owing to selective uniplanar orientation in the Cellophane, the A_3 planes are in a particularly favorable position with regard to reflection. The Table IV shows that this changes as orientation is randomized stepwise, first in two dimensions (in the roll) and then in three (in the pellet). The first A_0 peak, which is absent in the sheets, reappears in the pellet, and the intensity of the second A_3 peak (column 5 in Table IV) drops from 0.24 over 0.21 to 0.12 in the pellet.

This phenomenon is a striking illustration of the necessity of our procedure of randomizing orientation in all fiber samples through pellet formation, as indicated in Section E2.

It is further seen from Table IV that the value of $A_m/I_c \cdot n$ also changes upon randomization of selective orientation, though to a much less extent than $A_3/I_c \cdot n$. Similar differences were found when comparing pellets made from thin films of native bacterial cellulose with a pile consisting of several of such films irradiated perpendicular to the film plane.‡‡‡

The figure of 0.062 for $Am/I_c \cdot n$ found for the Cellophane pellet refers to a thickness equivalent to one sheet of Cellophane. The corresponding figure for the actual pellet thickness is 9.3 times greater and, hence, 0.58. This figure after correction (see below) becomes 0.54 and tallies well with that found for other regenerated celluloses. The same holds for the figure for the A_3 peak $0.12 \times 9.3 = 1.12$ (see Table VII).

The figures in Table V show that from absorption measurements on piles of several Cellophane sheets, each 0.09 mm thick, Eq. (4) could be checked (using $\mu = 11.3$). It is seen that the agreement is satisfactory when account is taken of the relatively large experimental error (estimated to be 5–10 percent) caused by the use of an exponential equation.

D. Experiments with Fiber Pellets

The objects are listed in Tables VI and VII. The standard cotton was prepared according to the prescription of the division of cellulose chemistry of the American Chemical Society. The other native fibers were purified and bleached samples. The cottonine consisted of flax separated into single fibers. The sulfite cellulose was a commercial grade of rayon pulp. The bacterial cellulose consisted of dried films grown on cultures of bacteria Xylinum, previously washed with water and repeatedly extracted with dilute potassium hydroxide solution.¶ Their nitrogen content could not be brought below 1 percent.

The rayon samples were desized. Rayon *A* had been spun with a minimum amount of stretch and rayon *B* was spun with 70 percent stretch (according to the two-bath process). Hence they represent low and high orientation.

‡ Since in this series one and the same substance (Cellophane) is dealt with and no variations in line width will occur, we have taken the height of the A_3 peak as a measure of intensity instead of its integrated surface, as in the main experiments.

‡‡ Admittedly, for obvious geometrical reasons the line breadth is somewhat increased on increasing the thickness of the Cellophane, but this increase is very small because it involves the sine of the deflection angle.

‡‡‡ An explanation of this striking observation remains to be found.

¶ The authors are indebted to Professor A. J. Kluyver, Delft, for this material.

The samples *u*, *v*, *w* at the bottom of Table IV consisted of cellulose IV. Mercerized ramie and Lilienfeld rayon were transformed into the so-called HT (high temperature) modification (cellulose IV) by heating in glycerol at 250°C.[7,9] The lattice transformation was about 90 percent completed in the ramie and 100 percent in the two Lilienfeld rayons (comprising the samples *A* and *B*, heated for 15 and 30 minutes, respectively).[9]

The results of the x-ray experiments are given in Table VI. In column 1 the value of the comparison interference I_c in the miniature camera is given, and in columns 2 and 3 the integrated surfaces of the two main peaks are given. Then follow, in columns 4 and 5, the uncorrected height of the amorphous maximum A_m and the total surface of the crystalline interferences above the background I_{cr}. In column 6 the total integrated intensity I_{tot} of all the radiation scattered (up to an angle of 42°) is listed (corrected for air scattering). All figures are given in arbitrary but comparable units.

In the last column the thickness of the pellets, as determined from absorption, is recorded. It is seen that figures of the same magnitude were found, and variations were within experimental error. The pellet of bacterial cellulose with $d=0.71$ is an exceptional case, since the pellet could not be made 3 mg in weight; correspondingly less material (2.5 mg) had to be taken in order to fit the mold.

Since there was no correlation between the *d*-values found from absorption and the diameters measured under the microscope (which varied between 1.58 and 1.64 mm), no corrections for diameter variations were applied, except in the case of bacterial cellulose. Here, the intensity readings listed in Table VI were multiplied by 0.84:0.71 to account for the lower density of the pellet. In Table VII the same experimental data are listed, now uniformly reduced to the value of $I_c=100$. The values of the amorphous maximum A_m are now also corrected for the share of the Compton plus thermal scattering as computed in Fig. 11 from sugar and diamond. The height of this curve being 20 mm at the locus of the amorphous maximum for $I_c=460$, the correction amounts to 100/460 times 20 mm for $I_c=100$, or 4.3 mm. For the native samples *a* to *e* and for the rayon samples *h* to *p* the probable error of the mean values of A_m, I_{cr}, and I_{tot} has been calculated (by the least square method).

The accuracy of the single determinations listed in Tables VI and VII is not very high. The magnitude of some of the relative errors was estimated to be as follows:

TABLE VI. Result of evaluation of the photometer curves.

Object	(1) I_c	(2) First peak	(3) Second peak	(4) A_m	(5) I_{cr}	(6) I_{tot} (−air)	(7) d (mm)
a. Standard cotton	45	26.1	54.7	15[b]	88	170	0.82
b. Ramie I	63	40.3	75.2	20	130[b]	259	0.88
c. Ramie II	42[b]	21.9	53.5	13[b]	83	173[b]	0.87
d. Cottonine (flax)	46	25.6	54.6	15	93[b]	184	0.84
e. Cotton linters	30	14.9	33.7	9[b]	54	112[b]	0.80
f. Woodpulp	34	19.8	40.8	13	64	144[b]	0.87
g. Bacterial cellulose	48	14.3	37.0	26	49[b]	184	0.71
h. Staple fiber	29	2.7	27.2	18	32	129	0.85
i. Rayon *A*	30[b]	2.1[b]	29.3	18[b]	34	141[b]	0.83
j. Rayon *B*	31	1.9	27.9	18	32	132[b]	0.86
k. Cellophane	34	2.8	33.8	19[b]	44	140	0.84
l. Cellophane	32	2.0[b]	27.9	18	37[b]	144	0.82
m. Tyre cord rayon I	26	1.6	25.3	16[b]	30[a]	114[b]	—
n. Tyre cord rayon II	31	—	—	18[b]	35	138[b]	0.81
o. Lilienfeld rayon	45	3.3[b]	40.7	28	48[b]	197	0.82
p. Bemberg rayon	33	3.0	28.4	19	32	145	0.82
q. Fortisan I	36	2.2[b]	33.7	19	39	143[b]	0.83
r. Fortisan II	43[b]	2.5	38.0	23[b]	47	179[b]	—
s. Merc. ramie	44	2.8	47.6	22[b]	55	186	0.86
t. Merc. bacterial cellulose	33	1.9	25.7	24	29[b]	143	0.80
u. Merc. ramie (IV)	39	11.6	35.4	46[b]	58	184	—
v. Lilienfeld rayon *A* (IV)	36[b]	12.9	27.2	41[b]	46[b]	158	—
w. Lilienfeld rayon *B* (IV)	35	10.0	26.2	40	40[b]	151[b]	—

[9] P. H. Hermans and A. Weidinger, J. Colloid. Sci. **1**, 495 (1946).

TABLE VII. Results of evaluation all reduced to $I_c=100$.

Object	(1) First peak	(2) Second peak	(3) A_m	(4) I_{cr}	(5) I_{tot} (−air)
Cellulose I					
a. Standard cotton	58	121	28	195	380
b. Ramie I	63	120	26	207	410
c. Ramie II	52	125	28	195	410
d. Cottonine (flax)	56	119	28[b]	203	405
e. Cotton linters	50	113	28	180	380
Average	56	116	28±0.5	198±5	398±7
f. Woodpulp	57	119	34	188	425
g. Bacterial cellulose	34	92	58[b]	119	440
Cellulose II					
h. Staple fiber	9[a]	94	58	110	445
i. Rayon *A*	7	96	56[b]	111	465
j. Rayon *B*	6[b]	90	54	105	428
k. Cellophane	8[a]	100	54	128	412
l. Cellophane	6[b]	92	52[b]	115	450
m. Tyre cord rayon I	6[a]	97	59	113	440
n. Tyre cord rayon II	—	—	56	116	448
o. Lilienfeld rayon	8	91	58	108	437
p. Bemberg rayon	9[a]	87	54	97	440
Average	(7[a])	93[a]	56±0.8	111[b]±2[b]	440±4
q. Fortisan I	6[a]	95	49	108	400
r. Fortisan II	5[a]	88	49	108	412
s. Merc. ramie	6[a]	108	47	125	423
t. Merc. bacterial cellulose	6[a]	83	66	29[b]	435
Cellulose IV					
u. Merc. ramie	25[b]	91	51	148	462
v. Lilienfeld rayon *A*	35	74	49	127	433
w. Lilienfeld rayon *B*	29	75	48[b]	116	433

TABLE VIII. Half-width of first and second peaks in mm on the film (computed from photometer traces with 12× linear magnification).

	First peak	Second peak
Standard cotton	3.0[b]	2.2
Ramie I	3.3[b]	2.5
Ramie II	3.4[b]	2.7
Cottonine	3.2	2.6
Cotton linters	2.9[b]	2.6
Woodpulp	3.2[b]	2.7
Bacterial cellulose	3.3[b]	2.7
Staple fiber	2.4[b]	3.3[b]
Rayon *A* (0% stretch)	2.0[b]	3.4[b]
Rayon *B* (70% stretch)	1.6[b]	3.4[b]
Cellophane I	2.0[b]	3.2
Cellophane II	2.2	3.2
Cord rayon II	—	—
Cord rayon I	1.6[b]	4.0
Lilienfeld rayon	2.4[b]	3.6
Bemberg rayon	2.0[b]	3.1
Fortisan I and II	1.5[b]	3.2
Merc. ramie	1.6[b]	3.1
Merc. bacterial cellulose	2.0[b]	3.1
Merc. ramie (IV)	2.4	3.6
Lilienfeld rayon *A* (IV)	2.8	3.6
Lilienfeld rayon *B* (IV)	2.5[b]	3.3[b]

Variations in thickness of pellet:	5 percent
Measurement of I_c:	2 percent
Intensity integration:	
Large surfaces	3–5 percent
Small A_0 surface in rayon, up to	40 percent

With the exception of the "first-peak" values for rayon, the total possible error in the other figures can, therefore, be estimated to be 10–15 percent. Actually, the maximum fluctuations are seen to be of this order of magnitude.

Line-breath measurements of the two main peaks were carried out on each exposure in determining their width at half-height above the background. For this purpose extra photometer curves were taken with a linear magnification factor of 12. The results are given in Table VIII, reduced to the actual half-width measured in mm on the film (at 40-mm specimen-to-film distance). These figures have only a relative meaning since their absolute value is affected by the large pinhole diameter and the thickness of the pellets. For cord rayon I no reliable figures could be obtained since the crystalline portion of this specimen consisted of cellulose II with some cellulose IV admixed, the sole case of this kind among the rayon samples investigated.

4. DISCUSSION

A. Relative Amounts of Crystalline and Disordered Substance

Starting from the empirical fact that the diffracted intensity in cellulose diagrams may be represented by a diffuse background exhibiting a flat maximum and a number of peaks superimposed thereon, we shall tentatively associate the former with the disordered and the latter with the crystalline portion. In Section 4C this point will be examined somewhat closer.

In Table VII the items of primary interest in this regard are A_m and I_{cr} (columns 3 and 4) as they represent a probable relative measure of the quantity of disordered and crystalline portions, respectively. It is seen that these figures are constant within experimental error within the group of the native fiber samples *a* to *e*. Woodpulp (*f*) shows a somewhat higher value of A_m, and bacterial cellulose a still higher value of A_m, combined with a distinctly lower value of crystallinity.

In the series of regenerated celluloses, all rayon and Cellophane samples (*h* to *p*), including Lilienfeld and Bemberg, have practically equal values of A_m as well as of I_{cr}. Fortisan (*q* and *r*) tends to be on the low side as regards A_m, and mercerized ramie (*s*) has a slightly higher I_{cr} value. The lowest value of I_{cr} and, simultaneously, the highest value of A_m are shown by the mercerized bacterial cellulose (*t*).

These results are in general conformity with

TABLE IX. Sorption ratios calculated from the height of the amorphous maximum Am and those observed (average from sorption and desorption).

	Calc.	Obs.
Woodpulp	1.2	1.2–1.3
Rayon samples *h* to *p*	2.0	1.95–2.02
Fortisan	1.75	1.64*
Mercerized ramie	1.68	1.60
Cellulose IV (Lilienfeld)	1.75	~1.5

* In order to avoid errors due to a possible remainder of acetate groups in the Fortisan, the sorption and desorption ratios were accurately determined from the original sample and from one treated for 5*h* with normal ammonia solution at 100°C. The average sorption ratios found were 1.64 and 1.63, respectively.

TABLE X. The sorption ratios of bacterial cellulose.

Percent rel. vapor pressure	85	65	35	17[b]	10	5
Sorption ratio (native)	1.26	1.22	1.38	1.79	2.0	—
Sorption ratio (mercerized)	1.68	1.73	1.77	2.00	2.05	2.49

expectations based on other physical data. In previous work it has been argued that the quantity of amorphous substance in cellulose fibers should be nearly proportional to their sorption ratio,[10] and also proportional to the difference between their density and that of crystalline cellulose as computed from x-ray measurements.[11] It has been shown that sorption ratios calculated from density determinations tally reasonably well with the experimental ones.

Now the sorptive capacity for water vapor is practically equal for the native samples *a* to *c*. If our assumption is correct, the sorption ratios of the other samples should be calculable from the proportion of their *Am* values. The result is shown in Table IX. There seems to be a satisfactory agreement, except in the case of cellulose IV, where the sorption ratio is only approximately known from one desorption series and more data are desired. Bacterial cellulose is not included in the table, since it was found that it behaved anomalously in sorption experiments in that, in contrast to other cellulose samples, its sorption ratio was not approximately constant at various relative vapor pressures, for reasons which remain to be explained.

According to the technique previously described[10] the following figures have been found at desorption (Table X).¶¶ The sorption ratios calculated from A_m are 2.1 and 2.35, respectively.

The anomalous behavior of bacterial cellulose with regard to sorption may be due either to remaining impurities or to unknown structural features. Anyhow, the native form is the first example of a native cellulose showing the x-ray pattern of cellulose I and having a very low degree of crystallinity (compare the low value for I_{cr}). The figures obtained from the samples transformed into cellulose IV would seem to give some support to the earlier presumption that crystallinity is somewhat increased as a result of the high temperature treatment.

The most important result arrived at, however, seems to be the fact that *there is no detectable difference in degree of crystallinity between all viscose rayons investigated, including Lilienfeld and cuprammonium yarns, with perhaps the only exception of Fortisan.* This yarn, a highly stretched cellulose acetate fiber, afterward saponified to cellulose, seems to exhibit a somewhat higher degree of crystallinity, although its I_{cr} value, which lies quite near to that of the other rayons, does not support this conclusion. Between "crystallinity" and orientation there seems to be little, if any, correlation, a fact surely significant, though difficult to explain.

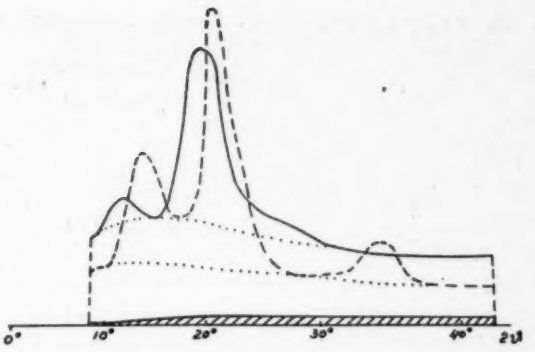

FIG. 12. Radial intensity distribution for native fibers (broken line) and rayon (fully drawn line) drawn on comparative scale.

In Fig. 12 average intensity curves for the native fibers and for rayon are shown superimposed to scale.

Besides the height *Am* of the background maximum, we might consider the integrated background intensity as another relative measure of the disordered portion, i.e., the total surface below the background line after subtraction of the air correction and the hatched area (Section 3B). The ratio of these integrated intensities for the average curves shown in Fig. 12 is equal to the ratio of the values $I_{tot}-I_{cr}-43$, or, 1.83. This figure, however, is not yet correct, since integration along the Debye-Scherrer circles has still to be carried out (Section 21).

Carrying out this integration as a control, the value 2.03 was found in conformity with the ratio 2.0 as computed from the heights of the maxima. It would seem, however, that computation from the heights is preferable, since the background surfaces are taken over a restricted range of diffraction angles, whereas the correct procedure would require integration over 180°. Anyhow, the good conformity obtained supports the reliability of the results.

The same restriction of limited diffraction angles seems to apply to the figures giving the integrated total I_{tot} of all the diffracted radiation listed in the last column of Table VII. According to the elementary rules of x-ray dif-

[10] P. H. Hermans, *Contribution to the Physics of Cellulose Fibers* (Elsevier, Publishing Company Amsterdam and New York, 1946); also A. J. Hailwood and S. Horrobin, "General discussion on swelling and shrinking," London (1946); Trans. Faraday Soc. to be published.

[11] P. H. Hermans, J. J. Hermans, and D. Vermaas, J. Polymer Sci. **1**, 162 (1946).

¶¶ The authors are indebted to Dr. D. Vermaas for carrying out the microsorption experiments.

TABLE XI. Correction of the crystalline intensities for integration along the Debye-Scherrer circles.

Cellulose I			Cellulose II		
Peak	r	$I \cdot r$	Peak	r	$I \cdot r$
1	3.9	218	1	3.3	25
2	6.0	696	2	5.6	521
3	11.8	307	3	7.8	103
	I_{cr}	1221		I_{cr}	649

fraction, I_{tot} should be equal in all cases examined.[12,13]¶¶¶ Table VII shows that this is borne out by our experiments in first approximation, though the average figure for the native samples (398) is distinctly (about 10 percent) lower than that for the rayons and cellulose samples (440). Since additional integration along the Debye-Scherrer circles might slightly change this result, we have carried out this operation. However, the figures still showed a difference of the order of 10 percent.

B. Absolute Quantity of Crystalline and Disordered Substance

From the foregoing we may venture to derive an approximate estimation of the absolute crystallinity figures. Let x and y be the average crystalline fractions in native and regenerated cellulose, then x/y follows from the ratio of the I_{cr} values, which is $198/112=1.77$. This ratio, however, cannot be taken directly from Table VII since integration along the Debye-Scherrer circle has still to be accounted for (see Section 21). The peak intensities, I times r, thus found are listed in Table XI together with the corresponding r-values. The ratio thus found is $1221:649=1.88$ against 1.77 without integration. These figures should still be corrected for the different moisture content in native and regenerated cellulose.

Under the conditions of the exposure the former contained 6 percent and the latter 12 percent moisture calculated on dry cellulose. Hence, the pellets contained 5.5 percent and 10.5 percent water calculated on their moist weight. The ratio $x/y=1.88$ found here actually represents the ratio $0.945x/0.895y$, and the corrected ratio x/y, hence, is 0.895:0.945 times 1.88, or 1.78.

[12] A. W. Coven, Phys. Rev. **41**, 422 (1932).
[13] G. E. M. Janncey and F. Pennell, Phys. Rev. **43**, 585 (1932); **44**, 128 (1933).
¶¶¶ The total scattering per atom is not dependent upon the physical state of the matter considered. The scattering per gram from a powdered crystal of KCl, for example, is nearly the same as that from argon gas; since the atomic number of potassium and chlorine is the same of that of argon (see references 12 and 13).

TABLE XII. Crystalline fraction in native cellulose and rayon derived from various physical data.

	Native	Rayon
Sorption isotherms*	0.68	0.35
Density	~0.60	~0.25
Orientation of model filaments from birefringence and x-ray diagram	—	$\leqslant 0.40$
Recrystallization of amorphous cellulose powder	—	~0.35
Present x-ray work	0.70	0.39

* A. J. Hailwood aud S. Horrobin, reference 10; D. Vermaas, Discussion remark to this paper (in preparation).

From the ratio of the A_m values from Table VII we find $(1-x)/(1-y)$. Hénce, we have:

$$\frac{x}{y}=1.78. \quad \frac{1-x}{1-y}=\frac{28}{56}=0.50.$$

Assuming a probable error of ±3 percent in both ratios, we obtain from these equations

$$x=0.69^5\pm0.02, \quad y=0.39\pm0.03.$$

The ratio $(1-x)/(1-y)$ is not liable to errors due to the difference in regain. The radiation diffracted by the water will contribute to the background only. Since the average atomic number of water (7.22) is practically equal to that of cellulose (6.68), and since the quantity of water is proportional to the fraction of amorphous substance, the ratio $(1-x)/(1-y)$ as derived from the background, using either A_m or the integrated surface, remains unchanged. (Correction of the separate A_m values, however, is not possible because we do not know the angular intensity distribution of the radiation scattered by the water, as the latter is not in the ordinary liquid state.)

We have also investigated whether the ratio x/y might be affected by the existence of crystalline interferences at high angles of diffraction, not accounted for in the investigated range from 0° to 42°. To that end, exposures of a ramie and of a rayon pellet were made in a Debye-Scherrer camera, covering the angular distance from 0° to 165°. Actually, some more relatively weak interferences appeared beyond 42°. The integrated intensities of these interferences were measured (accounting for integration along the Debye-Scherrer lines, which requires multiplication with the sine of the diffraction angle in this case). Though the two photographs were not directly comparable (over-all intensity measurements were lacking in this case), it could be shown that addition of the intensities of the high angle peaks to that of the peaks lying below 42° will not materially change the ratio of crystalline intensities between cellulose I and II.

It should be noted, moreover, that the magnitude of x and y is not very sensitive for relatively large variations in x/y. If, for instance, x/y is taken 1.70 instead of 1.78, the figures for x and y become 0.71 and 0.41, respectively; if x/y is taken 1.9, these figures become 0.68 and 0.36.

In Table XII the values found are compared with those recently estimated from other physical data.[14] Agreement as to the correct order of magnitude seems to be obtained when the imperfections of the applied methods are taken into consideration. On the other hand, there remains a considerable difference with figures arrived at by other workers from investigations of a chemical nature ("accessibility" measurements), e.g., those by Purves,[15] Nickerson,[16] Conrad and Scroggie,[17] Lowell and Goldschmidt,[18] and others. This is not surprising, however, since it may be expected that accessibility determinations based on chemical reactions will yield figures depending upon the particular reaction used.[14] A favorable exception may be the exchange reaction between cellulose and heavy water. Relevant investigations recently reported by Mark and co-workers[19] yield figures which seem to be in reasonable agreement with those listed in Table XI.

C. Relative Intensities and Width of the Separate Crystalline Peaks

We shall now consider the observed integrated intensities of the first and second crystalline peaks given in Table XI. The theoretical intensity ratio of the second to the first peak, according to the data calculated by Andress (see Table I), should be 3.15 in cellulose I and 7.35 in cellulose II. The experimental values computed from Table XI are $696/218 = 3.19$ and $521/25 = 20.8$, respectively. Hence, there is conformity only for cellulose I and not for cellulose II. (In the latter case, moreover, this value shows considerable variation from the average in the individual specimens investigated.) This may be due to either the incorrectness of Andress' theoretical values (difficulties in the exact computation of the Lorentz factor or incorrectness of the assumed lattice structure of cellulose II) or (more probably, in our opinion) to other reasons set forth in the next section.

The line-width values for the two peaks recorded in Table VIII do not reveal very significant variations within the various secimen groups, except for the first peak (101) in the rayon group. It would seem that the highly orientated rayons tend to exhibit a sharper first peak, except Lilienfeld rayon. The effect is certainly beyond experimental error, though admittedly, the error in measuring the small A_0 peaks in cellulose II was about double that in the other cases, where it was estimated to be 5 percent. The figures from Table VIII also demonstrate the difference between the line patterns of cellulose I and IV. The first peak, consisting of two interferences (101 and $10\bar{1}$) located near to each other in cellulose I, corresponds to only one interference (101) in cellulose IV and is, consequently, narrower in the latter case.

D. Discussion of the Concept of Crystallinity in Cellulose Fibers

Obviously, the subdivision of the fiber substance in a "crystalline" and an "amorphous" portion is but a rough approximation.[7] Between regions of three-dimensional lattice order and disordered regions transitionary states may be expected to occur. Baker *et al.*[20] have suggested the existence of "mesomorphous" components in systems of this kind. It is difficult to associate exact definitions of the physical state of the components with various degrees of order and still more difficult to predict how these will eventually contribute to the distribution of diffracted radiation.

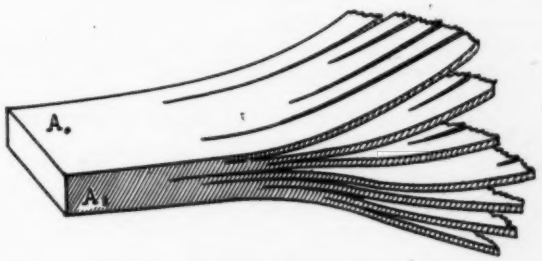

FIG. 13. Diagram of the transition from a crystalline region into a disordered region in cellulose II. Owing to the preferred cleavage parallel to the A_0 planes, A_0 plane order is sooner destroyed than A_3 plane order.

[14] Survey by P. H. Hermans, J. chim. phys. **44**, 135 (1947).
[15] C. B. Purves, J. Amer. Chem. Soc. **66**, 59 (1944).
[16] R. F. Nickerson, Ind. Eng. Chem. **34**, 85, 1480 (1945); **38**, 299 (1946).
[17] C. W. Conrad and H. G. Scroggie, Ind. Eng. Chem. **37**, 572 (1945).
[18] E. L. Lowell and O. Goldschmidt, Ind. Eng. Chem. **38**, 811 (1946).
[19] V. J. Frilette, J. Hanle and H. Wark, communicated at the XIth Intern. Congress of Pure and Applied Chemistry, London 1947.
[20] W. O. Baker, C. S. Fuller, and N. R. Pape, J. Am. Chem. Soc. **64**, 776 (1942).

By careful photometration of monochromatic exposures of highly oriented fibers we have established, that *the diffuse background does not exhibit a difference in intensity at various angular distances from the equator and, hence, no effects of orientation*. We may, therefore, with some right, associate this background with the "disordered component" of the fiber substance. Whether we may associate the peaks with the "crystalline fiber portion" remains perhaps a matter of further consideration. It is a well established fact that, in chemical reactions whereby the original lattice structure is gradually destroyed, the intensities of the various peaks do not diminish simultaneously, nor do their widths change to an equal extent. Usually, widening and intensity drop set in with the 101 line, and the 002 line remains less, if at all, affected.[21] This means that order may be disturbed in one direction without affecting order in another direction. In other words, three-dimensional order changes into two-dimensional order, and the latter may also contribute to the peak intensity.

The 101 planes which are first affected under such conditions are the lattice planes most densily populated by hydroxyl groups and, in cellulose II at least, they are also the preferred cleavage planes of the crystallites. Cellulose II crystallites tend to assume the form of lamellae, they are ribbon shaped rather than rod shaped as conclusively shown by Kratky from experiments on small angle scattering.[22] The 101 (or A_0) plane is the lamellar plane (see Fig. 13).

It is conceivable that in the transitional regions between the crystallites and the disordered portion a state of order may occur where the number of regular 002 spacings surpasses that of the 101 spacings. The diagram in Fig. 13 shows how the fringes protruding from a crystallite might split preferably along the 101 planes, while lattice order is less disturbed along the 002 planes.

Since integrated intensity at random orientation is primarily a function of the fraction of the relevant spacings having the correct values, it will be clear that in such a structure the relative 002 intensity will be enhanced as compared to the 101 intensity. A shift of the intensity ratio holding for an ordinary crystal may thus arise. In the preceding section we have seen that such a shift actually occurs in cellulose II and it may be that the explanation lies in the direction indicated. In cellulose II, the total crystalline intensity measured would then include an appreciable portion of radiation diffracted by regions of two-dimensional order. It is conceivable that also in this case there may still remain a close correspondence between the x-ray results and the sorptive capacity.

Obviously, when considering the total integrated intensity of the crystalline peaks as a measure of crystallinity, what we actually measure is the fraction exhibiting lateral order either in three or in two dimensions. In this broader sense the concept of crystallinity in fibers should be conceived of.

ACKNOWLEDGMENT

The x-ray exposures and photometer curves were taken by one of us (W) in the Laboratory for Technical Physics of the Technical College, Delft. The authors are indebted to Professor H. B. Dorgelo for liberal instrumental support by this laboratory and to Mr. P. M. de Wolff, Mr. J. J. Arlman, and Mr. H. G. de Winter for advice. Thanks are also due Professor J. M. Bijvoet and our colleagues Professor J. J. Hermans and Dr. D. Vermaas for helpful discussions on this subject.

[21] M. Mathieu, *La Nitration de la Cellulose* (Hermann and Cie, Paris, 1936); D. Vermaas and P. H. Hermans, J. Polymer Sci. **2**, 406 (1947).

[22] O. Kratky, A. Sekora, and R. Treer, Zeits. Elektrochem. **48**, 587 (1942).

Letters to the Editor

Convenient Methods for Obtaining d/n Values from X-Ray Diffraction Patterns

C. B. Stewart and E. S. Lutton
The Procter and Gamble Company, Ivorydale, Ohio
January 8, 1948

FOR deriving d/n values from x-ray powder patterns multiple graphs or elaborate tables or scales must generally be prepared unless the Bragg calculation is to be carried through in detail for each spacing. Relations accurate to $0.01kX$ ($1kX = 1.00202$A)[1] have been found which permit rapid slide rule calculations of d/n values for both (i) flat films, in conjunction with a single graph for d/n values below $3.0kX$ and (ii) cylindrical films.

(i) *Flat films.*—The well-known Bragg formula may be expressed

$$d/n = \lambda/2\sin\theta. \tag{1}$$

This relation can be approximated by the following simple equation

$$d/n = [10\lambda/(RD_5)] + A(RD_5), \tag{2}$$

since $2\sin\theta = \tan 2\theta$ for small angles, and $\tan 2\theta = (RD_5)/10$, (RD_5) being the diffraction ring diameter in cm for sample-to-film distance of 5 cm. A is a small constant calculated empirically. If Cu Kα-radiation is used and $\lambda = 1.539kX$,

$$d/n = [15.39/(RD_5)] + 0.055(RD_5).^2 \tag{3}$$

The most convenient form for use is

$$d/n = [15.39/(RD_5)] + 0.10\times[(RD_5)/2] + 0.01\times[(RD_5)/2]. \tag{4}$$

The first term is obtained by a single setting of an ordinary slide rule; the last two terms are readily added mentally with a minimum of practice. Relations (3) and (4) are accurate to $0.01kX$ down to $3.0kX$. In many cases, notably with long-chain compounds, there is little need for lower values. When they are required, a single graph, as in Fig. 1, will cover the range from 3.0 to $1.35kX$.

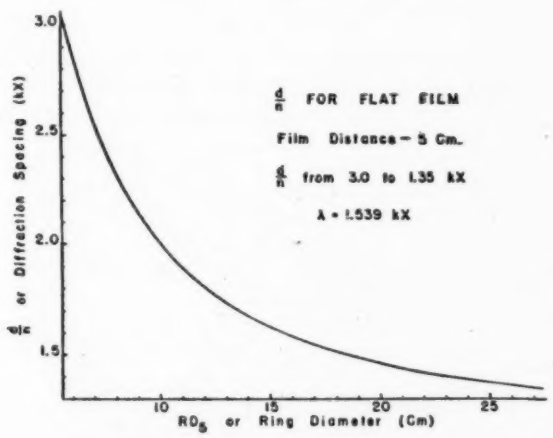

FIG. 1.

(ii) *Cylindrical films.*—For cylindrical films with fixed camera radius = 7.16 cm, the basic equation is

$$d/n = \lambda/[2\sin(4r)], \tag{5}$$

where r is the diffraction ring radius measured in cm, and $4r$ is the value of the angle θ measured in degrees.

Here an approximate relationship can be put in the form

$$d/n = \frac{\lambda}{2\times(4r/57.30)} + Br = \frac{7.16\lambda}{r} + Br, \tag{6}$$

since, for small angles, $2\sin\theta = 2\theta$ and θ in radians $= 4r/57.30$; B is a small constant evaluated empirically. For CuK α-radiation this becomes

$$d/n = (11.02/r) + 0.010r.^2 \tag{7}$$

Here, too, a single slide rule setting is sufficient; a simple mental addition follows. The equation is accurate to $0.006kX$ for d/n values from 0.9 to $22kX$ ($r = 0.50$ cm). Normally the upper limitation is without practical importance since cylindrical cameras are usually built so as to exclude from the film any lines corresponding to spacings greater than $22kX$.

For radiation other than CuK α, Eqs. (4) and (7) should be used and the results multiplied by $\lambda/1.539$ so that Eq. (4) for flat film becomes

$$d/n = [(15.39/RD_5) + (RD_5/2)\times(0.10+0.01)]\times(\lambda/1.539), \tag{8}$$

Error $\leq 0.010\times(\lambda/1.539)$ down to $3.0kX\times(\lambda/1.539)$,

and Eq. (7), for cylindrical film with 7.16-cm camera radius, becomes

$$d/n = [(11.02/r) + 0.010r]\times(\lambda/1.539), \tag{9}$$

Error $\leq 0.006\times(\lambda/1.539)$.

[1] E. A. Wood, Phys. Rev. **72**, 436 (1947).
[2] As has been pointed out to the authors by Dr. A. S. Richardson of this laboratory, the values of the small constants in relations (3) and (7) may be determined mathematically. To accomplish this, $2\sin\theta$ and $\tan 2\theta$ are expressed in terms of θ by means of infinite series. After the necessary operations, substitutions and elimination of smaller terms, equations almost identical with (3) and (7) appear.

Effect of Recrystallized Grain Size on Grain Growth

Paul A. Beck
Department of Metallurgy, University of Notre Dame, Notre Dame, Indiana
March 12, 1948

IN the discussion of a previous paper[1] it was briefly mentioned and in a recent note[2] it was stated in more detail that, according to results obtained with high purity aluminum, the instantaneous rate of grain growth at a given temperature depends only on the grain size D at the instant considered. The instantaneous rate of grain growth was found to be independent of the particular time-temperature schedule used previously to produce that grain size.

It would be of considerable fundamental interest to ascertain under what conditions or within what limits this principle retains its validity. An interesting question in

this connection is whether or not isothermal grain growth in specimens of the same material, starting from different recrystallized grain sizes, D_r, has the same instantaneous rate dD/dt at corresponding grain-size levels. The assumption that it has may be readily expressed in a form suitable for experimental verification, as shown in the present note.

It has been shown[1,3] that isothermal grain growth in a pure metal and in certain pure solid solutions follows the equation

$$D = K \cdot (t_g + A)^n. \tag{1}$$

Here t_g is that portion of the total annealing time t which is available for grain growth, i.e., the total annealing time less the time R necessary for complete recrystallization: $t_g = t - R$. The parameters n and K are functions of the temperature. When recrystallization is just completed $t_g = 0$, and from Eq. (1)

$$D_r = K \cdot A^n. \tag{2}$$

It is possible to eliminate A from Eqs. (1) and (2). By a slight rearrangement one then obtains

$$D^{1/n} - D_r^{1/n} = C \cdot t_g \tag{3}$$
where $C = K^{1/n}$.

Here n and C are parameters which depend on the temperature. Equation (3) is, of course, equivalent to Eqs. (1) and (2), which have already been published.[1] However, its presentation is warranted by the convenience it offers in certain applications.

Equation (2) leads to the interpretation of parameter A as the period of imaginary grain growth which would increase the grain size from zero to the recrystallized grain size D_r in accordance with the extrapolation of the formula describing grain growth subsequent to recrystallization, Eq. (1). These conditions are illustrated in Fig. 1. Here point *1* represents recrystallization just completed, and point *2* represents a condition obtained by recrystallization followed by grain growth along the solid curve 1–2 during the period t_g. This curve, a parabola of the nth order, corresponds to Eq. (1). According to Eq. (2) the value of A is determined so as to bring the apex of the dotted extension of the parabola exactly to the common origin of the time and the grain-size scales. The sum $t_g + A$, appearing in Eq. (1), is the total grain-growth time which would produce a final grain size D from an imaginary starting grain size of zero, according to the simple power law, Eq. (1). Actually, the dotted portion of the parabola (0–1) is not operative. Instead of grain growth, the process resulting in grain size D_r is recrystallization, a process involving nucleation and growth, during the period R, of virtually strain-free grains in a strained matrix.

Now, if the recrystallization process is so conducted as to lead to a different grain size D_r', the grain sizes obtained by grain growth starting with this D_r' cannot be predicted without some additional relationship. In the following the assumption is made that here too, as in the case previously investigated[2] where different starting grain sizes were produced by grain growth at different temperatures, the instantaneous rate of grain growth dD/dt at a certain temperature depends only on the instantaneous grain size D (see the first paragraph). With this assumption the D *vs.* t curve will be as shown in Fig. 2. The tangent of curve b at *3* (grain size D_r') will be the same as that of curve a at *2* (the same grain size). It is easy to see that curve b can be derived from curve a by a parallel displacement along the time axis. In other words, grain growth starting from a certain recrystallized grain size will, under such conditions, follow the same equation as grain growth starting from any other recrystallized grain size, provided that the parameter A is properly determined from Eq. (2) for each starting grain size. This implies that in Eq. (1) the parameters K and n are independent of the starting grain size. The same is true for parameter C in Eq. (3); the convenience in using this equation is now apparent. If $D^{1/n} - D_r^{1/n}$ is plotted against t_g, the same straight line describes grain growth regardless of the starting grain size. In a case like that of 70–30 brass, where n is independent of the temperature, the same ordinate scale can be used throughout, and the lines representing grain growth at various temperatures will be straight lines of different slope, intersecting each other at the origin.

In the log D *vs.* log t plot which was used in previous publications to represent grain-growth data for high purity aluminum, for an Al+2 percent Mg alloy and for 70–30 brass, the consequences of the above assumption can be expressed as shown in Fig. 3. For a certain grain size D_r the time for complete recrystallization R may be the same as parameter A calculated from Eq. (2). For that particular starting grain size Eq. (1) is simplified to

$$D = K \cdot t^n, \tag{4}$$

where $t = t_g + R = t_g + A$, and the logarithmic grain-growth line is a straight line (a in Fig. 3). If D_r' is such that $A > R$ a curve is obtained (b in Fig. 3), which starts higher than

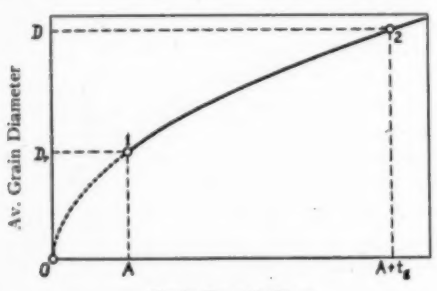

FIG. 1.

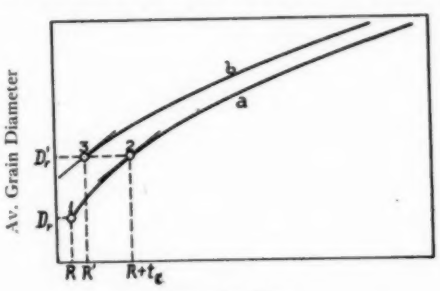

FIG. 2.

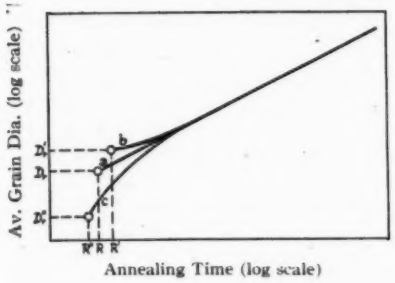

FIG. 3.

the straight line, but approaches it asymptotically. If for a certain $D_r''A < R$, the curve approaches the straight line from below (line *C*, Fig. 3). Examples of all three types of logarithmic grain-growth lines have actually been recorded in previous work.[1,2] This may now be interpreted to indicate that the time for complete recrystallization *R*, leading to a recrystallized grain size of D_r, may be either larger or smaller than or equal to the time *A* during which a grain size D_r would develop from zero size by means of the hypothetical "extrapolated grain growth."

For 70–30 brass of a grain size of 0.028 mm, reduced 33 percent by rolling, the log *D vs.* log *t* plot of the grain sizes produced by annealing at 450° very closely approximates a straight line all the way to the recrystallization point. In this case, therefore, *A* is approximately equal to *R*, i.e., the hypothetical grain-growth mechanism would lead to the same grain size in the same period of annealing as recrystallization does. Work is at present under way in this laboratory to study grain growth in brass after recrystallization to various grain sizes. The results of these experiments, plotted in either one of the two ways discussed, should tell whether or not the above assumption is correct.

[1] Paul A. Beck, J. C. Kremer, L. J. Demer, and M. L. Holzworth, "Grain growth in high purity aluminum and in an aluminum-magnesium alloy," AIME Tech. Pub. No. 2280 Metals Tech. (September 1947).
[2] Paul A. Beck, M. L. Holzworth, and Haun Hu, "Instantaneous rates of grain growth," Phys. Rev. **73**, 526 (1948).
[3] Paul A. Beck, John Towers, Jr., and William D. Manly, "Grain growth in 70–30 brass," AIME Tech. Pub. No. 2326, Metals Tech. (February 1948).

New Booklets

Minnesota Mining and Manufacturing Company, 901 Fauquier Avenue, St. Paul 6, Minnesota, has issued a 28-page brochure entitled *3M Adhesives in Industry*. Forty photographs, 18 "case histories." Free on request.

Bausch and Lomb Optical Company's *The Educational Focus* for February 1948, published at Rochester 2, New York, features an article on "Phase contrast microscopy" by J. Magliozzi.

Sound Apparatus Company, 233 Broadway, New York 7, New York, announces a bulletin entitled *Sound Advances*, which discusses the company's new high speed recorder. 8 pages, free on request.

Tracerlog, published by Tracerlab, Inc., 55 Oliver Street, Boston 10, Massachusetts, in its February 1948 issue describes a new laboratory monitor and also features an article entitled "Practical aspects of the administration and operation of a laboratory for radioisotopes." 12 pages.

Electro-Tech Equipment Company, 117 Lafayette Street, New York 13, New York, has published a 66-page catalog which gives comprehensive coverage of standard makes of instruments and controls.

Machlett Laboratories, Inc., Springdale, Connecticut, publishes a quarterly journal named *Cathode Press*, which is mailed without cost to executives, engineers, and others interested in the development, manufacture, distribution, and use of electron tubes. The fall 1947 issue contained 48 pages.

Eastman Kodak Company, Rochester 4, New York, has issued a 4-page pamphlet describing Eastman isotope concentrates, compounds containing stable isotopes of carbon or nitrogen for use in basic research. Available on request. Address the Organic Chemical Sales Division.

Metallizing Engineering Company, Inc., 38–12 30th Street, Long Island City, 1, New York, publishes a journal named Metco News, described as "briefs from industry on the latest developments and applications of the metal spraying process." Free on request. 12 pages.

Howard B. Jones Division of Cinch Manufacturing Corporation, 2460 West George Street, Chicago 18, Illinois, has published a new Howard B. Jones catalog No. 16, describing its line of electrical connecting devices. 36 pages, free on request.

Dow Corning Corporation, Midland, Michigan, has issued *Silastic Facts No. 5*, a 16-page booklet on the Dow Corning silicone rubber.

National Bureau of Standards announces publication of the following bulletins, available from the Superintendent of Documents, Government Printing Office, Washington 25, D.C.:

RP1824 *Validity of the Cosine-Fourth-Power Law of Illumination*, by Irvine C. Gardner, 7 pages, 10 cents.

RP1828 *Freezing Points of Cobalt and Nickel*, by Milton S. Van Dusen and Andrew I. Dahl, 5 pages, 10 cents.

RP1829 *Influence of the Atmosphere upon the Precision of Telescope Pointing*, by Francis E. Washer and Leo W. Scott, 6 pages, 10 cents.

Cannon Electric Development Company, 3209 Humboldt Street, Los Angeles 31, California, has announced the publication of bulletin No. DP-547 entitled *Rack and Panel Type Connectors for Radio and Instrument Applications*. 24 pages. Free on request to the Catalog Department of the company.

Here and There

New Appointments

Three new appointments to the staff of the National Bureau of Standards were recently announced. Russell E. Dorrell will work in the Electron Tube Laboratory as an electronics engineer, William B. Haliday will be engineer in charge of model tube construction in the same laboratory, and Paul V. Horton has been appointed to the Engineering Electronics Section, Ordnance Development Division.

J. V. Pennington, consulting engineer and petroleum technologist of Houston, Texas, has accepted appointment as Associate Director of Southwest Research Institute.

E. P. Wigner will join the staff of the Department of Physics, University of Wisconsin, as a visiting professor for the summer session of 1948.

M.I.T. Receives Texas Company Grant

A $250,000 grant for atomic research and training of nuclear scientists has been made to the Massachusetts Institute of Technology by The Texas Company. The funds will be used for long-range pure research in nuclear fission and related basic studies on the ultimate nature of matter and energy, to construct high voltage equipment of advanced design, and to train scientists in nuclear theory and its application. This work will be carried on primarily in the Laboratory for Nuclear Science and Engineering, which will coordinate its efforts with the departments of physics, chemistry, chemical, electrical, and mechanical engineering, metallurgy, and biology, for maximum interchange of information.

John H. Curtiss Honored

John H. Curtiss, Chief of the National Applied Mathematics Laboratories of the National Bureau of Standards, was elected a fellow of the American Statistical Association by "unanimous vote of the Committee on Honors" for "his outstanding contribution to the profession" at the Association's annual meeting in New York, December 28–31, 1947.

W. C. White to Head National Electronics Conference

The National Electronics Conference, Inc., which will hold its annual technical forum at the Edgewater Beach Hotel, Chicago, November 4–6, has selected W. C. White of General Electric Company, Schenectady, New York, as chairman of the board of directors for the current year.

Physics Lectures at Iowa State

The Department of Physics and the Institute for Atomic Research at Iowa State College, Ames, Iowa, sponsored a special series of lectures on nuclear physics and cosmic rays during February and March. Dr. T. W. Bonner of Rice Institute delivered the first series, and Dr. Marcel Schein of the Institute for Nuclear Studies, University of Chicago, gave the March lectures.

1948–1949 Jewett Fellowship Awards

Nine young scientists have been named by the American Telephone and Telegraph Company to receive the 1948–49 Frank B. Jewett Fellowships for research in the physical sciences. The awards grant $3,000 to the recipient and $1,500 to the institution at which he chooses to do his research. Winners of the fellowships are Warren John Brehm, Ernest Max Grunwald, Leon Albert Henkin, James Allister Jenkins, Robert Karplus, Alvin Ira Kosak, Joaquin M. Luttinger, Paul Olum, and Richard Nelson Thomas. Three of the winners are mathematicians, three chemists, two physicists, and one an astronomer.

Division of Solid State Physics

The annual meeting of the Division of Solid State Physics was held in conjunction with the 1947 annual meeting of the American Physical Society at Columbia University, January 29–31. At this meeting a symposium of papers was presented under the auspices of the Division, consisting of:

Crystallographic Factors in Lattice Imperfections, by R. Smoluchowski, Carnegie Institute of Technology.
Basic Principles of Operations of Crystal Counters, by Frederick Seitz, Carnegie Institute of Technology.
Ferromagnetic Domains, by H. J. Williams, Bell Telephone Laboratories, Inc.
Ferromagnetic Resonance, by J. L. Snoek, Philips Research Laboratories, Eindhoven.

There were also three sessions, comprising a total of 36 contributed papers.

The following were elected as officers of the Executive Committee: R. Smoluchowski, Chairman; W. Shockley, Vice Chairman; A. W. Lawson, Secretary-Treasurer; T. A. Read, Member; and S. Siegel, Member.

Symposium on Electron and Light Microscopy

A Symposium emphasizing the supplementary relationship between electron and light microscopy, sponsored by Armour Research Foundation and the Physics Department of Illinois Institute of Technology, is to be held at The Stevens Hotel, Chicago, Illinois, June 10–12. Information may be obtained from W. C. McCrone or C. F. Tufts of Armour Research Foundation (35 W. 33rd Street, Chicago 16, Illinois).

An instrument display of interest to workers in microscopy will be a feature, and arrangements have been made to exhibit photomicrographs and electron micrographs. Anyone wishing to exhibit should submit material to Howard T. Betz, Armour Research Foundation, before June 6.

Wear Conference Planned at M. I. T. for June

A summer conference on mechanical wear to be sponsored by the Massachusetts Institute of Technology, the A.S.M.E., the General Motors Corporation, and the Chrysler Corporation, will be held in Cambridge, Massachusetts on June 14, 15, and 16. The conference will be devoted to consideration of all aspects of wear between solid surfaces—its causes, symptoms, and cures. In addition to the engineering aspects of this problem, papers will also be presented on the physical and chemical factors in wear. The speakers will include F. P. Bowden, R. Holm, H. Blok, R. H. Savage, R. G. Larsen, and R. W. Dayton.

Particulars may be obtained from Professor J. T. Burwell, Mechanical Engineering Department, Massachusetts Institute of Technology, Cambridge, Massachusetts.